5-2021

Essays on management of scarce resources

Qian LUO
Singapore Management University

ESSAYS ON MANAGEMENT OF SCARCE RESOURCES

QIAN LUO

SINGAPORE MANAGEMENT UNIVERSITY

2021

Essays on Management of Scarce Resources

by

Qian Luo

Submitted to Lee Kong Chian School of Business
in partial fulfillment of the requirements for the Degree of
Doctor of Philosophy in Business

Dissertation Committee:

Onur Boyabatlı (Chair)

Associate Professor of Operations Management

Lee Kong Chian School of Business, Singapore Management University

Buket Avcı

Assistant Professor of Operations Management

Lee Kong Chian School of Business, Singapore Management University

Zhichao Zheng (Daniel)

Associate Professor of Operations Management

Lee Kong Chian School of Business, Singapore Management University

Niyazi Taneri

Senior Lecturer of Operations & Technology Management

Judge Business School, University of Cambridge

Rowan Wang

Associate Professor

College of Business, Southern University of Science and Technology

SINGAPORE MANAGEMENT UNIVERSITY

I hereby declare that this dissertation is my original work
and it has been written by me in its entirety.
I have duly acknowledged all the sources of information
which have been used in this dissertation.

This dissertation has also not been submitted for any degree
in any university previously.

Qian Luo
10 May 2021

Abstract

Efficient management of scarce resources is critical to the improvement of economic, social and/or environmental performances. In this dissertation, I focus on the management of two scarce resources: i) healthcare resources and ii) water, and investigate two important problems: i) the estimation of patients' health transition to support healthcare resources control under the context of sequential medical treatments, and ii) the urban water system control with a specific focus on the wastewater recycling capacity investment in the presence of climate change and urban water scarcity.

The first chapter studies how to estimate patients' health transition considering the effects of treatment-effect-based policies. Treatment-effect-based decision policies are increasingly used in healthcare problems, which leverage predictive information on patient health transitions and treatment outcomes for specific medical treatment decisions. However, treatment-effect-based policies will significantly censor patients' observed health transitions and distort the estimation of transition probability matrices (TPMs). I propose a structural model to recover the underlying true TPMs from censored transition observations to address this issue. I show that the estimated TPMs from the structural model are consistent, asymptotically normally distributed and maximize the log-likelihood function on observed censored data. I compare the proposed model with other estimation methods through numerical experiments and demonstrate its advantages in various performance metrics, e.g., deviations from the ground truth TPMs. I also implement the proposed model to estimate patient health transitions using real censored data in ICUs extubation problems. Formulating the

extubation problem as a classical optimal stopping Markov Decision Process model, I show that the proposed model, with more accurate estimated TPMs considering censored data, can reduce the length of stay of patients in ICU compared to other benchmark transition estimation methods.

In the second chapter, considering multiple urban water resources (e.g., freshwater from reservoirs, recycled water, and desalinated water/imported freshwater) and multiple streams of urban water demand (e.g., household and non-household demands), I examine the economic and sustainable implications of wastewater recycling capacity investment under rainfall and recycling cost uncertainties. To this end, I formulate the problem as a two-stage stochastic minimization model and characterize the optimal wastewater recycling capacity. I find that the optimal recycling capacity first decreases and then increases in the freshwater capacity, suggesting that they are substitutes when the freshwater capacity is relatively small and complements otherwise. I also perform sensitivity analysis on how the uncertainties (rainfall and recycling cost variabilities and their correlation) affect the optimal recycling capacity and the optimal expected cost and find that the water utility always benefits from a higher correlation coefficient but a lower rainfall variability. In this chapter, I also discuss urban water sustainability using the measures such as urban water vulnerability and characterize the specific conditions under which urban water may become more vulnerable.

The third chapter calibrates the economic model presented in the second chapter based on the publicly available data from the urban water supply practice in Adelaide, the capital city of South Australia. To complement the analytical results, I conduct comprehensive numerical analysis in this chapter to investigate the effects of uncertainties on the optimal expected cost and optimal recycling capacity. Moreover, I study the value of wastewater recycling and how rainfall and recycling cost variabilities, correlation and demand expansion affect it. For example, the results show

that the value of wastewater recycling increases in the correlation coefficient and decreases in the rainfall variability. Based on the calibrated baseline scenario, I find that the expansion of both the household and non-household demands increase the value of recycling; moreover, the expansion of non-household demand tends to have a larger impact when the deviations from the baseline scenario become relatively large. I further study the leakage reduction, water vulnerability and overflow risk. The insights from the numerical analysis in this chapter complement the analytical results presented in Chapter 2. I put forward important practical implications relevant to both urban water utilities and water policymakers based on the findings.

Contents

Acknowledgements

First and foremost, I would like to express my deepest gratitude and appreciation to my advisor Professor Onur Boyabatı, research committee members Professor Zhichao Zheng and Professor Buket Avcı for their inspiration, excellent guidance and continuous support of my research. I would not have been able to finish my thesis without their immeasurable support. Their excellence and strictness always motivate me to pursue high-quality research.

Special thanks must go to my research committee member Professor Rowan Wang, who inspired me a lot on critical thinking and how to conduct and write good research papers. I also would like to thanks another research committee member Professor Niyazi Taneri for his effort and time on my thesis.

My sincere thanks goes to my colleagues Yan He, Nicholas Yeo and Peng Wang for the stimulating discussions, for the sleepless nights we were working together before deadlines, and for all the fun we have had in the last five years.

Last but not least, my sincere gratitude goes to my families for their endless love, trust and support in the past years. Their unconditional support gave me the confidence, courage and opportunity to pursue a Ph.d. degree.

Chapter 1

Estimating Patients Health Transitions From Data Censored By Treatment-Effect-Based Policies

1.1 Introduction

Discrete-time Markov Chain (DTMC) is widely used to characterize patient health transitions, and Markov Decision Process (MDP) are broadly applied to describe sequential medical decision problems, e.g., liver transplant (Alagoz et al. 2004) and cancer screening (Chhatwal et al. 2010). Transition probability matrices (TPMs) are critical to understanding patients' disease progression, and hence, to decision-making problems under MDP framework (Mannor et al. 2012). Traditionally, TPMs are usually estimated under an assumption that data is fully observed, which may cause mistakes since patients' health transitions are censored oftentimes. Data censoring, the situation in which some end-points of interest cannot be observed, arises in a range of contexts and is common in medical studies in particular (Huang 2009). For example, data censoring may occur when study termination, participant dropout and treatment selection. As pointed out by Feiler et al. (2013), censoring can distort observations; hence, it can result in the estimation bias of TPMs. In this chapter, I propose a novel framework to estimate TPMs considering data censoring from treat-

ment selection.

Different treatment selection/decision policies may yield different data censoring results, and hence, may impose different distortions on TPMs estimation. In medical practice, physicians usually make treatment decisions base on patients' current severity. For example, given a severity threshold, patients will receive or continue treatment if and only if their health conditions are not better than the threshold. This decision policy is termed as *severity-based policy* in this research. Physicians may also make decisions base on the effect of treatment methods (i.e., treatment effect) such that the treatment method with the largest treatment benefit can be selected. This decision policy, which is based on the treatment effect, is termed as *treatment-effect-based policy*. The treatment-effect-based policy is also referred to as personalized medicine or uplift modeling (Zhao et al. 2017, Schork 2015), which has been receiving considerable attention from practitioners and scholars; for example, it has been used to ration ventilators during the coronavirus disease 2019 (COVID-19) pandemic (**?**Truog et al. 2020) and broadly discussing in literature (e.g., Lee et al. (2018), Bertsimas et al. (2019a), KC et al. (2020), Gupta et al. (2020) and Keskinocak and Savva (2020)).

As I mentioned, treatment selections lead to data censoring and then may distort TPMs estimation. I use a toy example in Figure 1.1 to illustrate the censoring mechanisms and their impacts on TPMs estimation under severity-based and treatment-effect-based policies, repectively.

Patients are classified into two states: state 1 is better than state 2. For a patient who is under treatment at state 2 at current stage, a physician needs to decide whether to continue the treatment. Under the severity-based policy, if the current state is better (not better) than the threshold, the decision/action is no treatment (treatment), so the transitions under treatment (no treatment) are censored. I define it as *severity-based censoring*, which is also discussed in Shechter (2006) that focuses

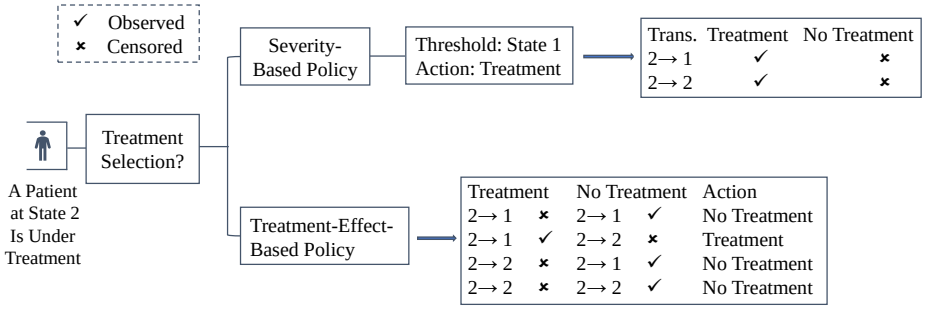

Figure 1.1: Transition Censoring Under Different Policies.
(1) $2 \to 1$ and $2 \to 2$ denote transitions;
(2) under the severity-based policy, assuming the threshold is state 1, the action is "treatment" as the patient' state is not better than the threshold. Hence, transitions under action "no treatment" are censored;
(3) under the treatment-effect-based policy, assuming the treatment effect threshold is zero, if the future state under "treatment" is not better than that under "no treatment", the action is "no treatment" and then the transitions under action "treatment" are censored.

on the impact of censoring under no treatment. Given the threshold, Figure 1.1 shows that the severity-based censoring only depends on current status and, given the health state, we either observe all or cannot observe any transitions under each action.

The censoring under the treatment effect-based policy, which is termed as *treatment-effect-based censoring*, depends on future health states. For example, in Figure 1.1, the transition from state 2 to state 1 under treatment is censored (or observed) if the patient transits to state 1 (or state 2) under no treatment. Recall that state 1 is better than state 2, the treatment effect then is 0 (or -1, which indicates heath state improvement under treatment). Hence, the treatment-effect-based policy censors transitions with worse future outcomes. Moreover, it is more likely for us to observe transitions with better outcomes under the treatment-effect-based policy when comparing with the severity-based policy.

To be more concrete, I assume the gound truth TPMs under treatment and no treatment are $\left(\begin{smallmatrix} 0.6 & 0.4 \\ 0.5 & 0.5 \end{smallmatrix}\right)$ and $\left(\begin{smallmatrix} 0.4 & 0.6 \\ 0.2 & 0.8 \end{smallmatrix}\right)$, respectively. I estimate TPMs using observed transitions, of which the transition probabilities are represented by the proportions of observed transitions. Under the severity-based policy, assuming state 1 is the

threshold, then all patients receive treatment, which implies that all transitions under no treatment are censored. Hence, the TPM under treatment is estimated as $\left(\begin{smallmatrix} 0.6 & 0.4 \\ 0.5 & 0.5 \end{smallmatrix}\right)$, which is the same as the ground truth TPM, while the TPM under no treatment is not well defined since there is no observed data. Under the treatment-effect-based policy, no transition to state 2 with treatment is observed, then the TPM of observed transitions under treatment is $\left(\begin{smallmatrix} 1 & 0 \\ 1 & 0 \end{smallmatrix}\right)$. Similarly, the observed TPM under no treatment is $\left(\begin{smallmatrix} 0.625 & 0.375 \\ 0.333 & 0.667 \end{smallmatrix}\right)$[1]. The results show that these two observed TPMs tend to overestimate the effects of the actions (i.e., comparing with the ground truth TPMs, these two observed TPMs specify that patients are more likely to transit to better states) and are significantly different from the ground truth TPMs. To be more specific, I find that the severity-based censoring only reduces frequencies of observed transitions, while the treatment-effect-based censoring not only reduces observed frequencies but also shifts the observed transition structures from the underlying transition structures, and hence, distort the TPMs estimation. Under most circumstances, we only know that both severity-based and treatment-effect-based decisions are included in datasets, but we are unable to (exactly) disentangle severity-based decisions from treatment-effect-based decisions. For such datasets, without properly addressing data censoring, biased TPMs estimations may be derived, which greatly mislead follow-up medical decisions, e.g., decisions using MDP models.

Despite the prominence of the treatment-effect-based policy in healthcare, machine learning, and marketing literature, its impacts on data censoring have received little attention to date. In this chapter, given the popularity of MDP models and then the importance of TPMs, I consider a TPMs estimation problem where patients' health transitions are characterized by a DTMC and data are obtained under

[1]To derive this matrix, for example, transition $2 \to 1$ under no treatment can be observed with probability 0.2 while transition $2 \to 2$ under no treatment is observed with probability $0.8 \times 0.5 = 0.4$ (i.e., conditioning on the transition is $2 \to 1$ under treatment); hence, the observed transition probabilities for $2 \to 1$ and $2 \to 2$ under no treatment are $\frac{0.2}{0.2+0.4} = 0.333$ and $\frac{0.4}{0.2+0.4} = 0.667$, respectively.

both severity-based and treatment-effect-based policies. Focusing on the treatment-effect-censoring problem, I propose a structural model to estimate the ground truth TPMs. The proposed model is valuable because it provides a framework to understand the behind mechanisms of observations and to recover the ground truth TPMs in an interpretable way. Moreover, as pointed out by Kaynar and Siddiq (2019), an interpretable structural model provides a more credible framework for the assessment of counterfactual.

The main contributions of this research are summarized as follow:

- I propose a structural model that embeds treatment-effect-based censoring to recover ground truth TPMs under the framework that patients' health transitions are characterized by DTMC. The proposed model captures the mechanism of data censoring in the transitions and provides a systematic and interpretable way to recover TPMs. To the best of my knowledge, this is the first research to discuss the treatment-effect-based censoring problems in literature. Although I use health transition estimation as examples, the model can also be applied to other contexts in which treatment-effect-based policy is involved in decision making.

- I analytically prove that the TPMs estimation solution of the structural model is unique, and the estimators are consistent and asymptotically normally distributed under some conditions. Moreover, I prove that the proposed estimators maximize the likelihood of observing the data with treatment-effect-based censoring incorporated.

- In the numerical experiments, I compare the proposed model with other estimation methods (e.g., the method with using predictive models to predict the censored observations and estimating TPMs by incorporating the recovered censored data) and demonstrate its advantages in terms of various performance

metrics. I also implement the proposed model in ICUs extubation problem to estimate patient health transitions using real censored data. Formulating the extubation problem as a classical optimal stopping Markov Decision Process model, I show that the proposed model is able to reduce the length of stay of patients in ICU comparing to other benchmark transition estimation methods that do not properly address censored data.

In what follows, I review literature in Section 1.2; I develop the structural model and show the asymptotic behaviors of the estimators in Section 1.3; I then present numerical experiments in Section 1.4 and a case study in Section 1.5. I conclude the chapter in Section 1.6.

1.2 Literature Review

As illustrated in Figure 1.2, the applications of MDP models in general and the severity-based and treatment-effect-based policies in particular affect the observed data and then affect the MDP application itself through the TPMs and/or treatment effect estimations on data with censoring/selection bias. Hence, this work is mainly related to the literature on TPMs estimation but also contributes to the literature of estimating treatment effect on data with selection bias, the application of MDP (including partially observable Markov decision process, POMDP) models in medical areas (i.e., the application of severity-based policies) and personalized medicine and uplift modelling (i.e., the application of treatment-effect-based policies).

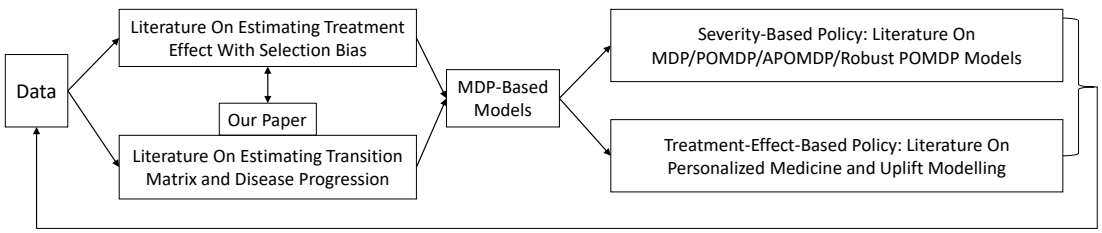

Figure 1.2: Relationship Between My Work and The Literature

There are extensive research on TPMs estimation. Some focus on the estimation with complete observations. For example, Miller (1952) and Madansky (1959) estimate transition probabilities using restricted least square (LS) method by minimizing the sum of squares of the differences between predicted probabilities and observed probabilities. However, they do not consider that each row of transition matrix sums to one and the probabilities are positive. Theil and Rey (1966) address this problem using a quadratic programming approach under the LS framework. The best known and most popular method to estimate TPMs is Maximum Likelihood Estimation (MLE) as in (Wu and Noé 2010). MLE is proved to be consistent and asymptotically normally distributed (Kendall and Alan 1961) and shown to be superior to LS estimation in Lee et al. (1970). Besides, Martin (1967) and Lee et al. (1968) suggest a Bayesian approach to estimate TPMs. Jilkov and Li (2004) estimate TPMs with online minimum mean-square error (MMSE) estimation under a Bayesian framework. Storm et al. (2015) develop a Bayesian framework to estimate non-stationary transition probabilities. I refer the readers to Pasanisi et al. (2012) for a more comprehensive review of the application of Bayesian methods to TPMs estimation. Moreover, Kolmogorov equation is also applied to estimate disease progression under continuous-time Markov Chains, e.g., Asena and Goshu (2017) and Meenaxi and Singh (2018). These literature assume a dataset with complete observations, and do not address the data incompleteness and censoring.

Some research study TPMs estimation with incomplete or partially observed data samples. For example, observations from the dataset may have greater time intervals than desired by the Markov models, which means the disease progression paths that individuals have followed during certain intervals are unobservable. To address this problem, Welton and Ades (2005) adopt a Bayesian framework and compute the TPM using Kolmogorov equation with the estimated transition rate matrix as input. An alternative solution is to apply matrix decomposition methods to observed TPMs,

e.g., Craig and Sendi (2002), Chhatwal et al. (2010) and Chhatwal et al. (2016). This approach requires that the eigenvalues of observed TPMs are non-negative; otherwise, an invalid transition matrix is derived. Charitos et al. (2008) also address the problem that the model interval is not equal to the observed interval in the data base on matrix decomposition techniques. They do not require non-negative eigenvalues; instead, they apply regularization techniques which aim to replace rows with negative entries in the invalid TPM with rows with non-negative entries using a distance criterion. Craig and Sendi (2002) consider the situation that observed time intervals are unequal. They use the expectation-maximization (EM) algorithm to estimate TPMs of interest. Applying the EM algorithm and MLE, Leaf (2017) propose a unified framework to estimate TPMs with incomplete data. In addition, Alagoz et al. (2004) estimate TPMs with the Natural History Model (NHM) proposed by Alagoz et al. (2002). Pasanisi et al. (2012) apply Monte Carlo Markov Chain algorithms to perform Bayesian inference and then evaluate the posterior distributions of the transition probabilities considering partially observed state sequence.

My work is closest to the research on the estimation of TPMs with data censoring. Aalen and Johansen (1978) investigate the transition probability estimation problem for non-homogeneous Markov chains considering censored observations using a general censoring random process. They show that the estimator can be expressed as a product integral. Lagakos et al. (1978) consider a semi-Markov model with right-censored data and estimate transition probabilities using nonparametric MLE. These research focus on the estimation of transition probabilities under a continuous-time Markov setting and consider randomly censored observations; however, I focus on the discrete-time Markov setting with treatment-effect-based censoring. In a discrete-time Markov setting, Dasbach et al. (1991) estimate one-year natural disease transition probabilities using MLE method considering data censoring caused by initiation of treatment. In a similar context, Craig et al. (1999) develop a Markov model to

characterize the progression of a chronic condition. Unlike Dasbach et al. (1991), Craig et al. (1999) incorporate covariate information, and create a non-homogeneous Markov chain. They use a Bayesian approach to estimate annual transition probabilities under intervention considering the time of intervention is interval-censored. Borrowing ideas in Dasbach et al. (1991), Shechter (2006) and Shechter et al. (2008) derive empirical estimations of transition probabilities by hypothesizing how the censored observations distribute among states when therapy had not been initiated at the time. My work differs from the literature in two main aspects. First, instead of only considering the estimation of natural disease transitions with and without treatment, I estimate TPMs under different actions simultaneously. Second, I focus on treatment-effect-based censoring, which, to the best of my knowledge, has not been discussed in TPMs estimation.

As treatment selection censoring may result in selection bias, my work is also related to the researches on addressing selection bias. More specifically, because my work attempts to address the selection bias problem by recovering the censored observations (i.e., the assessment of counterfactual) in a structural way, within this literature, it is closest to the papers on causal inference. Ho et al. (2017) discuss the application of causal inference models in operations management when there are different types of selection bias. Stukel et al. (2007) compare the effects of four analytical methods on removing treatment selection bias when doing causal inference. A more comprehensive review of this stream of literature is referred to Infante-Rivard and Cusson (2018). My research differs from them by addressing the selection bias problem during TPMs estimation.

DTMC models (MDP and POMDP) are widely applied to address healthcare problems, such as organ transplant (Alagoz et al. 2004, Boloori et al. 2020), diagnostic screening (Chhatwal et al. 2010, Zhang et al. 2012, Ayer et al. 2012, Erenay et al. 2014, Ayer et al. 2016), vascular access (Skandari et al. 2015) and ICU bed

rationing (Chan et al. 2012, Ouyang et al. 2020). My work directly contributes to this stream of researches as TPMs are critical input for them. Furthermore, from the perspective of TPMs estimation under MDP frameworks, this work is broadly related to the literature which addresses the ambiguity of TPMs estimation using data under MDP framework, e.g., Nilim and Ghaoui (2005), Wiesemann et al. (2013), Zhang et al. (2017), and Goh et al. (2018). There is an increasingly trend of implementing treatment-effect-based policies in personalized/precision medicine, see e.g., Ibrahim et al. (2016), Lee et al. (2018), Bertsimas et al. (2017), Hopp et al. (2018), Cheng et al. (2019), Gupta et al. (2020) and references therein. As I described, treatment-effect-based policies censors observations in a specific way (i.e., observations with worse future outcomes are censored). Data censoring is one of the greatest challenges when using observed data for causal inference (Imbens and Rubin 2015, Bertsimas et al. 2019b) in personalized medicine. My research can be seen as a contribution to this literature by providing a framework to understand the censoring mechanisms under personalized medicine, which can be useful to build predictive models for personalized treatment effects.

My work is also related to research which considers data censoring in general operations management. For example, Chu and Lai (2013) investigate a salesforce contracting problem with censored demand. Rudi and Drake (2014),Jain et al. (2015),and Zhang et al. (2018) analyze the demand censoring in inventory problems. Ban (2020) develop an estimation procedure for the (S, s) inventory policy and show the consistency and asymptotic efficiency of the estimator when there is demand censoring. Similarly, in this chapter, I also conduct asymptotic analysis of the proposed model and show the efficiency of the estimated TPMs.

1.3 Model Development and Analysis

I consider a TPMs estimation problem using data from a medical decision framework, where physicians make medical treatment decisions using severity-based or treatment-effect-based policies. As described, treatment-effect-based censoring shifts transition structures, and it is usually impossible to disentangle severity-based decisions from treatment-effect-based decisions. In this section, I propose a structural model to address the treatment-effect-based censoring in TPMs estimation.

To construct the model, I structurally link the ground truth TPMs with the censored observations. Specifically, given ground truth TPMs, I derive the probability that any particular transition can be observed under severity-based and treatment-effect-based policies, respectively. Given the probabilities of using severity-based and treatment-effect-based policies by decision makers (e.g., the physicians), I obtain the probability that any transition can be observed in the dataset, which is the observed transition probability. As the name suggests, the observed probabilities can be estimated using observed data directly, which then can be used to derive the ground truth TPMs inversely.

In the modeling framework, I only consider severity-based and treatment-effect-based policies and I believe that almost all medical decisions are made under these two policies in practice. Under these two policies, the key specification is the threshold (i.e., severity and treatment-effect thresholds, respectively), which determines physicians' actions. In general, physicians may be inconsistent in the decision criteria such that they may choose different values as the threshold when making decisions. Moreover, the decision criteria may also vary with operational conditions (KC et al., 2020), e.g., ICU occupancy level and workload, and other factors such as patients' insurance types and financial conditions. In this regard, different thresholds may be used under both policies in practice.

Another important issue I want to emphasize is, in medical practice, the treatment

effects are often estimated based on physicians' prognosis, which is challenging and cannot be perfectly accurate. Physicians' prognostic information is usually unavailable, which makes it difficult to capture the ground truth treatment-effect-censoring in the estimation. Through the discussions with physicians, they mention that they only make decisions base on the prognostic outcomes when they are very confident in their prognosis. Therefore, in the following sections, I first develop a structural model assuming physicians' prognosis on future health states are error-free in Section 1.3.1, and then analyze the properties of the proposed structural model in Section 1.3.2. In Section 1.3.3, I extend my model to capture prognostic errors when the prognostic information is given.

1.3.1 Structural Model

Consider a dataset from sequential medical treatment decisions made by physicians periodically based on either health states or treatment effects of patients. Let $s \in \mathcal{S} = \{1, 2, ..., N\}$ denote the health state, and a larger s indicates a worse health condition. Let $a \in \mathcal{A} = \{0, 1\}$ denote the action, where $a = 1$ represents "treatment" and $a = 0$ represents "no treatment". Under each action, the health transitions over time periods are characterized by a DTMC. Let $\boldsymbol{P}^a$ denote the ground truth TPM under action a, with $P^a_{ij} \in [0, 1]$ for all $i, j \in \mathcal{S}$. Although I consider two actions in this chapter, the model can be easily extended to the decision frameworks with multiple actions.

Consider a finite time horizon with period $t \in \mathcal{T} = \{1, 2, ..., T\}$. I define the personalized treatment effect for a patient whose state is s in period t is $\delta_t = (s^{a=1}_{t+1} - s_t) - (s^{a=0}_{t+1} - s_t) = s^{a=1}_{t+1} - s^{a=0}_{t+1}$, where s_t is the state in period t and s^a_{t+1} denotes the state in period $t + 1$ if I take action a in period t (recall that I assume s^a_{t+1} is prognosticated by physicians without prognostic errors). Hence, a negative δ_t indicates that the "treatment" can benefit the patient more than "no treatment". I

formally define the following two decision policies.

Definition 1.1 (Severity-based policy)**.** Given a state threshold $\bar{s} \in \mathcal{S}$, for any patient in time period $t \in \mathcal{T}$, s/he will receive treatment if and only if $s_t \geq \bar{s}$.

Definition 1.2 (Treatment-effect-based policy)**.** Given a treatment-effect threshold $\bar{\delta}(i)$, for any patient of state i in time period $t \in \mathcal{T}$, s/he will receive treatment if and only if $\delta_t \leq \bar{\delta}(i)$.

In medical practice, physicians may apply multiple thresholds under both severity-based and treatment-effect-based frameworks. For simplicity and without loss of generality, I consider a single treatment-effect threshold under treatment-effect-based policy. The general model with multiple treatment-effect thresholds is presented in Appendix A.2, and the results also hold.

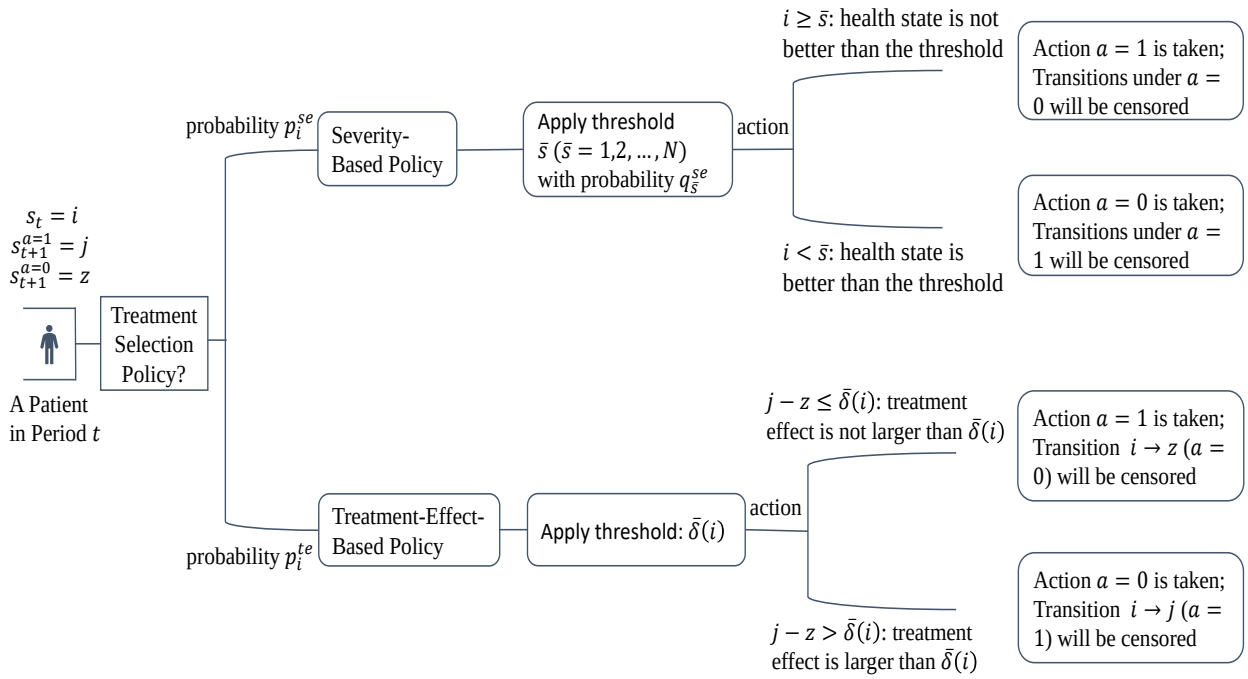

Figure 1.3: Illustration of Model Framework and Transition Censoring

Figure 1.3 illustrates the modeling framework and censoring mechanisms. Considering a patient with state i ($i \in \mathcal{S}$) in any period $t < T$. The patient will transit to state j under action $a = 1$ (i.e., $s_{t+1}^{a=1} = j$) and state z under action $a = 0$ (i.e.,

$s_{t+1}^{a=0} = z$), respectively. Then, the treatment effect of this patient in period t can be computed as $\delta_t = s_{t+1}^{a=1} - s_{t+1}^{a=0} = j - z$. Physicians make medical decisions base on either current severity s_t (i.e., severity-based policy) or treatment effect δ_t (i.e., treatment-effect-based policy). I assume that the probability of using treatment-effect-based policy for patients at state i is $p_i^{te} \in (0,1)$ and the probability of using severity-based policy is $p_i^{se} = 1 - p_i^{te}$. Under the severity-based policy, decisions are made by comparing the patient's current state $s_t = i$ with the state threshold $\bar{s}$. I assume state $k \in \mathcal{S}$ will be selected as the threshold with probability $q_k^{se} \in (0,1)$. Suppose $\bar{s} = k$, then if $i \geq k$, the patient will receive treatment (i.e., $a = 1$ is taken), which implies that transitions under $a = 0$ for this patient are censored and cannot be observed; otherwise, transitions under $a = 1$ for the patient are censored. Under the treatment-effect-based policy, decisions are made by comparing patient's treatment effect δ_t with the treatment-effect threshold $\bar{\delta}(i)$. If $j - z \leq \bar{\delta}(i)$, the patient will receive treatment, which implies that transitions from i to z under action $a = 0$ will be censored and cannot be observed; otherwise, if $j - z > \bar{\delta}(i)$, the patient will not receive treatment and then transitions from i to j under action $a = 1$ will be censored.

If the transition is from state i to state j under action $a = 1$, the probability that this transition will be observed is $\sum_{k=1}^{N} q_k^{se} \mathbb{I}_{i \geq k}$ and $\sum_{k=j-\bar{\delta}(i)}^{N} P_{ik}^{a=0}$ under severity-based and treatment-effect-based policy, respectively. If the transition is from state i to state j under action $a = 0$, the probability that this transition will be observed is $\sum_{k=1}^{N} q_k^{se}(1 - \mathbb{I}_{i \geq k})$ and $\sum_{k=\max(j+\bar{\delta}(i)+1,1)}^{N} P_{ik}^{a=1}$ under severity-based and treatment-effect-based policy, respectively.

Therefore, the total probability that the transition from state i to state j with action $a = 1$ and $a = 0$ can be observed is $P_{ij}^{a=1}(p_i^{te} \sum_{k=j-\bar{\delta}(i)}^{N} P_{ik}^{a=0} + p_i^{se} \sum_{k=1}^{N} q_k^{se} \mathbb{I}_{i \geq k})$ and $P_{ij}^{a=0}(p_i^{se} \sum_{k=1}^{N} q_k^{se}(1 - \mathbb{I}_{i \geq k}) + p_i^{te} \sum_{k=\max(j+\bar{\delta}(i)+1,1)}^{N} P_{ik}^{a=1})$, respectively. For convenience, I let $\boldsymbol{p}^{te} = (p_1^{te}, p_2^{te}, ..., p_N^{te})$, $\boldsymbol{p}^{se} = (p_1^{se}, ..., p_N^{se})$, and $\boldsymbol{q}^{se} = (q_1^{se}, q_2^{se}, ..., q_N^{se})$.

Without lose of generality, I assume the total number of patients in state i is M,

then I can derive the expected number of observed transitions from i to j under action $a = 1$ and $a = 0$ as

$$\bar{Y}_{ij} = MP_{ij}^{a=1}\left(p_i^{te}\sum_{k=j-\bar{\delta}(i)}^{N} P_{ik}^{a=0} + p_i^{se}\sum_{k=1}^{N} q_k^{se}\mathbb{I}_{i\geq k}\right)$$

and

$$\bar{X}_{ij} = MP_{ij}^{a=0}\left(p_i^{se}\sum_{k=1}^{N} q_k^{se}(1-\mathbb{I}_{i\geq k}) + p_i^{te}\sum_{k=\max(j+\bar{\delta}(i)+1,1)}^{N} P_{ik}^{a=1}\right)$$

I define $\hat{\mathbf{\Pi}}^a$ as the observed TPM under action a, where $\hat{\Pi}_{ij}^a$ is the ratio of the number of observed transitions from i to j over the total number of observed transitions out of state i. Hence, I have

$$\hat{\Pi}_{ij}^{a=1} = \frac{\bar{Y}_{ij}}{\sum_{z\in\mathcal{S}}\bar{Y}_{iz}}, \quad \hat{\Pi}_{ij}^{a=0} = \frac{\bar{X}_{ij}}{\sum_{z\in\mathcal{S}}\bar{X}_{iz}}$$

Combining the results above, for any $i, j \in \mathcal{S}$, I obtain:

$$\begin{aligned}
\hat{\Pi}_{ij}^{a=1} &= \frac{P_{ij}^{a=1}\left(p_i^{te}\sum_{k=j-\bar{\delta}(i)}^{N} P_{ik}^{a=0} + p_i^{se}\sum_{k=1}^{N} q_k^{se}\mathbb{I}_{i\geq k}\right)}{\sum_{z=1}^{N} P_{iz}^{a=1}\left(p_i^{te}\sum_{k=z-\bar{\delta}(i)}^{N} P_{ik}^{a=0} + p_i^{se}\sum_{k=1}^{N} q_k^{se}\mathbb{I}_{i\geq k}\right)} \\
\hat{\Pi}_{ij}^{a=0} &= \frac{P_{ij}^{a=0}\left(p_i^{se}\sum_{k=1}^{N} q_k^{se}(1-\mathbb{I}_{i\geq k}) + p_i^{te}\sum_{k=\max(j+\bar{\delta}(i)+1,1)}^{N} P_{ik}^{a=1}\right)}{\sum_{z=1}^{N} P_{iz}^{a=0}\left(p_i^{se}\sum_{k=1}^{N} q_k^{se}(1-\mathbb{I}_{i\geq k}) + p_i^{te}\sum_{k=\max(z+\bar{\delta}(i)+1,1)}^{N} P_{ik}^{a=1}\right)}
\end{aligned} \tag{1.1}$$

The bilinear system of equations is a structural model that (1.1) forms the interactions of the ground truth transition probabilities P under $a = 0$ and $a = 1$ as nonlinear terms. Solving the system of equations by using $\hat{\mathbf{\Pi}}^a$, $\boldsymbol{p}^{se}$ and $\boldsymbol{q}^{se}$ as the inputs, I can derive estimator $\hat{\boldsymbol{P}}^a$ for the ground truth $\boldsymbol{P}^a$. Furthermore, as I defined, the left-hand side of the equations (1.1) represent the observed TPMs and the right-hand side show how the ground truth TPMs are censored under the decision framework. The equations build the relationship between the observations and the ground truth transitions considering treatment-effect-based censoring, which can help us understand the censoring mechanism in a more systematic and interpretable way.

For convenience, I summarize some key notation in Table 1.1.

a: action; $a = 1$ represents "treatment" and $a = 0$ represents "no treatment"
s: state variable with s_t is the state in period t
δ_t: treatment effect in period t
p_i^{te}: probability of using the treatment-effect-based policy for patients at state i
p_i^{se}: probability of using the severity-based policy for patients at state i
q_k^{se}: probability that the severity threshold is state k
$\boldsymbol{P}^a$: ground truth TPM (under action a)
$\hat{\boldsymbol{\Pi}}^a$: observed TPM (under action a)
$\hat{\mathbf{P}}^a$: estimated TPM (under action a) using the structural model (termed as *one-stage estimator* later)

Table 1.1: Notation

1.3.2 Model Analysis

In this section, I present and discuss some analytical properties of the structural model and its performance.

First, I need to solve the system of equations to derive the estimators $\hat{\boldsymbol{P}}^a$. Since the structural model has a nonlinear system of equations, intuitively, I may expect there are multiple solutions, which is not desirable for the estimation of TPMs. In following theorem, I show that $\hat{\boldsymbol{P}}^a$ can be uniquely identified, given the existence of solution(s) in system of equations (1.1).

Theorem 1.1. For any $i, j \in \mathcal{S}$, given the existence of solution(s), the system of equations (in the structural model) has an unique solution.

The proof of Theorem 1.1, given in Appendix A.1, relies on the construction of contradiction. By contradiction, I assume that there are two different solutions $(\mathbf{P}_i^{a=1(1)}, \mathbf{P}_i^{a=0(1)})$ and $(\mathbf{P}_i^{a=1(2)}, \mathbf{P}_i^{a=0(2)})$ to the nonlinear system of equations, and then derive the results that $\sum_{j=1}^N P_{ij}^{a=1(1)} < 1$ and $\sum_{j=1}^N P_{ij}^{a=0(1)} > 1$, which contradict to the fact that $\sum_{j=1}^N P_{ij}^{a=1(1)} = \sum_{j=1}^N P_{ij}^{a=0(1)} = 1$.

Theorem 1.1 implies that the structural model has a very nice property on the estimation of TPMs (for the discussions onward, I assume the existence of solutions), which frees us from the dilemma of choosing among multiple solutions given the nonlinearity of the system of equations. Moreover, the uniqueness property is critical to the analysis of asymptotic properties of the estimators, which are discussed subsequently.

The existence of solutions to the structural model with $N \leq 2$ is easy to show. However, the existence of solutions of such a general bilinear system is difficult and remains as an open question in the literature (Johnson et al. 2014). Intuitively, there should exist solutions as long as I can obtain well defined $\hat{\mathbf{\Pi}}^a$ from data. Besides, I conduct thousands of numerical experiments with randomly generated parameters (i.e., $\hat{\mathbf{\Pi}}^a$, $\boldsymbol{p}^{se}$ and $\boldsymbol{q}^{se}$) and find that the structural model is always solvable. In the analysis afterwards, I assume the existence of solutions.

I am also interested in the asymptotic properties of the estimators. The observed TPM $\hat{\mathbf{\Pi}}^a$ can be estimated from data, which is affected by data sample size. I assume the observed transitions are multinomially distributed. Hence, there exists a ground truth $\mathbf{\Pi}^a$ such that, for any state $i \in \mathcal{S}$, I have

$$Y_{i1}, ..., Y_{iN} \sim multinomial(K_i^{a=1}, \Pi_{i1}^{a=1}, ..., \Pi_{iN}^{a=1})$$

and

$$X_{i1}, ..., X_{iN} \sim multinomial(K_i^{a=0}, \Pi_{i1}^{a=0}, ..., \Pi_{iN}^{a=0})$$

where Y_{ij} and X_{ij} are random variables which represent the number of observed transitions from i to j under actions $a = 1$ and $a = 0$, respectively. K_i^a is the total number of observed transitions from i to other states. Moreover, I let $f_i^{a=1}$ and $f_i^{a=0}$ be the probability mass functions for Y_{ij} and X_{ij}, respectively.

For $i \in \mathcal{S}$ and $j = 1, 2, ..., N-1$, I further define

$$g_{ij}^{a=1}(\boldsymbol{P}_i^{a=0}, \boldsymbol{P}_i^{a=1}) = \frac{P_{ij}^{a=1}\left(p_i^{te}\sum\limits_{k=j-\bar{\delta}(i)}^{N} P_{ik}^{a=0} + p_i^{se}\sum\limits_{k=1}^{N} q_k^{se}\mathbb{I}_{i\geq k}\right)}{\sum\limits_{z=1}^{N} P_{iz}^{a=1}\left(p_i^{te}\sum\limits_{k=z-\bar{\delta}(i)}^{N} P_{ik}^{a=0} + p_i^{se}\sum\limits_{k=1}^{N} q_k^{se}\mathbb{I}_{i\geq k}\right)}$$

$$g_{ij}^{a=0}(\boldsymbol{P}_i^{a=0}, \boldsymbol{P}_i^{a=1}) = \frac{P_{ij}^{a=0}\left(p_i^{se}\sum\limits_{k=1}^{N} q_k^{se}(1-\mathbb{I}_{i\geq k}) + p_i^{te}\sum\limits_{k=\max(j+\bar{\delta}(i)+1,1)}^{N} P_{ik}^{a=1}\right)}{\sum\limits_{z=1}^{N} P_{iz}^{a=0}\left(p_i^{se}\sum\limits_{k=1}^{N} q_k^{se}(1-\mathbb{I}_{i\geq k}) + p_i^{te}\sum\limits_{k=\max(z+\bar{\delta}(i)+1,1)}^{N} P_{ik}^{a=1}\right)}$$

with $P_{iN}^a = 1 - \sum\limits_{j=1}^{N-1} P_{ij}^a$ for $a \in \{0, 1\}$. I then define the mapping

$$\mathbf{G}_i = (g_{i1}^{a=1}, g_{i2}^{a=1}, ..., g_{i,N-1}^{a=1}, g_{i1}^{a=0}, g_{i2}^{a=0}, ..., , g_{i,N-1}^{a=0})$$

I want to clarify that P_{iN}^a is not included in the independent variable set as $P_{iN}^a = 1 - \sum_{j=1}^{N-1} P_{ij}^a$. However, for notation convenience, I still use arguments $\boldsymbol{P}_i^{a=0}$ and $\boldsymbol{P}_i^{a=1}$ in the mapping $\mathbf{G}_i$. Based on these settings, I characterize the asymptotic behaviors of the estimators in Theorem 1.2.

Theorem 1.2. Given the existence of solution(s) of the structural model. Let $\hat{\mathbf{\Pi}}^a(n)$ and $\hat{\boldsymbol{P}}^a(n)$ denote the estimators of $\mathbf{\Pi}^a$ and $\boldsymbol{P}^a$ with sample size n. For any arbitrary small $\epsilon > 0$, when $n \to \infty$, I have

(1) $\mathbb{P}(||\hat{\mathbf{\Pi}}^a(n) - \mathbf{\Pi}^a|| > \epsilon) \to 0$

(2) $\mathbb{P}(||\hat{\boldsymbol{P}}^a(n) - \boldsymbol{P}^a|| > \epsilon) \to 0$

(3) Assume the Jacobian matrix $J_{\boldsymbol{G}_i}$ has the property that $\det(J_{\boldsymbol{G}_i}) \neq 0$. Then I have $\sqrt{n}[\hat{\boldsymbol{P}}_i^a - \boldsymbol{P}_i^a] \sim \mathcal{N}(0, \boldsymbol{\Delta}_i \boldsymbol{V}^{-1} \boldsymbol{\Delta}_i')$ asymptotically, where $\boldsymbol{P}_i = (\boldsymbol{P}_i^{a=1}, \boldsymbol{P}_i^{a=0})$ and $\hat{\boldsymbol{P}}_i = (\hat{\boldsymbol{P}}_i^{a=1}, \hat{\boldsymbol{P}}_i^{a=0})$, $\boldsymbol{\Delta}_i = \nabla_{\mathbf{\Pi}_i^a}[\mathbf{G}_i^{-1}]$ and $\boldsymbol{V}$ is

$$\boldsymbol{V} = \begin{pmatrix} \boldsymbol{V}^{a=1} & \mathbf{0} \\ \mathbf{0} & \boldsymbol{V}^{a=0} \end{pmatrix}$$

and

$$\boldsymbol{V}^{a=1} = \left\{ - E \left[\frac{\partial^2 Log\left(f_i^{a=1}(\boldsymbol{Y}_i; \boldsymbol{\Pi}_i^{a=1})\right)}{\partial \Pi_{ik}^{a=1} \partial \Pi_{ij}^{a=1}} \right] \right\}$$

$$\boldsymbol{V}^{a=0} = \left\{ - E \left[\frac{\partial^2 Log\left(f_i^{a=0}(\boldsymbol{X}_i; \boldsymbol{\Pi}_i^{a=0})\right)}{\partial \Pi_{ik}^{a=0} \partial \Pi_{ij}^{a=0}} \right] \right\}$$

The proof of Theorem 1.2 is relegated to Appendix A.1. For a brief overview, Theorem 1.2(2) is proved by using the uniqueness property presented in Theorem 1.1 and the continuous mapping theorem. Theorem 1.2(3) is derived following Lemma 3.9 from Wooldridge (2010).

Theorem 1.2 shows that $\hat{\mathbf{\Pi}}^a$ and $\hat{\mathbf{P}}^a$ are asymptotically consistent. The estimators are normally distributed asymptotically given that the Jacobian matrix of the mapping $\boldsymbol{G}_i$ is non-singular. This allows us to derive the confidence intervals for the estimators. Besides, I want to claim that, in general, it is very difficult to show $\det(J_{\boldsymbol{G}_i}) \neq 0$ analytically for a very complicate mapping $\boldsymbol{G}_i$. To support the assumption that $\det(J_{\boldsymbol{G}_i}) \neq 0$, I perform thousands of numerical experiments, and the results show that $J_{\boldsymbol{G}_i}$ is non-singular in general.

As the observed transitions are assumed to be multinomially distributed, and I build the relationship between $\boldsymbol{P}^a$ and $\hat{\mathbf{\Pi}}^a$ in the structural model, then the ground truth TPMs can also be estimated by MLE. Specifically, for $i \in \mathcal{S}$, I derive the log-likelihood functions as

$$\log(L(\boldsymbol{P}_i^{a=0}, \boldsymbol{P}_i^{a=1})) = \log(L_1(\boldsymbol{P}_i^{a=0}, \boldsymbol{P}_i^{a=1})) + \log(L_2(\boldsymbol{P}_i^{a=0}, \boldsymbol{P}_i^{a=1}))$$

where

$$\log(L_1(\boldsymbol{P}_i^{a=0}, \boldsymbol{P}_i^{a=1})) = \log(\frac{K_i^{a=1}!}{Y_{i1}!...Y_{iN}!}) + \sum_{j=1}^{N} \left(Y_{ij} \log(g_{ij}^{a=1}(\boldsymbol{P}_i^{a=0}, \boldsymbol{P}_i^{a=1})) \right)$$

and

$$\log(L_2(\boldsymbol{P}_i^{a=0}, \boldsymbol{P}_i^{a=1})) = \log(\frac{K_i^{a=0}!}{X_{i1}!...X_{iN}!}) + \sum_{j=1}^{N} \left(X_{ij} \log(g_{ij}^{a=0}(\boldsymbol{P}_i^{a=0}, \boldsymbol{P}_i^{a=1})) \right)$$

I characterize the relationship between the estimator $\hat{\mathbf{P}}^a$ derived by solving structural model (1.1) and the maximum likelihood estimator in the following theorem.

Theorem 1.3. Given $(\hat{\mathbf{P}}_i^{a=1}, \hat{\boldsymbol{P}}_i^{a=0})$ is the solution to the system of equations. $(\hat{\mathbf{P}}_i^{a=1}, \hat{\mathbf{P}}_i^{a=0})$ maximizes the log-likelihood function $\log(L(\boldsymbol{P}_i^{a=0}, \boldsymbol{P}_i^{a=1}))$.

Theorem 1.3 implies that the estimators from the proposed structural model are maximum likelihood estimators. This property is important in the sense that it bridges the gap between my novel structural model and the traditional ML estimation method. The proof of Theorem 1.3 is presented in Appendix A.1.

As I mentioned, the proposed model builds the relationship between $\hat{\mathbf{\Pi}}^a$ and $\boldsymbol{P}^a$, which provides a structural framework to investigate the deviation between $\hat{\mathbf{\Pi}}^a$ and $\boldsymbol{P}^a$. Specifically, I define $\bar{\mathbf{\Delta}}^a = \hat{\mathbf{\Pi}}^a - \boldsymbol{P}^a$ with

$$\begin{aligned}\bar{\Delta}_{ij}^{a=1} &= \hat{\Pi}_{ij}^{a=1} - P_{ij}^{a=1} \\ &= \frac{P_{ij}^{a=1}\left(p_i^{te}\sum\limits_{k=j-\bar{\delta}(i)}^{N} P_{ik}^{a=0} + p_i^{se}\sum\limits_{k=1}^{N} q_k^{se}\mathbb{I}_{i\geq k}\right)}{\sum\limits_{z=1}^{N} P_{iz}^{a=1}\left(p_i^{te}\sum\limits_{k=z-\bar{\delta}(i)}^{N} P_{ik}^{a=0} + p_i^{se}\sum\limits_{k=1}^{N} q_k^{se}\mathbb{I}_{i\geq k}\right)} - P_{ij}^{a=1}\end{aligned}$$

and

$$\begin{aligned}\bar{\Delta}_{ij}^{a=0} &= \hat{\Pi}_{ij}^{a=0} - P_{ij}^{a=0} \\ &= \frac{P_{ij}^{a=0}\left(p_i^{se}\sum\limits_{k=1}^{N} q_k^{se}(1-\mathbb{I}_{i\geq k}) + p_i^{te}\sum\limits_{k=\max(j+\bar{\delta}(i)+1,1)}^{N} P_{ik}^{a=1}\right)}{\sum\limits_{z=1}^{N} P_{iz}^{a=0}\left(p_i^{se}\sum\limits_{k=1}^{N} q_k^{se}(1-\mathbb{I}_{i\geq k}) + p_i^{te}\sum\limits_{k=\max(z+\bar{\delta}(i)+1,1)}^{N} P_{ik}^{a=1}\right)} - P_{ij}^{a=0}\end{aligned}$$

The proposition below shows the properties of the deviation between $\hat{\mathbf{\Pi}}^a$ and $\boldsymbol{P}^a$.

Proposition 1.1. For any $i \in \mathcal{S}$ and $a \in \{0, 1\}$,

(1) There exists a threshold $\bar{s}_i^a$ such that $\bar{\Delta}_{ij}^a \geq 0$ if $j \leq \bar{o}_i^a$, and $\bar{\Delta}_{ij}^a < 0$ otherwise;

(2) $\frac{\bar{\Delta}_{ij}^a}{P_{ij}^a}$ is decreasing in j if $j \leq \bar{o}_i^a$ and increasing in j otherwise.

Proposition 1.1 shows that $\hat{\mathbf{\Pi}}^a$ tends to overestimate the effect of action a as $\bar{\Delta}_{ij}^a \geq 0$ if $j \leq \bar{o}_i^a$. This is because physicians keep selecting actions with better future outcomes under the treatment-effect-based policy, then from censored data we

observe that patients tend to transit to better states. As the transitions with better outcomes are less likely to be censored, the relative deviation, $\bar{\Delta}^a_{ij}/P^a_{ij}$, is decreasing in j when $\bar{\Delta}^a_{ij} \geq 0$ and increasing in j when $\bar{\Delta}^a_{ij} < 0$.

1.3.3 Structural Model with Prognostic Errors

In this section, I construct the structural model with physicians' prognostic errors incorporated. Let $\kappa^a_{sj} = Pr(\hat{s}^a_{t+1} = s | s^a_{t+1} = j)$ denote the probability that the prognosticated state in next period is s condition on the true state in next period is j under action a. Then, following the same process presented in Section 1.3.1, I have

$$\hat{\Pi}^{a=1}_{ij} = \frac{P^{a=1}_{ij}\left(p^{te}_i \sum_{s=1}^{N} \kappa^{a=1}_{sj} \sum_{\tau=1}^{N} P^{a=0}_{i\tau} \sum_{k=s-\bar{\delta}(i)}^{N} \kappa^{a=0}_{k\tau} + p^{se}_i \sum_{k=1}^{N} q^{se}_k \mathbb{I}_{i\geq k}\right)}{\sum_{z=1}^{N} P^{a=1}_{iz}\left(p^{te}_i \sum_{s=1}^{N} \kappa^{a=1}_{sz} \sum_{\tau=1}^{N} P^{a=0}_{i\tau} \sum_{k=s-\bar{\delta}(i)}^{N} \kappa^{a=0}_{k\tau} + p^{se}_i \sum_{k=1}^{N} q^{se}_k \mathbb{I}_{i\geq k}\right)}$$

and

$$\hat{\Pi}^{a=0}_{ij} = \frac{P^{a=0}_{ij}\left(p^{se}_i \sum_{k=1}^{N} q^{se}_k (1-\mathbb{I}_{i\geq k}) + p^{te}_i \sum_{s=1}^{N} \kappa^{a=0}_{sj} \sum_{\tau=1}^{N} P^{a=1}_{i\tau} \sum_{k=\max(s+\bar{\delta}(i)+1,1)}^{N} \kappa^{a=1}_{k\tau}\right)}{\sum_{z=1}^{N} P^{a=0}_{iz}\left(p^{se}_i \sum_{k=1}^{N} q^{se}_k (1-\mathbb{I}_{i\geq k}) + p^{te}_i \sum_{s=1}^{N} \kappa^{a=0}_{sz} \sum_{\tau=1}^{N} P^{a=1}_{i\tau} \sum_{k=\max(s+\bar{\delta}(i)+1,1)}^{N} \kappa^{a=1}_{k\tau}\right)}$$

I can show that the solution uniqueness, asymptotic properties, and the log-likelihood maximization also hold under this case. The major concern on this case is physicians' prognostic information (i.e., $\kappa^a_{sj} = Pr(\hat{s}^a_{t+1} = s | s^a_{t+1} = j)$) is usually unavailable and barely possible to be recovered from observations. Therefore, I focus on the error-free model in this chapter.

In the following section, I further compare the performance of the error-free model with the performances of other estimation methods/models by using simulation experiments.

1.4 Simulation Experiments

Instead of only using real data to estimate TPMs with the structural model, I first conduct a set of simulation experiments and investigate the performance of the error-free structural model on simulated data with prognostic errors in the context of ICU extubation. The simulation experiments are necessary and important as they provide convincing frameworks to compare the structural model with other estimation methods by using the ground truth TPMs as benchmark. I first introduce the background and medical practice of the extubation problem in Section 1.4.1. I then describe simulation settings in Section 1.4.2. In Section 1.4.3, I illustrate the performance of the error-free structural model with comprehensive simulation results.

1.4.1 Extubation Problem: Background

Acute respiratory failure is associated with very high mortality rate of more than 40% in critically ill patients (Vincent et al. 2002). In ICUs, invasive mechanical ventilation (MV) is one of the most common interventions to provide support for respiratory failure patients to breathe. For intubated patients (i.e., receiving invasive MV), physicians regularly check and evaluate their respiratory conditions. For each evaluation, a critical decision faced by physicians is when to extubate (i.e., stop invasive MV). On the one hand, long time ventilation is associated with high prevalence rates of complications, e.g., volutrauma and lung and airway injuries (Miller and Carlo 2008); on the other hand, premature extubation may result in a high extubation failure rate and, as a result, a higher mortality rate (Thille et al. 2013). In ICUs practice, traditionally, a severity-based policy is used to make extubation decisions. For this decision-making process, it is also straightforward to use the optimal stopping MDP framework to optimize the extubation decisions, which implies that understanding health transitions is critical. Nowadays, physicians in ICUs may prognosticate pa-

tients' future outcomes under ventilation and extubation and then extubate patients according to the prognosticated treatment effect of the actions. Moreover, according to the discussion with the physicians, they tend to make extubation decisions base on the treatment effect when they are very confident in their prognosis. As treatment-effect-based policy structurally censors health transitions data, the ICU extubation context is perfect for applying the proposed model to estimate ground truth TPMs.

In the partner ICU, respiratory rate is used as a major reference clinical variable when making extubation/intubation decisions. Moreover, the respiratory rate serves as an effective and natural risk predictor for respiratory failure in the literature (Rivera and Weissman 1997, Meade et al. 2001). Hence, I classify patients into four states base on their respiratory rate values. Specifically, patients with Respiratory Rate values in $(0, 22]$, $(22, 30]$, $(30, 38]$, and $(38, +\infty)$ are classified into state 1, 2, 3, and 4 according to Rivera and Weissman (1997) and Meade et al. (2001), as well as the suggestions from physicians in the partner ICU. In a relative sense, state 1 patients have the best health condition and state 4 patients have the worst health condition.

1.4.2 Simulation: Settings

In this section, I simulate patients' health transitions through the evolution of respiratory rate (RR). Based on the simulated ground truth transitions, I derive the ground truth TPM $\boldsymbol{P}^a$. I implement both severity-based and treatment-effect-based policies on the simulated data to decide actions of ventilation or extubation and observe patients' health conditions. Moreover, physicians' prognosis on future respiratory conditions is simulated with error so that I can investigate the performance of the error-free model on datasets with prognostic errors. I apply the method proposed in Section 1.3.1 to derive the observed TPM $\hat{\mathbf{\Pi}}^a$ and the estimated ground truth TPM $\hat{\mathbf{P}}^a$. As a benchmark, another way to address the censoring problem is to recover the censored results by predictions: I simulate predictive clinical variables of RR and

construct predictive models to predict the censored RR values, and I then derive the estimated TPM ($\tilde{\mathbf{P}}^a$) using the predictions. In the simulation, I also apply the quadratic programming method discussed in Theil and Rey (1966) and Schneider and Zenios (1990) to estimate the ground truth TPM (denoted by $\breve{\boldsymbol{P}}^a$, and the details of quadratic method are presented in Appendix A.6).

RR of patients under ventilation is simulated across a time horizon with $T = 28$ by using the Gaussian process, which is widely used to fit time series clinical data in medical research (Clifton et al. 2012, Colopy et al. 2017, Cheng et al. 2019). Specifically, I let RR_t^1 and RR_t^0 denote the RR values in period $t+1$ under ventilation and extubation, respectively. I simulate $RR_{t+1}^1 = RR_t^1 + \xi_t$ and $RR_{t+1}^0 = RR_t^1 + \epsilon_t$, where $\xi_t \sim \mathcal{N}(0, v_1)$ and $\epsilon_t \sim \mathcal{N}(0, v_0)$ are normal random variables. For any patient under ventilation, the initial RR value is randomly generated from $[22, 43]$ in period 1. This is because RR values no less than 22 are classified into the abnormal status, and the RR values of 99% patients in the first period of their ventilation are less than 43 in the dataset. In each period, the treatment-effect-based policy is adopted to make decisions with probability $p_j^{te} = p$. I assume $\bar{\delta}(i) = -1$ for all i, since physicians in the partner ICU tend to keep the patients under ventilation as long as the patients can benefit more from intubation when using the treatment-effect-based policy. Patients' next period states under $a = 0$ (extubation) and $a = 1$ (continue the ventilation) are prognosticated by physicians with an accuracy level $\alpha^a = Pr(\hat{s}_{t+1}^a = j | s_{t+1}^a = j)$ ($\hat{s}_{t+1}^a$ denotes, under action a, the state in period $t+1$ is prognosticated to be $\hat{s}_{t+1}^a$). For simplicity and without loss of generality, I let $\alpha^{a=1} = \alpha^{a=0} = \alpha$ in the simulation. Given the current state is i and the next state under action a is j, if the prognosis is inaccurate, then the probability that the prognosticated state in next period is s is assumed to be $\frac{1-\alpha}{N-1}$ with $s \neq j$.

For each patient, following the medical practice in ICU, I assume that s/he will not be extubated in period 1. I use t_0 to denote the first period that the action is

$a = 0$ (i.e., extubation), then I select all simulated data from period 1 to period t_0 and use $\mathcal{D}$ to denote the selected dataset. I simulate the predictive variables pv^0 and pv^1 on dataset $\mathcal{D}$. Specifically, I set $pv_t^0 = \mu_0 RR_{t+1}^0 + \mu_1 + \varepsilon_0$ and $pv_t^1 = \gamma_0 RR_{t+1}^1 + \gamma_1 + \varepsilon_1$, where $\varepsilon_0 \sim \mathcal{N}(0, \sigma_0)$ and $\varepsilon_1 \sim \mathcal{N}(0, \sigma_1)$ are normal random variables. I train a linear model to predict the censored RR values under action a, of which the model accuracy is β^a (details are presented in Appendix A.3). The predicted RR values are classified into different states, and then, I know the predicted censored transitions. Using the proportions of transitions on data with both observed and predicted censored transitions in the simulation, I then derive $\tilde{\mathbf{P}}^a$.

Note that, in the simulation, I need to set the ground truth values of p and $\boldsymbol{q}^{se}$ to simulate the decision-making process. Hence, I know values of p and $\boldsymbol{q}^{se}$, which allow us to solve the proposed structural model and then compare it with other estimation methods. However, in practice, p and $\boldsymbol{q}^{se}$ are unknown, and how to estimate p and $\boldsymbol{q}^{se}$ is challenging in the sense that it is usually unable to disentangle the severity-based decisions from treatment-effect-based decisions in data. In this chapter, I propose a two-stage estimation method. In the first stage, I build an ensembled tree model considering the severity and treatment effect information to predict the decisions and then select the $\hat{p}$ and $\hat{\mathbf{q}}^{se}$ that maximize the log-likelihood of observing the decisions as the estimators of p and $\boldsymbol{q}^{se}$ (details are shown in Appendix A.3)[2]. In the second stage, I use $\hat{p}$, $\hat{\mathbf{q}}^{se}$ and $\boldsymbol{\Pi}^a$ to solve the structural model and derive the estimated TPM ($\hat{\mathbf{P}}_E^a$: termed as *two-stage estimator*).

The treatment effect values used in the ensembled model are derived based on the predictions of censored observations. Hence, $\hat{\mathbf{P}}_E^a$ is affected by the prediction accuracy β^a (affected by σ). For comparison, I also use the ground truth values of p and $\boldsymbol{q}^{se}$ to solve the structural model to estimate TPM under action a, which is denoted by $\hat{\mathbf{P}}^a$ for $a = 0, 1$ (termed as *one-stage estimator*).

[2]It should be noted that, for the first stage estimation, I are unable to show the identifiability analytically.

In the simulation, I set $p = 0.45$ and $\boldsymbol{q}^{se} = [0.2, 0.55, 0.2, 0.05]$, which are close to the estimated values from the real data. v_0 and v_1 are randomly selected from $[3, 10]$ with 100 pairs. For each pair of v_0 and v_1, I simulate $30,000$ patients and consider α from 0.6 to 1.0 with a step 0.02. Without lose of generality, I further let $\sigma_0 = \sigma_1 = \sigma$, $\mu_0 = \gamma_0 = 2$ and $\mu_1 = \gamma_1 = 1$, where σ takes value from 0 to 10 with a step size 1. To account for the potential randomness, for each σ, I repeat the simulation of the predictive variables 30 times. Then I generate β^0 and β^1, the estimators and the performances of each estimation method.

1.4.3 Simulation: Results Analysis

In the simulation, I actually know physicians' ground truth prognostic accuracy. The structural model considering prognostic errors (see Section 1.3.3) can also be used to estimate the TPMs under the two-stage estimation framework. I find that the error-free model generally outperforms the prognostic-error embedded model unless the actual prognostic accuracy is low (e.g., $\alpha < 0.65$, more results are relegated in Appendix A.4.4). As I mentioned, physicians tend to make treatment-effect-based decisions when they are very confident in their prognosis. Moreover, the physicians' prognostic information is usually unavailable in practice. Hence, in the analysis onwards, I focus on the comparisons between the error-free model and other estimation methods.

To show the performance, I define $Dist\_Struct = ||\boldsymbol{P}^a - \hat{\mathbf{P}}^a||_{norm}$, $Dist\_Struct\_E = ||\boldsymbol{P}^a - \hat{\mathbf{P}}^a_E||_{norm}$, $Dist\_Pred = ||\boldsymbol{P}^a - \tilde{\mathbf{P}}^a||_{norm}$, $Dist\_Obs = ||\boldsymbol{P}^a - \hat{\mathbf{\Pi}}^a||_{norm}$ and $Dist\_Quad = ||\boldsymbol{P}^a - \breve{\mathbf{P}}^a||_{norm}$ as the distances between the estimators and ground truth TPMs, respectively. The smaller the distance is, the better the performance is. I employ max-norm, 2-norm, and Frobenius-Norm as the matrix distance metrics and use max-norm as a representation to illustrate the results (more results are relegated to Appendix A.4.1). I summarize the key new notations in Table 1.2 for more

convenient reference.

$\hat{\mathbf{P}}^a_E$: two-stage estimator
$\tilde{\mathbf{P}}^a$: estimated TPM (prediction incorporated)
$\breve{\mathbf{P}}^a$: estimated TPM (quadratic programming)
Dist_Obs: $\|\boldsymbol{P}^a - \hat{\mathbf{\Pi}}^a\|_{norm}$
Dist_Struct: $\|\boldsymbol{P}^a - \hat{\mathbf{P}}^a\|_{norm}$
Dist_Struct_E: $\|\boldsymbol{P}^a - \hat{\mathbf{P}}^a_E\|_{norm}$
Dist_Pred: $\|\boldsymbol{P}^a - \tilde{\mathbf{P}}^a\|_{norm}$
Dist_Quad: $\|\boldsymbol{P}^a - \breve{\mathbf{P}}^a\|_{norm}$
α: simulated prognostic accuracy
β^a: accuracy of the predictive model
σ: the standard deviation for generating predictive variables (a lager σ implies smaller β^a)

Table 1.2: Additional Notation In Simulation Experiments

In Figure 1.4, I show the results of *Dist_Pred*, *Dist_Struct*, *Dist_Struct_E*, *Dist_Obs* and *Dist_Quad* under different values of α and σ.

Comparisons Among $\hat{\mathbf{P}}^a$, $\hat{\mathbf{\Pi}}^a$ and $\hat{\mathbf{P}}^a_E$

Observation 1.1. (1) The performance of the estimated TPM using the error-free structural model, i.e., $\hat{\mathbf{P}}^a$, and the observed TPM, i.e., $\hat{\mathbf{\Pi}}^a$, are increasing and decreasing in α, respectively; (2) The two-stage estimator, i.e., $\hat{\mathbf{P}}^a_E$, outperforms $\hat{\mathbf{P}}^a$ if α is relatively small and outperformed by $\hat{\mathbf{P}}^a$ otherwise; (3) The observed TPM is outperformed by the two-stage estimator when α is relatively large.

For Observation 1.1(1), since the structural model I used is assumed to be error-free, the performance of $\hat{\mathbf{P}}^a$ is negatively affected by physicians' prognostic error (I term this effect as NE_{err}). Obviously, NE_{err} is decreasing in α as a larger α results in less prognostic error. Therefore, $\hat{\mathbf{P}}^a$ is closer (i.e., *Dist_Struct* is smaller) to $\boldsymbol{P}^a$ as α increases. The performance of the observed TPM $\hat{\mathbf{\Pi}}^a$ is negatively affected by ignoring treatment-effect-based censoring (I term this effect as NE_{te}). If α is small enough such that transitions are (nearly) uniformly randomly censored under

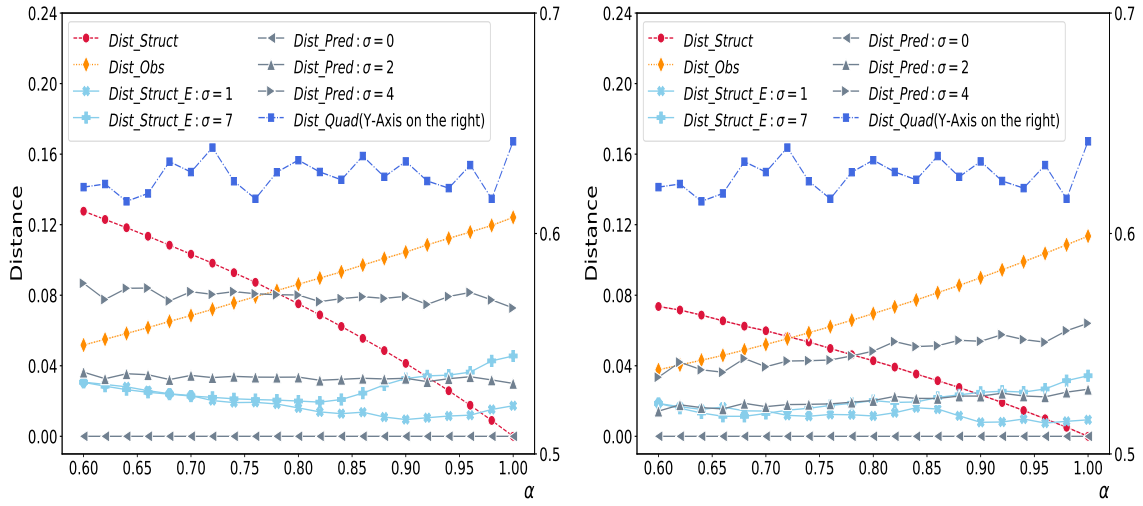

(a) Action $a = 0$ (b) Action $a = 1$

Figure 1.4: Performances Comparison under Max Norm
$\sigma = 0$: $\beta^0 = \beta^1 = 1$; $\sigma = 1$: $\beta^0 \in (0.951, 0.957)$, $\beta^1 \in (0.960, 0.966)$; $\sigma = 2$: $\beta^0 \in (0.925, 0.930)$, $\beta^1 \in (0.915, 0.920)$; $\sigma = 4$: $\beta^0 \in (0.850, 0.855)$, $\beta^1 \in (0.830, 0.840)$; $\sigma = 7$: $\beta^0 \in (0.726, 0.733)$, $\beta^1 \in (0.680, 0.687)$.

treatment-effect-based policy, then, *Dist_Obs* tends to be 0. If physicians' prognosis become more accurate (i.e., α is larger), NE_{te} becomes larger; hence, I observe that *Dist_Obs* is increasing (i.e., the performance is decreasing) in α for $a = \{0, 1\}$. I also find that there exists a threshold α^a (e.g., $\alpha^0 = 0.78$) such that *Dist_Obs* is smaller than *Dist_Struct* if $\alpha < \alpha^a$ and *Dist_Obs* is larger than *Dist_Struct* otherwise. These observations suggest that it is better to use $\hat{\mathbf{\Pi}}^a$ to represent $\boldsymbol{P}^a$ if physicians' prognosis is not very accurate; otherwise, it is better to use $\hat{\mathbf{P}}^a$ as a proxy of $\boldsymbol{P}^a$.

Given α, I can also find that the performance of $\hat{\mathbf{P}}^{a=1}$ is better than that of $\hat{\mathbf{P}}^{a=0}$ (i.e., *Dist_Struct* is smaller under $a = 1$). I know that, under treatment-effect-based policy, $a = 1$ is selected if $\delta \leq -1$, while $a = 0$ is selected if $\delta \geq 0$. Conditioning on the treatment-effect-based policy is used and the transition is from state i to state j under action $a = 1$ ($a = 0$), then the probability that this transition will be observed in the data is $\sum_{k=j+1}^{N} P_{ik}^{a=0}$ under $a = 1$ ($\sum_{k=\max(1,j)}^{N} P_{ik}^{a=1}$ under $a = 0$) if physicians' prognosis is error-free; however, physicians' prognosis is imperfect, which

implies that the actual probability of observing the corresponding transition will be different. Hence, the prognostic errors affect the performance of the error-free model through terms $\sum_{k=j+1}^{N} P_{ik}^{a=0}$ and $\sum_{k=\max(1,j)}^{N} P_{ik}^{a=1}$. Comparing with the summation: $\sum_{k=j+1}^{N} P_{ik}^{a=0}$, there are more elements in the summation: $\sum_{k=\max(1,j)}^{N} P_{ik}^{a=1}$, then more prognostic errors involved (i.e., NE_{err} is larger) in $\sum_{k=\max(1,j)}^{N} P_{ik}^{a=1}$, which may result in worse performance for $\hat{\mathbf{P}}^{a=0}$. I further test this by assuming $a = 1$ is selected if $\delta \leq 0$ and $a = 0$ is selected otherwise, and the results show that $\hat{\mathbf{P}}^{a=0}$ tends to have better performance.

Interestingly, from Observation 1.1(2), I find that $\hat{\mathbf{P}}^{a}$ (i.e., one-stage estimator) is outperformed by $\hat{\mathbf{P}}_{E}^{a}$ (i.e., two-stage estimator) under most situations even when σ is large (e.g., *Dist_Struct_E* with $\sigma = 7$ is smaller than *Dist_Struct* when α is not very large, e.g., $\alpha \leq 0.9$). For the two-stage estimation, I find that the estimated $\hat{p}$ tends to be smaller than the ground truth p, which implies that, compared with the one-stage estimator (the ground truth p is used), the two-stage estimator will receive less negative impacts from prognosticated errors (i.e., reduced NE_{err}, which benefits the two-stage estimator) but more negative effects from ignoring the treatment-effect-based censoring (i.e., increased NE_{te}, which deteriorates the two-stage estimator). As I described above, when α becomes larger, NE_{err} and NE_{te} become smaller and larger, respectively

Bearing these results in mind, I discuss the relationship between the performances of $\hat{\mathbf{P}}^{a}$ and $\hat{\mathbf{P}}_{E}^{a}$. When α is very large, e.g., α approaches 1, there is (nearly) no prognostic error such that, comparing with the one-stage estimator, the performance loss due to increased NE_{te} dominates the performance gain from reduced NE_{err} for the two-stage estimation; hence, *Dist_Struct_E* is greater than *Dist_Struct* (i.e., $\hat{\mathbf{P}}_{E}^{a}$ is outperformed by $\hat{\mathbf{P}}^{a}$). As α decreases, then NE_{err} increases and NE_{te} decreases, and the performance gain from reduced NE_{err} tends to dominate the performance loss due to increased NE_{te}. Therefore, as observed in the figure, *Dist_Struct_E* tends

to be smaller than *Dist_Struct* when α is relatively small. Similar arguments on the interplay between NE_{te} and NE_{err} can be applied to explain the relationship between *Dist_Struct_E* and *Dist_Obs*, which is presented by Observation 1.1(3).

The discussions above show that *Dist_Struct_E* depends on the marginal effects of physicians' prognostic errors and treatment-effect-based censoring. I find that *Dist_Struct_E* tends to present a first decreasing and then increasing trend as α increases, which suggests that, when α starts to increase from α_0 (recall that under α_0 the treatment-effect-based censoring is (nearly) random), the marginal effect of ignoring the treatment-effect-based censoring is dominated by the marginal effect of reducing prediction error. As α further increases and passes a certain tipping point, the positive marginal benefit from the increase of α becomes small. It then is dominated by the marginal loss of ignoring treatment-effect-based censoring. I validate these insights by choosing the probability of using a treatment-effect-based policy from the interval $(0, p)$ and then do the estimation (details are shown in Appendix A.4.1).

Comparisons Among $\tilde{\mathbf{P}}^a$, $\hat{\mathbf{P}}^a$ and $\hat{\mathbf{P}}^a_E$

Observation 1.2. (1) The performance of estimated TPMs based on predictions,i.e., $\tilde{\mathbf{P}}^a$, decreases as the prediction accuracy decreases (i.e., σ increases); (2) $\tilde{\mathbf{P}}^a$ is outperformed by $\hat{\mathbf{P}}^a$ even when the predictive accurate rate β^a is greater than the prognostic accuracy α; (3) The performance of the two-stage estimator $\hat{\mathbf{P}}^a_E$ under $\sigma = \ddot{\sigma}_1$ is better than that of $\tilde{\mathbf{P}}^a$ under $\sigma = \ddot{\sigma}_1$ even when $\ddot{\sigma}_1$ is much larger than $\ddot{\sigma}_2$.

Observation 1.2(1) is intuitive. Moreover, the fluctuation of lines which represent *Dist_Pred* is because β^a is not necessarily equal for any given σ under different values of α. As for Observation 1.2(2), I have, for example, when $\beta^0 \in (0.850, 0.855)$, *Dist_Struct* is less than *Dist_Pred* under action $a = 0$ as long as $\alpha > 0.75$. These insights also hold for other cases with different values of σ and the case that $a = 1$.

For *Dist_Pred* under action a, it is affected by β^a in the sense that a larger β^a implies a smaller *Dist_Pred*. However, there are several driven forces behind the performance of the error-free structural model. As I discussed before, *Dist_Struct* is explicitly affected by α. Given the value of α and $\beta^a = \alpha$, intuitively, *Dist_Struct* is not necessarily smaller than *Dist_Pred*. However, the decisions made under the wrong prognosis may be the same as the decisions made without prognostic errors. From this perspective, the structural model can hedge the risk from inaccurate prognosis and then improve the overall decision making accurate rate, which is referred to as the effective decision accurate rate and illustrated in Figure 1.5 under different α. The red line denotes the overall effective decision accurate rate, and the blue line denotes the effective decision accurate rate under the treatment-effect-based policy. In line with the intuitions, the presented effective decision accurate rates are much higher than α. I know that there is no prognosis involved under severity-based policy, then the severity-based policy can also hedge prognostic errors. Combining the risk hedging effects from both severity-based policy and the effective decision accurate rate, I can observe that *Dist_Struct* is smaller than *Dist_Pred* even when α is less than β^a.

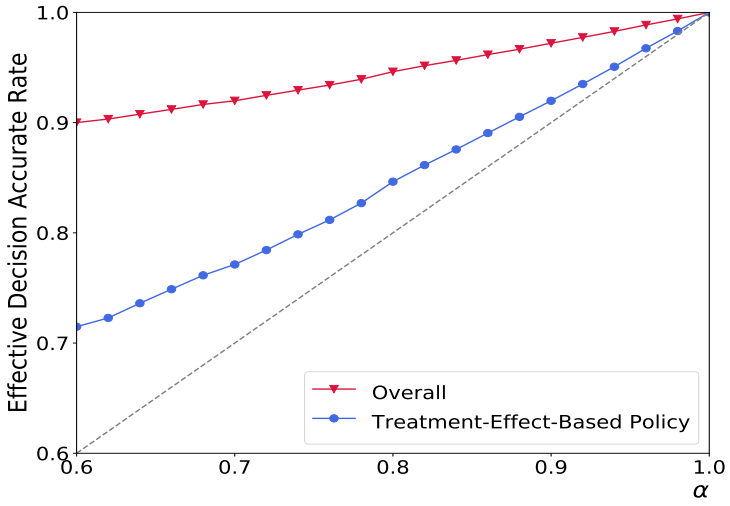

Figure 1.5: Effective Decision Accurate Rate

Following the analysis above, it is not surprising that *Dist_Struct_E* dominates *Dist_Pred* even when the σ for *Dist_Struct_E* is much larger than the σ for *Dist_Pred*, e.g., *Dist_Struct_E* with $\sigma = 7$ is not greater than *Dist_Pred* with $\sigma = 2$ under most values of α. Moreover, I also find that treatment-effect-based censoring has significantly negative impact on β^a in the sense that high ρ_0 and ρ_1 values result in very low prediction accuracy, e.g., when $\rho_0 = \rho_1 = 0.82$, β^a is smaller than 0.55 under $a = 0$ and $a = 1$ (more details are presented in Appendix A.4.2). These findings suggest that using a predictive model to recover the censored RR values may end up with very low accuracy and, as a result, a very low performance of $\tilde{\mathbf{P}}^a$. However, the performances of two-stage estimators are not very sensitive to the changes of σ.

For the performance of the quadratic programming method, I can see that *Dist_Quad* exceeds 0.6 under all cases, which suggests that $\breve{\mathbf{P}}^a$ deviate from $\boldsymbol{P}^a$ significantly and it is not a good estimator of the underlying TPM. From all these comparisons, I can find that the error-free structural model outperforms other estimation methods when physicians' prognostic accuracy is reasonably high, and more specifically, the two-stage error-free estimators, in general, dominate other estimators.

To further demonstrate the good performance of the proposed structural model, in Appendix A.4.3, I derive the deviation matrices for the aforementioned estimators. I show that, in the average sense, $\hat{\mathbf{P}}_E^a$ is much closer to $\boldsymbol{P}^a$ when compared with other estimators and $\hat{\mathbf{\Pi}}^a$ tends to overestimate the effects of action a as the treatment-effect-based policy keeps censoring transitions with worse future outcomes. In the Appendix, I also investigate the percentage of entries in $\hat{\mathbf{P}}_E^a$ that are closer to the ground truth values when compared with $\tilde{\mathbf{P}}^a$ and $\hat{\mathbf{\Pi}}^a$. The results also suggest that the structural model outperforms the other two methods in the sense that most entries in $\hat{\mathbf{P}}_E^a$ are closer to the corresponding entries in $\boldsymbol{P}^a$.

MDP Performance

To illustrate the impacts of different estimators on the performance of MDP policy, in the simulation, I formulate the extubation problem as an optimal stopping problem under an MDP framework. I consider a finite horizon problem with 28 periods. To mimic the medical practice, I further consider an initial period of $t = 1$, in which patients under intubation will not be extubated. For the subsequent periods, the physicians need to decide to continue the ventilation ($a = 1$) or to extubate the patients ($a = 0$). Let $c(s, a)$ denote the immediate state-dependent cost under action a and state s. $c(1, 0)$, $c(2, 0)$, $c(3, 0)$ and $c(4, 0)$ are randomly sampled from sets $[10, 15]$, $[18, 25]$, $[38, 45]$, and $[67, 75]$, respectively, and $c(s, 1) = 8$.

I let $V^{Struct\_E}(s)$, $V^{pred}(s)$ and $V^{obs}(s)$ denote the costs of patients whose initial state is s by using the optimal policies obtained with $\hat{\mathbf{P}}_E^{a=1}$ (under $\sigma = 7$ for the illustration), $\tilde{\mathbf{P}}^{a=1}$ and $\hat{\mathbf{\Pi}}^{a=1}$, respectively. I further let $V(s)$ denote the optimal cost (i.e., derived under the ground truth TPMs) associated with patients whose initial state is s. I repeat the sampling of $c(s \in \mathcal{S}, 0)$ 500 times, for each time, I solve the MDP model, and then I present the average results of $(V^{Struct\_E}(s) - V(s))/V(s)$, $(V^{Pred}(s) - V(s))/V(s)$ and $(V^{Obs}(s) - V(s))/V(s)$ when $s = 3, 4$ (the performance gaps of $s = 1$ and $s = 2$ are very small) in Figure 1.6.

I find that $\hat{\mathbf{P}}_E^{a=1}$ dominates $\hat{\mathbf{\Pi}}^{a=1}$ in the sense that $(V^{Struct\_E}(s) - V(s))/V(s)$ is very small and always smaller than $(V^{Obs}(s) - V(s))/V(s)$ even when α is small and σ is large. From this figure, in most cases, $(V^{Obs}(s) - V(s))/V(s)$ are greater than 1% and even reach up to 4%, which are much worse than that from $\hat{\mathbf{P}}_E^{a=1}$. In terms of the comparison between $\hat{\mathbf{P}}_E^{a=1}$ and $\tilde{\mathbf{P}}^{a=1}$, given $\sigma = 7$, I can see that $(V^{Struct\_E}(s) - V(s))/V(s)$ (i.e., nearly 0) is much smaller than $(V^{Pred}(s) - V(s))/V(s)$ (i.e., larger than 2% and reach up to 3%). I also find that the performance of $\hat{\mathbf{P}}_E^{a=1}$ with $\sigma = 7$ is better than that of $\tilde{\mathbf{P}}^{a=1}$ under $\sigma = 3$. I want to emphasize that these results are only used as supplement shreds of evidence to further illustrate the

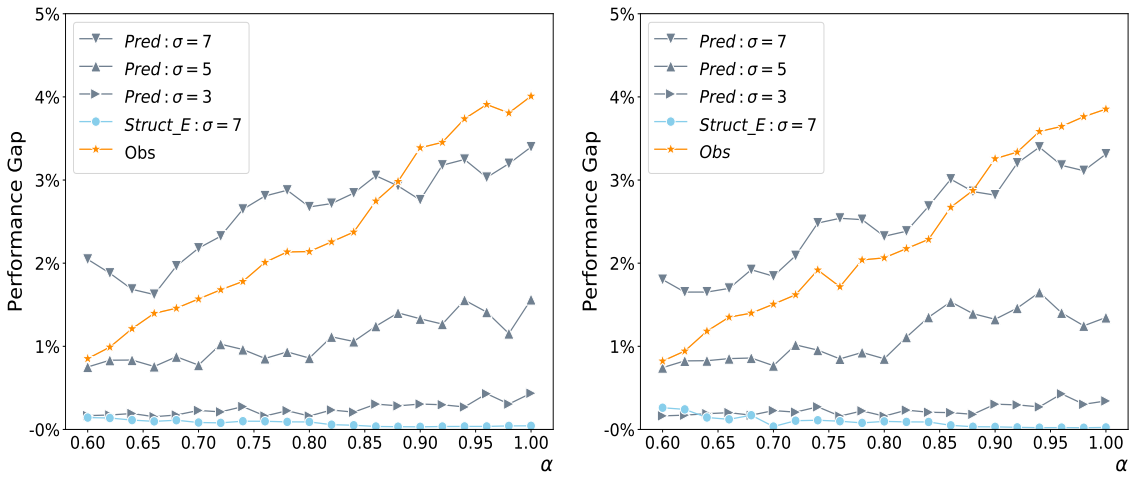

(a) State 3 (b) State 4

Figure 1.6: MDP Performance Comparison
$\sigma = 3$: $\beta^1 \in (0.869, 0.874)$; $\sigma = 5$: $\beta^1 \in (0.781, 0.789)$; $\sigma = 7$: $\beta^1 \in (0.680, 0.687)$.

superiority and benefits of the structural model in TPMs estimation. When the cost structure changes, the benefit of using $\hat{\mathbf{P}}_E^{a=1}$ may also be changed.

Through the comparisons above, I can conclude that considering treatment-effect-based censoring is critical during the estimation of patients' health transitions, and the proposed structural model is more informative and greatly outperforms other potential estimation methods.

1.5 Case Study

In this section, I conduct a case study to estimate ground truth TPMs under the intubation/extubation framework of an ICU. The analysis in this case study is quite similar to that in the simulation except that the ground truth values of the probabilities of using the two policies and correponding thresholds are unknown. In Section 1.5.1, I present the clinical settings and discuss the sample selection procedure. Parameters and TPMs estimations are described in Section 1.5.2. I use the MDP framework to illustrate the necessity of considering treatment-effect-based censoring

in Section 1.5.3.

1.5.1 Clinical Setting and Data Selection

I consider a dataset of patients who visit the cardiothoracic ICU of a tertiary hospital in Singapore from March 2010 to October 2016. The dataset has 5,566 ICU admissions during the study period, and each admitted patient contains detailed data that include demographics, timestamps (admission time, discharge time, intubation time, extubation time, chart time for clinical variables, etc.), and physiological data. The dataset also provides comprehensive information on MV. Clinical results are recorded every 15 minutes to 4 hours, except for laboratory tests, which usually are updated daily. In the partner ICU, physicians will review the health conditions of patients under invasive MV every 6 hours. For each visit, they will evaluate patients' respiratory conditions and then decide whether to extubate the patients.

In the dataset, I first exclude cases without MV performed during the ICU stays. Besides, abnormal extubation (extubation at the end of life, extubation required by patients, and unplanned extubation) cases are also not considered in this study. Due to the high prevalence rate of complications associated with MV, the physicians in the partner ICU seek to extubate patients under ventilation within one week except for those who are in much more complicated health conditions. Hence, I remove the patients with more than seven days of ventilation from the data sample. 30-day ICU readmission cases and patients with too long LOS (i.e., longer than two months) are also removed from the sample as such patients may have very different health conditions (e.g., much severer than others). Moreover, patients who died within one week after intubation, and intubated patients whose intubation time and extubation time cannot be identified are also excluded from the sample. After the clean-up of the dataset, I end up with 3122 patient entries.

1.5.2 TPMs Estimation

Based on the clinical setting and medical practice in the ICU, I first set the decision time interval equal to 6 hours. As patients' states are well classified by RR values, now I can estimate the observed TPMs $\hat{\mathbf{\Pi}}^{a=1}$ and $\hat{\mathbf{\Pi}}^{a=0}$, which are potentially distorted, from the data directly.

$$\hat{\mathbf{\Pi}}^{a=1} = \begin{pmatrix} 0.805 & 0.128 & 0.052 & 0.015 \\ 0.570 & 0.284 & 0.121 & 0.025 \\ 0.210 & 0.259 & 0.395 & 0.136 \\ 0.173 & 0.156 & 0.233 & 0.448 \end{pmatrix} \quad \hat{\mathbf{\Pi}}^{a=0} = \begin{pmatrix} 0.052 & 0.313 & 0.510 & 0.125 \\ 0.018 & 0.211 & 0.557 & 0.214 \\ 0.015 & 0.143 & 0.518 & 0.324 \\ 0.027 & 0.182 & 0.442 & 0.350 \end{pmatrix}$$

Physicians' prognostic information is unavailable and cannot be recovered from the data. Hence, I apply the error-free structural model in this case study. The ground truth values of $\boldsymbol{p}^{te}$ and $\boldsymbol{q}^{se}$ are also unknown. Similar to the simulation, I use the two-stage estimation method. Recall that, in the first stage estimation, the treatment effect values are used in the ensembled model to predict the actions; however, I do not have the treatment effect data directly. Hence, the predictions of treatment effects are required. I train the predictive models with XGBoost(i.e.,Extreme Gradient Boosting) methods and 10-folds cross-validation to predict the censored outcomes under $a = 0$ and $a = 1$. The details of predictive models are relegated to the appendix A.5. In terms of the prediction performance, the out-of-sample accurate rate is up to 0.685. I use the predictions to approximate physicians' prognosis to derive the predicted treatment effects.

Following the suggestions from the ICU physicians, I consider $p_i^{te} = p$ and $\bar{\delta}(i) = -1$ for all $i \in \mathcal{S}$. By enumerating over the potential value of p and $\boldsymbol{q}^{se}$, I obtain $p_i^{te} = 0.437$ $(i = 1, 2, 3, 4)$ and $\boldsymbol{q}^{se} = [0.173, 0.511, 0.231, 0.085]$. Next I can estimate

the TPM $\hat{\mathbf{P}}_E^a$ using the proposed error-free structural model as follows:

$$\hat{\mathbf{P}}_E^{a=1} = \begin{pmatrix} 0.661 & 0.139 & 0.138 & 0.062 \\ 0.507 & 0.275 & 0.173 & 0.045 \\ 0.171 & 0.218 & 0.407 & 0.204 \\ 0.120 & 0.116 & 0.213 & 0.551 \end{pmatrix} \quad \hat{\mathbf{P}}_E^{a=0} = \begin{pmatrix} 0.033 & 0.292 & 0.529 & 0.146 \\ 0.008 & 0.145 & 0.553 & 0.294 \\ 0.007 & 0.079 & 0.375 & 0.539 \\ 0.019 & 0.143 & 0.400 & 0.438 \end{pmatrix}$$

I also estimate the TPMs with censored outcomes predicted by the predictive models. Combining the predictions and observations, I estimate $\tilde{\mathbf{P}}^a$ with MLE as follow:

$$\tilde{\mathbf{P}}^{a=1} = \begin{pmatrix} 0.885 & 0.089 & 0.025 & 0.002 \\ 0.637 & 0.265 & 0.095 & 0.003 \\ 0.519 & 0.227 & 0.234 & 0.020 \\ 0.517 & 0.087 & 0.330 & 0.066 \end{pmatrix} \quad \tilde{\mathbf{P}}^{a=0} = \begin{pmatrix} 0.581 & 0.149 & 0.160 & 0.110 \\ 0.363 & 0.231 & 0.294 & 0.112 \\ 0.303 & 0.328 & 0.332 & 0.037 \\ 0.201 & 0.177 & 0.330 & 0.292 \end{pmatrix}$$

The results show that both $\hat{\mathbf{\Pi}}^a$ and $\tilde{\mathbf{P}}^a$ are significantly different from $\hat{\mathbf{P}}_E^a$ for $a = \{0, 1\}$.

I also apply the quadratic programming method to estimate the TPM $\breve{\mathbf{P}}^a$ with the identity matrix be the weighting matrix:

$$\breve{\mathbf{P}}^{a=1} = \begin{pmatrix} 0.788 & 0.124 & 0.051 & 0.037 \\ 0.644 & 0.070 & 0.276 & 0.010 \\ 0.000 & 0.780 & 0.008 & 0.213 \\ 0.000 & 0.304 & 0.696 & 0.000 \end{pmatrix} \quad \breve{\mathbf{P}}^{a=0} = \begin{pmatrix} 0.028 & 0.281 & 0.474 & 0.217 \\ 0.022 & 0.309 & 0.669 & 0.000 \\ 0.073 & 0.000 & 0.593 & 0.334 \\ 0.000 & 1.000 & 0.000 & 0.000 \end{pmatrix}$$

I find that there are many transitions with probability 0; however, from the observed TPMs, I know that all transitions can be observed in the data, which indicates that the quadratic programming method is not appropriate in this context.

As I described, physicians tend to make treatment-effect-based decisions only when they are very confident in the prognosis; moreover, physicians' prognostic accuracy may be higher than the accuracy of predictive models described in this chapter as the physicians possess additional experience which are not captured by the predictive models. Hence, it is reasonable to assume that physicians' prognostic accuracy is

able to be higher than 0.7. From the simulation results in Figure 1.4, I find that $\hat{\mathbf{P}}_E^a$ greatly outperforms $\hat{\mathbf{\Pi}}^a$, $\tilde{\mathbf{P}}^a$ and $\breve{\mathbf{P}}^a$ when physicians' prognostic accuracy is higher than 0.7. Hence, in the case study, two-stage estimators are the best proxies of the ground truth TPMs.

1.5.3 MDP Model and Performance Comparison

Similar to the simulation, I formulate the extubation problem as an optimal stopping problem with a finite horizon MDP framework. Physicians in my partner ICU usually consider extubating patients within seven days. Furthermore, physicians regularly check ventilated patients every 6 hours. Then, I consider a decision period time is 6 hours, and consequently the total number of decision period is 28, i.e., $t = 1, 2, ..., 28$. My objective is to minimize patient length of stay (LOS), which is one of the main metrics of patients and healthcare providers. I assume that patients' LOS is geometrically distributed (Chan et al. 2012), which essentially assumes that the LOS after intubation/extubation is independent of the ICU stay before the intubation/extubation. From the data, I also do not find significant correlation between the LOS prior and after intubation/extubation (correlation coefficient=0.01, p value=0.95). Hence, I exclude the impact of prior intubation/extubation ICU stays on the estimation of the cost associated with ventilation/extubation. Hereafter, LOS denotes ICU LOS counted from intubation. Then I have $c(s, a = 1) = 6$ hours for all $s \in \mathcal{S}$. While for $c(s, a = 0)$, it is state-dependent and estimated as the expected remaining LOS after extubation (ELOS). For state $s \in \mathcal{S}$, I define $\text{ELOS}(s) = \sum_{i=1}^{N_s} \text{RLOS}_i(s)/N_s$, where N_s is the number of patients extubated from state s and $\text{RLOS}_i(s)$ is the remaining LOS after extubation of patient i with state s. $\text{ERLOS}(j|s) = \sum_{i=1}^{N_{j|s}} \text{RLOS}_i(j|s)/N_{j|s}$ is the expected remaining LOS after extubation of patients transit from state s to state j under extubation. $N_{j|s}$ and $\text{RLOS}_i(j|s)$ denote the number of patients and the remaining LOS after extubation of patient i transits from state s to state j with

extubation.

It is important to note that the observational data has a potential selection bias on extubation. Specifically, physicians may tend to extubate patients in relatively good health conditions or with larger extubation associated treatment effects. Hence, the potential costs of censored observations are not accounted for by ELOS. To justify this problem, I apply a widely used method, propensity score weighting (PSW) adjustment (Lee 2006), to correct the selection bias for cost estimation. The bias-corrected cost, which is denoted by BLOS, is presented in Table 1.3.

	Sample Size	ELOS	BLOS
State 1	1,792	90.74	94.03
State 2	548	94.53	106.85
State 3	249	98.47	120.75
State 4	115	115.77	140.13

ELOS: Biased cost; BLOS: Bias-corrected cost.

Table 1.3: Estimated Cost and Sample Size

I define the policies π^o, π^p and π^* as the optimal policies derived with $\hat{\mathbf{\Pi}}^{a=1}$, $\tilde{\mathbf{P}}^{a=1}$ and $\hat{\mathbf{P}}_E^{a=1}$, respectively (recall that in the optimal stopping MDP model, only the TPMs under action $a = 1$ are used). By solving the MDP model, I present the policies in Figure 1.7.

I find that π^o, π^p and π^* are significantly different. π^p shows that it is optimal to extubate patients only when $s = 1$ and optimal to continue the ventilation otherwise. π^o implies that patients at state 2 should be extubated when the time is approaching the end. While π^* is even less conservative in the sense that all patients at state 2 should be extubated. Such differences are due to the fact that $\hat{\mathbf{\Pi}}^{a=1}$ and $\tilde{\mathbf{P}}^{a=1}$ tend to overestimate the effect of ventilation when compared with $\hat{\mathbf{P}}_E^{a=1}$.

As I mentioned, the two-stage estimators are the best proxies of the ground truth TPMs, then I further show the difference between costs incurred by policy π^o (π^p) and policy π^* by using the two-stage estimators to represent the ground truth TPMs. Let $V(s|\pi)$ be the expected cost of applying policy π to state s patients in the initial

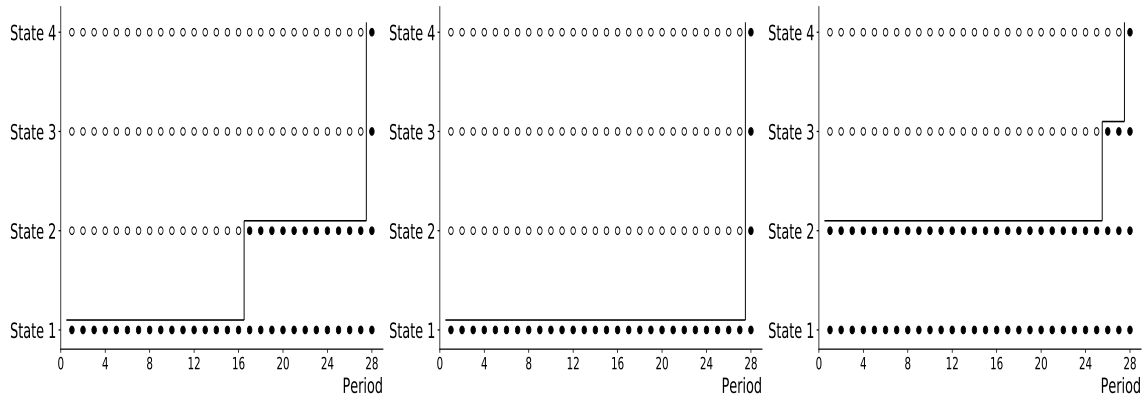

(a) Optimal Policy π^o (b) Optimal Policy π^p (c) Optimal Policy π^*

Figure 1.7: Comparison of Optimal Markov Decision Process Policies:
(1) π^o, π^p and π^* are the optimal MDP policies derived with $\hat{\mathbf{\Pi}}^{a=1}$ (i.e.,the observed TPM), $\tilde{\mathbf{P}}^{a=1}$ (i.e.,the estimated TPM based on predictions) and $\hat{\mathbf{P}}^{a=1}$(i.e.,the two-stage estimator), respectively.
(2) Black dots: extubation; white dots: ventilation. Areas below the black lines represent extubation.

period. Then, I show the cost differences between π^o(and π^p) and π^* in Table 1.4.

State	$s=1$	$s=2$	$s=3$	$s=4$
$V(s\|\pi^o) - V(s\|\pi^*)$: hrs	0.89	1.43	1.99	1.87
$V(s\|\pi^p) - V(s\|\pi^*)$: hrs	0.91	1.45	2.01	1.91

Table 1.4: Cost Gap Between Different Policies

In Table 1.4, for example, applying policy π^o results in a longer LOS by 1.99 hours for State 3 patients in period 0 compared with applying policy π^*. This is equivalent to say that about 8.3% patients with an initial state 3 may spend one extra day in the ICU when applying policy π^o (since 1.99 hours are 8.3% of one day). Given the fact that about 5 million patients are admitted to ICUs annually in the US (Barrett et al. 2014) and 40% of patients admitted to ICUs require mechanical ventilation (Vincent et al. 2002), then prolonged LOS will lead to high monetary cost (at least $3,968 per day for mechanically ventilated patients (Dasta et al. 2005)) and also bring risk of infections. Moreover, longer LOS cause delayed admissions for other critical

illness patients and, as a result, lead to higher mortality risks overall. Therefore, such differences are significant in medical practice. All these results demonstrate that estimating TPMs without (properly) addressing the treatment-effect-based censoring can cause significantly higher costs.

1.6 Conclusion

Treatment-effect-based policies have become increasingly common in healthcare research and practice due to the development of predictive techniques. Researchers and practitioners also increasingly recognize the importance of accounting for censoring during causal inference and/or empirical estimations. However, the researches on addressing the treatment-effect-based censoring in the estimation of health transitions remain silent. This chapter fills this void by considering the impacts of treatment-effect-based censoring on health transition during TPMs estimation. Specifically, I propose a structural model to estimate TPMs. I analytically show the asymptotic properties of the estimated TPMs derived by the structural model and illustrate the structural model's advantages by comparing it with other estimation methods with comprehensive simulation experiments. I also implement the proposed model to estimate patient health transitions using real censored data in ICUs extubation problem. Formulating the extubation problem as a classical optimal stopping Markov Decision Process model, I show that the proposed model, with more accurate estimated TPMs considering censored data, can reduce the length of stay of patients in ICU compared to other benchmark transition estimation methods. Therefore, my research demonstrates that it is critical to consider treatment-effect-based censoring when estimating health transitions in medical research and practice.

This work suggests several future research directions. First, as described, the proof of the existence of solutions to a general bilinear system is still an open question in

academic research. I partially address this issue by conducting extensive numerical experiments, which show that the solution always exists in my context. Then, analytically prove the existence of solutions to the structural model will greatly contribute to not only this type of research but also mathematical problems on bilinear systems and its applications. Second, my main model assumes a prognostic error-free environment. In this chapter, I also present the structural model with prognostic errors incorporated and show that patients' health transitions can be consistently recovered as long as physicians' prognostic information (e.g., accuracy and misclassification matrix) is known. However, physicians' prognostic information is usually unavailable in a standard dataset utilized in the literature. The problem on how to estimate physicians' prognostic information could be very interesting and important. Third, I only consider treatment-effect-based censoring in this study. Future studies may combine this type of censoring with other data sample features or problems during the estimation.

Chapter 2

Wastewater Recycling Capacity Investment In Urban Water Management

2.1 Introduction

Global urban water utilities have been facing unprecedented challenges to achieve water sustainability. On one hand, the global water resources are shrinking (Boretti and Rosa 2019). Richey et al. (2015) estimate that more than 30% of the world largest groundwater systems are now in distress. Urban water demand, on the other hand, is rising because of rapid urbanization, economic development and population growth. Flörke et al. (2018) project that urban water demand is expected to rise by 80 percent by 2050. Such a hike means urban water demand will be more prominent to exceed the current accessible supplies while these supplies are becoming increasingly unreliable as climate change kicks in. Therefore, moving towards more holistic, integrated approaches to urban water management is becoming more popular for meeting increasing water needs. A number of cities, such as Los Angeles, Singapore or Adelaide, have had substantial success tackling water sustainability by diversifying water resources and supply strategies. In particular, wastewater plays a pivotal role in water sustainability by closing the urban water cycle and serving as a consistent

and reliable water source. Conventionally, wastewater is collected and then disposed after a series of basic treatments (e.g., screening and grit removal, sedimentation, filtration and disinfection) in wastewater treatment plants (WWTPs). Recent innovations in water treatment technologies have paved the way for the wastewater to be recycled (e.g., organics and dissolved solids removal by advanced membrane technologies) and used for several purposes, including industrial cooling and landscape irrigation. Wastewater recycling requires an upfront capacity investment and this investment decision is influenced by the availability of other water resources (e.g., freshwater and imported/desalinated water) as well as other idiosyncratic features of urban water systems including different demand streams and uncertainties. This work's main objective is to study the water utility's wastewater recycling capacity investment decision as a part of the integrated urban water management system while considering the important idiosyncratic features of these systems.

In the operations management (OM) literature there is a vast amount of research that studies the value of recycling/reusing items in the context of closed-loop supply chains (see Atasu et al. 2008a, Guide Jr and Van Wassenhove 2009 and Souza 2013 for overviews). The results derived by these papers are not directly applicable to urban water systems because of their unique characteristics. In a typical urban water system (see Figure 2.1), water demand is in multiple streams and each stream can be satisfied with a different combination of alternative water resources. Specifically, conventional freshwater can be treated to potable water, which is suitable for human consumption and used to satisfy household demand. Wastewater, on the other hand, is usually recycled to non-potable water and then used to meet non-household demand, e.g., for industrial purposes and landscape irrigation. Potable water can also be used to meet non-household demand. In addition, desalinated seawater and/or imported freshwater[1] also serves as alternative urban water resources and can be treated to

[1]In Figure 2.1, for the ease of exposition, I use desalinated water to represent the last resort.

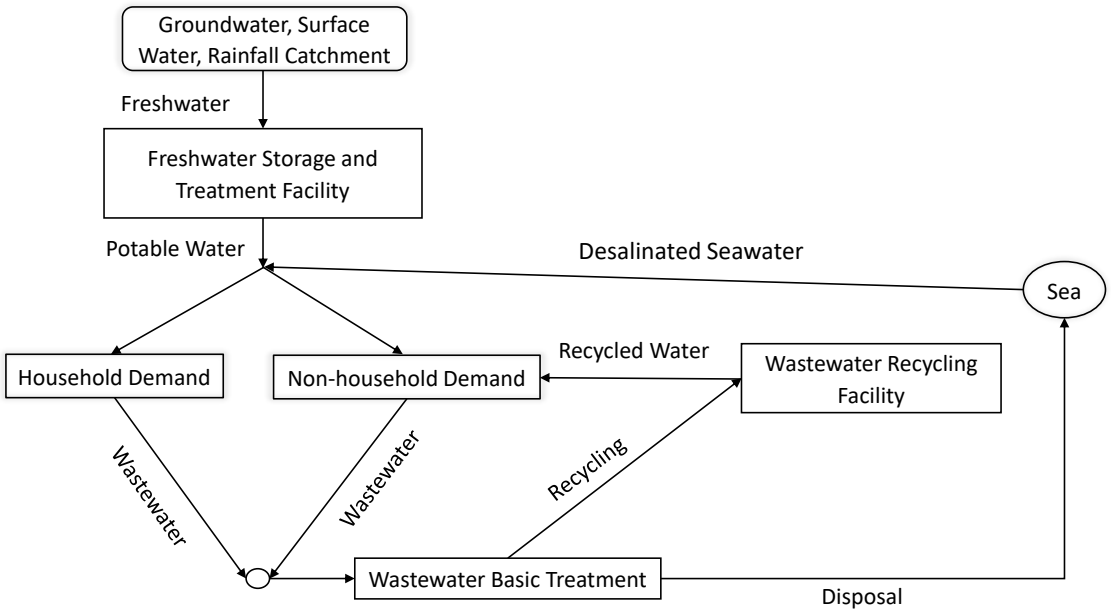

Figure 2.1: Urban Water Supply Framework

potable water to satisfy both household and non-household demands.

Among these alternative water resources, freshwater is the cheapest, but it is exposed to rainfall uncertainty. In addition, heavy rainfall events due to climate change may result in the instantaneous maximum flows out of catchment areas, which lead to storm overflows and urban floods that are costly to handle (Mun et al. 2021). Recycled water is more expensive (from Figure 2.1, we know that the cost of recycled water includes basic wastewater treatment cost and recycling cost) than freshwater as wastewater treatment is more energy-intensive (Rygaard et al. 2011). Moreover, as energy prices are uncertain due to climate change, the cost of recycled water is subject to uncertainty. Desalinated seawater or imported freshwater, being the most expensive water resource, serves as the last resort to satisfy any type of demand and can provide an abundant supply. These unique features play significant roles in the economic and sustainable implications of wastewater recycling investment in urban water management.

Motivated by the need to move toward more integrated approaches in urban water management, I analyze the wastewater recycling capacity investment and allocation

decisions of a water utility by considering the unique characteristics of an urban water system described above. The water utility operates an urban water system in which all demands should be satisfied. For an exogenously given freshwater capacity, the water utility chooses the wastewater recycling capacity to minimize the expected cost in a single planning period. I model the decisions as a two-stage stochastic problem in a stylized manner. In the first stage, the wastewater recycling capacity is chosen under rainfall and recycling cost uncertainties[2]. In the second stage, after these uncertainties are realized, given the capacity investment levels the water utility allocates the freshwater, recycled water and desalinated/imported water to meet the household and non-household demands in the most cost-effective way. Using this framework, I answer the following main research questions:

i) What is the optimal wastewater recycling capacity to invest under rainfall and recycling cost uncertainties?

ii) What are the impacts of rainfall and recycling cost uncertainties on the optimal expected cost and the optimal recycling capacity?

iii) Are wastewater recycling capacity and freshwater capacity complements or substitutes?

iv) Which water pipe system (freshwater or recycled water) should be prioritized to reduce leakage to improve the urban water sustainability?

v) How does the investment on wastewater recycling affect urban water vulnerability and overflow risk?

My main results can be summarized as follows.

[2]As I described, the cost of recycled water consists two parts: basic treatment cost and recycling cost, and is uncertain due to fluctuating energy prices. In the urban water system, all collected wastewater must go through the basic treatment processes. Hence, the variability from basic treatment processes will not play a role in the model. Hereafter, instead of using cost of recycled water uncertainty, I focus on the recycling cost uncertainty.

Solution to the Capacity Planning and Allocation Problems. I first solve for the optimal water allocation scheme. The desalinated/imported water always serves as the last resort to satisfy the unmet demand once the freshwater and recycled water are completely used. Effectively, freshwater is the cheapest source; however, it is not always the first resort to satisfy demand. As I described, all collected wastewater has to go through a basic treatment regardless of whether it is disposed or recycled, the optimal allocation is determined by the additional cost associated with the recycling process (i.e., recycling cost), and this cost can be lower than the freshwater cost. I find that the recycled water is dispatched in priority to meet non-household demand if the recycling cost is sufficiently small or moderate and the amount of rainfall is not too high to result in an overflow of freshwater from reservoirs.

For the optimal capacity decision, when it is profitable to invest, the firm invests in the minimum investment level, which is the difference between the total demand and freshwater capacity when the capacity cost is high. When the capacity cost is low, the firm invests in the maximum investment level, which is the minimum of total wastewater collected and non-household demand. In between, the optimal recycling capacity is implicity characterized by a first-order condition.

Impacts of Freshwater Capacity and Uncertainties. I analyze the relationship between the optimal recycling capacity and the freshwater capacity. Common intuition may suggest that these two types of capacities are substitutes. I prove that this intuition is correct when there is no overflow cost. However, I find that this intuition can be wrong and these two components can be complements when the freshwater capacity is relatively large and the overflow cost is positive. This is because the risk of overflow is lower with a larger freshwater capacity; hence recycled water can be prioritized in a larger range of rainfall realizations. Thus, a higher recycling capacity is preferred.

I then conduct sensitivity analysis, both analytically and numerically, to investi-

gate the impacts of rainfall and recycling cost variabilities and their correlation on the optimal expected cost and the optimal recycling capacity. To this end, I assume that the recycling cost and rainfall follow a bivariate Normal distribution. I find that the utility firm always benefits (i.e., the cost decreases) from a higher correlation but a lower rainfall variability. Moreover, I find that the firm benefits from a lower recycling cost variability when this variability is small, correlation is negative, and the mean recycling cost is relatively large; otherwise, the firm benefits from a higher recycling cost variability. The sensitivity results associated with the optimal recycling capacity are structurally similar to those associated with the optimal expected cost.

Urban Water Leakage Reduction, Vulnerability and Overflow Risk. I also discuss the sustainability of the integrated urban water system through water leakage reduction, urban water vulnerability and overflow risk. I find that the optimal expected cost increases in urban water leakage ratios (freshwater or recycled water). Which water pipeline system gets the priority in leakage reduction depends on the relationship between the freshwater and recycled water leakage ratios. An interesting observation is that, given the recycled water and freshwater leakage ratios, if the freshwater leakage ratio is small than a threshold, it is better to prioritize reducing freshwater leakage; otherwise, the reduction of recycled water leakage should be prioritized. The vulnerability reflects to what extent the urban water system fails to satisfy the demand when the last water resort is excluded. I use the expected amount of desalinated /imported water used to measure the vulnerability. The common intuition may suggest that the urban water system is less vulnerable when the freshwater capacity is large. I provide specific conditions under which this intuition is correct and extend it by showcasing the conditions under which a larger freshwater capacity increases the system's vulnerability. The impacts of the uncertainties on the vulnerability are similar to the effects on the optimal expected cost characterized above. Water overflow or flood may also greatly impact urban water sustainability by destroying water infrastructures and re-

sulting in economic loss. This work investigates the urban water system overflow risk and how the uncertainties and freshwater capacity affect the overflow risk. I find that the overflow risk increases in the rainfall variability. As the cost variability increases, the overflow risk increases if the correlation is positive and the mean recycling cost is not very small.

I further complement my structural analysis with numerical studies based on practical instances in Chapter 3. Towards this end, I calibrate my model to represent the urban water utility located in Adelaide, the capital city of South Australia. I use publicly available data from the annual National Performance Reports and National Water Account published by the Australia Bureau of Meteorology (ABM), complemented by the data obtained from the extant literature and technical reports.

The remainder of this chapter is organized as follows. Section 2.2 reviews the related literature and discusses the contribution of this work. In Section 2.3, I introduce the research problem in subsection 2.3.1 and present the mathematical model and optimal solutions in subsection 2.3.2. Subsection 2.3.3 studies the effects of uncertainties on the optimal recycling capacity and the optimal expected cost. From subsection 2.3.4 to subsection 2.3.6, I investigate the measures on sustainability including water leakage reduction, vulnerability and overflow risk and examine the effects of uncertainties and correlation on these measures. I conclude this work and discuss the limitations as well as the future research directions in Section 2.4.

2.2 Literature Review

This research is closely related to the OM literature that studies water-related management problems. The papers in this literature study a broad range of operational issues related to water management, including water quality control (Sobel 1971, Taylor 1973, Fiacco and Ghaemi 1982, Mulligan and Ahlfeld 2002), irrigation man-

agement (Stoecker et al. 1985, Rabinowitz et al. 1988, Huh and Lall 2013), and flood management (Eijgenraam et al. 2017). Similar to my work, a stream of papers in this domain investigates water allocation problems. For example, Murali et al. (2015) consider the municipal groundwater management problem in the presence of a water trading market. Using a deterministic model, they maximize social welfare by optimally deciding the quantities of groundwater to extract, export and import. Zhang et al. (2016) analyze the water allocation problem in a developing region in Tucson. They determine the optimal water allocation policy to minimize the expected distribution and freshwater treatment costs while controlling the risk of water shortage. I, in addition to the allocation problem, also consider the capacity planning problem in an urban water system with rainfall and recycling cost uncertainties. Capacity planning problems in water systems have also been studied in the OM literature. Avi-Itzhak and Ben-Tuvia (1963) analyze the optimal reservoir and pumping capacities to minimize the cost per cubic meter of water pumped. Erlenkotter et al. (1989) develop a model to determine the optimal timing for initiating a water capacity expansion project when the future water demand exceeds the forecasted demand. Closest to my work, Armstrong and Willis (1977) investigate the economic implications of capacity planning and allocation decisions in a deterministic setting. Similar to my work, they also consider multiple water resources, including imported water, desalinated water, and freshwater, but do not incorporate recycled water in their model. Different from Armstrong and Willis (1977), I focus on the wastewater recycling capacity and incorporate other important features (i.e., rainfall and recycling cost uncertainties) of an urban water system in my model.

Capacity planning problems have also received considerable attention from the water management literature. Srinivasan et al. (2010) propose a simulation framework to evaluate the economic and supply risk performances of efficiency improvement approaches such as reducing pipeline leakage and water supply augmentation

via desalination and rainfall harvesting. Beh et al. (2015) develop a multi-objective adaptive optimization approach under various uncertainties (e.g., rainfall, temperature and demand) to investigate the optimal capacity investment path for water resources, including seawater desalination and rainfall harvesting. Similarly, Fletcher et al. (2017) develop a multi-stage simulation-based decision framework under supply and demand uncertainties to evaluate the economic performance of urban water investment schemes with a special focus on the optimal desalination capacity decision. Different from these papers, I focus on wastewater recycling capacity investment. There are papers in this literature that consider wastewater recycling plants investment. For example, Woods et al. (2013) analyze the value of wastewater recycling and compare the economic and environmental performances of centralized and decentralized treatment schemes. Wu et al. (2017) study a multi-objective urban water supply problem in the context that freshwater, recycled water and desalinated water are used to meet urban demand. However, in terms of capacity decisions, they focus on operating capacity adjustment. Similarly, assuming the design capacities are given, Bhushan and Ng (2016) also integrate seawater desalination and wastewater recycling into urban water systems under climate change and use a multi-objective optimization embedded simulation method to optimize the operating capacities of desalination and wastewater recycling. In this paper, they also consider multiple streams of demand and wastewater is recycled for potable use. However, my work differs from Bhushan and Ng (2016) in several aspects. First of all, I consider an uncertain recycling cost that is subjected to climate change. Second, in my setting, recycled water can only satisfy non-household use (or non-potable use), as commonly observed in practice. Third, I specifically investigate the wastewater recycling capacity problem and try to understand how the variabilities and correlation between the amount of rainfall and recycling cost affect the value of wastewater recycling.

This research is also related to the growing OM literature on closed-loop sup-

ply chain (CLSC) management. As reviewed by Atasu et al. (2008a), the papers in this literature capture the unique features of CLSCs and study various challenging operational, tactical and strategic problems. For operational and tactical problems, a bunch of papers focuses on topics such as returned products acquisition and disposition (Ferguson et al. 2009, Galbreth and Blackburn 2010), reverse channel and logistic management (Savaskan and Van Wassenhove 2006, Angelus and Özer 2020), and inventory control (Van der Laan et al. 1999, Toktay et al. 2000, DeCroix and Zipkin 2005, Calmon and Graves 2017). On the strategic side, research topics such as the profitability of remanufacturing (Debo et al. 2005, Ferrer and Swaminathan 2006, Atasu et al. 2008b), the impact of remanufacturing on new product design (Atasu and Souza 2013), CLSC network design (Fleischmann et al. 2001, Üster and Hwang 2017), product take-back strategies or legislations (Agrawal et al. 2012, Oraiopoulos et al. 2012, Atasu and Subramanian 2012) and collection strategies (Savaskan et al. 2004) have been studied. Like the papers in this literature, I study a closed-loop urban water system in which water is reused through wastewater recycling. However, my research differs from the papers in this literature in several aspects. First of all, most of the papers in this literature study product reuse considering the competition between OEMs and remanufacturers and focus on cannibalization between new and remanufactured products. In my research, competition is not an issue as a central planner (the water utility) manages the whole urban water system to satisfy demand in the least costly way. Cannibalization is also irrelevant as I assume that the demand for potable and non-potable water is exogenously given. Moreover, remanufacturing is a cheaper alternative to new product manufacturing, and the capacities are either infinite or limited with exogenously given values. In my work, wastewater recycling is more expensive than freshwater treatment, and wastewater recycling capacity is optimized to minimize the cost. In CLSC literature, some papers are studying the capacity investment decisions of remanufacturing and recycling

facilities. Among these papers, Georgiadis et al. (2006), Vlachos et al. (2007) and Georgiadis and Athanasiou (2010) study a dynamic capacity planning problem in CLSCs using simulation methods under different contexts. These papers investigate how the product life cycles and products return patterns affect the expansion of used product collection and remanufacturing capacities. Debo et al. (2006) consider the joint life-cycle dynamics of new and remanufactured products and determine their optimal diffusion path. Using numerical optimization, they show how the capacity requirements for new products manufacturing and used products remanufacturing evolve over the product life cycle. Francas and Minner (2009) examines the capacity decisions of two alternative manufacturing network configurations. Like in my work, they formulate the problem as a two-stage stochastic optimization model. In the first stage, the capacities of remanufacturing and new production plants are selected. In the second stage, the quantity of new and remanufactured items is determined after the demand and product return uncertainties are resolved. They numerically solve the model and show the impacts of investment cost, network size and market structure on the decisions and performances. Unlike these papers, my research focuses on optimizing wastewater recycling capacity under rainfall and recycling cost uncertainties in a setting where freshwater and recycled water are partially substitutable to serve urban demand or perfectly substitutable to serve non-household demand. My work attempts to provide an analytical framework to understand the implications of wastewater recycling capacity optimization on sustainable urban water management and how the uncertainties affect these implications.

2.3 Wastewater Recycling Capacity Planning: Problem, Model, and Analysis

In this section, I analyze the wastewater recycling capacity investment problem using a mathematical optimization model. I describe the research setting and introduce the notations in subsection 2.3.1. The optimization model and optimal solutions are discussed in subsection 2.3.2. I then conduct extensive analysis on the effects of uncertainties on the optimal recycling capacity and optimal expected cost (section 2.3.3), leakage reduction (section 2.3.4) the urban water vulnerability (section2.3.5) and overflow risk (section 2.3.6).

2.3.1 Problem Description

The following mathematical representation is used throughout the text: a realization of the random variable $\tilde{y}$ is denoted by y. The expectation operator and probability are denoted by $\mathbb{E}$ and $\mathbf{Pr}$, respectively. The monotonic relations are used in the weak sense unless otherwise stated. Subscripts f, r, and d denote freshwater, recycled water and desalinated water-related parameters and decision variables. All the proofs are relegated to the appendix.

I consider an urban water utility that decides on the wastewater recycling capacity and allocation of different water resources (freshwater, recycled water and desalinated/imported water) to satisfy household and non-households demand to minimize the expected cost in a single planning period. I assume that all demand should be satisfied and treat that the household demand and non-household demand as the maximum potential demand in the planning period. I model the utility's decisions as a two-stage problem. In the first stage, the wastewater recycling capacity K_r is chosen at a unit cost w_r under rainfall and wastewater recycling cost uncertainties. The amount of available freshwater, which is uncertain due to rainfall uncertainty,

and the wastewater recycling cost are denoted by $\tilde{s}$ and $\tilde{c}_r$, respectively. In the second stage, after realizing these uncertainties, the quantities of fresh water, wastewater for recycling and seawater/imported freshwater are decided to meet household and non-household demands in the most cost-effective way. Specifically, q_f units freshwater is dispatched from the reservoirs and treated at a unit treatment cost c_f. The quantity q_f is subjected to $\tilde{s}$ and the freshwater storage and treatment capacities. In the analysis, for the ease of exposition, I assume that freshwater storage and treatment capacities are the same and termed as freshwater capacity, which is denoted by K_f. After the treatment, the freshwater is turned into $\beta_f q_f$ units of potable water, where $\beta_f \in (0,1)$ is the freshwater recovery ratio (i.e., the amount of potable water recovered from a unit of freshwater). The potable water is then supplied to meet household demand D_h and/or non-household demand D_{nh}. If the remaining freshwater in the reservoir after dispatching is too much and exceeds a certain level (i.e., $s - q_f > \alpha K_f$, $\alpha \in (0,1]$ measures the safety water storage level for reservoirs), as discussed and modelled in Mun et al. (2021), there is overflow/flood. Like in Mun et al. (2021), I also consider the economic loss resulting from overflow and use o_f to denote the unit overflow cost. Without loss of generality, I set $\alpha = 1$ throughout the text; hence, the overflow cost is $o_f(s - q_f - K_f)^+$.

The amount of wastewater water collected from households and non-households is equal to $q_u = \beta_h D_h + \beta_{nh} D_{nh}$ where β_h and β_{nh} denote the wastewater collection rates from household and non-household, respectively. The collected wastewater will undergo a series of basic treatments in WWTPs by incurring a unit basic treatment cost $\tilde{c}_b$. The treated wastewater, instead of being discharged, may be further recycled to non-potable water in water recycling plants (WRTs) to satisfy non-household demand. Let $\tilde{c}_r$ denote the unit recycling cost; hence, the total cost of a unit of recycled water is $\tilde{c}_t = \tilde{c}_b + \tilde{c}_r$. I let q_r be the quantity of collected wastewater that is recycled and $\beta_r \in (0,1)$ be the recovery ratio of recycled water (i.e., β_r unit of recycled water

is obtained from a unit of wastewater). Hence, $\beta_r q_r$ units of recycled water is used to satisfy non-household demand. Moreover, q_r is constrained by q_u and K_r. The utility also use desalinated seawater/imported water to satisfy the demand streams at a unit cost c_{sd}. For brevity, I focus on desalinated seawater hereafter unless otherwise stated. In this text, I let q_d be the amount of desalinated water (i.e., potable water desalinated from seawater) required to meet the demand. The corresponding water recovery ratio is denoted by β_d; hence $c_d = c_{sd}/\beta_d$ denotes the effective unit desalination cost. I further assume that the desalination capacity is sufficiently large; hence there is no constraint on the amount of desalinated water available.

I assume that $(\tilde{s}, \tilde{c}_r)$ follow a bivariate distribution with $\tilde{s} \in [s_0, +\infty)$ and $\tilde{c}_r \in [\underline{c}_r, \bar{c}_r]$ ($s_0 \geq 0$ represents the deterministic amount of freshwater available at the beginning of the period, and $\underline{c}_r > 0$), bounded expectation (μ_s, μ_c) with covariance matrix $\mathbf{\Sigma}$, where $\mathbf{\Sigma}_{00} = \sigma_s^2$, $\mathbf{\Sigma}_{11} = \sigma_c^2$, $\mathbf{\Sigma}_{01} = \mathbf{\Sigma}_{10} = \rho\sigma_s\sigma_c$, and ρ denotes the correlation coefficient.

It should be noted that pipeline transportation may also be costly in some cases; hence, the mentioned freshwater treatment cost c_f, wastewater basic treatment and recycling costs ($\tilde{c}_b$ and $\tilde{c}_r$) and seawater desalination cost c_{sd} also incorporate the associated water transportation and distribution costs. Without loss of generality, I assume that the effective freshwater treatment cost is less than the potential smallest effective total cost of recycled water (i.e., $\underline{c}_t/\beta_r > c_f/\beta_f$) and the effective desalination cost is the largest of the three such that $c_d > \bar{c}_t/\beta_r$, where $\tilde{c}_t \in [\underline{c}_t, \bar{c}_t]$. This assumption is consistent with the fact that desalinated water is used as the last resort to satisfy household and non-household demands in practice. For the ease of exposition, I further assume $K_f \leq \frac{D_h + D_{nh}}{\beta_f}$ (the results presented also hold under the case that $K_f > \frac{D_h + D_{nh}}{\beta_f}$). I also highlight that the capacities K_f and K_r in this context can be interpreted as the capability of treating K_f units of freshwater and recycling K_r units of wastewater (after basic treatment) in a single period.

2.3.2 Model and Optimal Solutions

This section presents the optimization model and the optimal solutions for the urban water utility's wastewater recycling capacity and water allocation decisions. I solve the problem using backward induction.

In stage 1, the urban water utility chooses the recycling capacity K_r. In stage 2, the utility observes the rainfall and recycling cost realizations (s, c_r). In this stage, constrained by the freshwater capacity K_f and the recycling capacity K_r, the utility optimally decides on q_f, q_r and q_d to satisfy the demand. The amount of desalinated water dispatched (q_d) can be expressed as a function of the amount of freshwater (q_f) and wastewater for recycling (q_r) as seawater desalination serves as the last resort to satisfy unmet demand (if any), i.e., $q_d = D_h + D_{nh} - \beta_r q_r - \beta_f q_f$. I formulate the urban water utility's problem as a multi-variable cost minimization problem as follows:

$$\min_{q_f, q_r} Z(q_f, q_r)$$

$$s.t. \quad q_f \leq \min(K_f, s), \tag{2.1}$$

$$q_r \leq \min(\beta_h D_h + \beta_{nh} D_{nh}, \frac{D_{nh}}{\beta_r}, K_r), \tag{2.2}$$

$$\beta_r q_r + \beta_f q_f \leq D_h + D_{nh}, \tag{2.3}$$

$$q_f \geq, 0 \tag{2.4}$$

$$q_r \geq 0 \tag{2.5}$$

with

$$Z(q_f, q_r) \doteq c_b(\beta_h D_h + \beta_{nh} D_{nh} - q_r) + c_t q_r + o_f \left(s - q_f - K_f\right)^+ +$$

$$c_f q_f + c_d(D_h + D_{nh} - \beta_r q_r - \beta_f q_f)$$

In the objective function $Z(q_f, q_r)$, the first term represents the basic treatment cost of wastewater for disposal, the second term is the cost of recycled wastewater, the third term denotes the overflow cost and the last two terms are the freshwater treatment and desalination costs, respectively. Constraint (2.1) ensures that the quantity of

freshwater dispatched is limited by the capacity K_f and the realized amount of rainfall, constraint (2.2) guarantees that the quantity of recycled wastewater is limited by the amount of wastewater collected, the recycling capacity and the non-household demand and constraint (2.3) makes sure that the total quantity of freshwater and recycled water dispatched does not exceed the total demand. As all collected wastewater undergoes the basic treatment procedures, the objective function is rewritten as

$$Z(q_f, q_r) = c_b(\beta_h D_h + \beta_{nh} D_{nh}) + c_r q_r + o_f \left(s - q_f - K_f\right)^+ + \\ c_f q_f + c_d(D_h + D_{nh} - \beta_r q_r - \beta_f q_f)$$

I define the following parameters for ease of exposition:

- Let $S^f_{max} = \beta_f \min(K_f, s)$, which is the maximum amount of potable water that can be treated from freshwater.
- Let $S^r_{max} = \min(\beta_r(\beta_h D_h + \beta_{nh} D_{nh}), D_{nh}, \beta_r K_r)$, which is the maximum amount of recycled water that can be dispatched to satisfy non-household demand.
- Let $\tau_1(K_r) = \frac{D_h + D_{nh} - S^r_{max}}{\beta_f}$, which is the minimum amount of freshwater required to satisfy demand when the maximum amount of recycled water is dispatched and desalinated water is not available
- Let $\tau_2 = \frac{D_h + D_{nh}}{\beta_f}$, which is the minimum amount of freshwater required to satisfy demand when the recycled water and desalinated water are not available
- Let $\tau_3(K_r) = \tau_1(K_r) + K_f$, which is the maximum amount of freshwater that the system can handle such that no overflow occurs when the maximum amount of recycled water is dispatched and desalinated water is not available
- Let $\tau_4 = \tau_2 + K_f$, which is the maximum amount of freshwater that the system can handle such that no overflow occurs when the recycled water and desalinated water are not available

To rule out uninteresting cases, I assume $(c_f - o_f)/\beta_f > \underline{c}_r/\beta_r$ and $c_f/\beta_f < \bar{c}_r/\beta_r$. Proposition 2.1 characterizes the optimal amount of freshwater, recycled water and desalinated water dispatched that minimize $Z(q_f, q_r)$.

Proposition 2.1. *If $K_f < \tau_1(K_r)$, then the optimal solution is:*

$$(q_f^*, q_r^*, q_d^*) = \left(S_{max}^f/\beta_f, S_{max}^r/\beta_r, D_h + D_{nh} - S_{max}^r - S_{max}^f\right)$$

Otherwise,

$$(q_f^*, q_r^*, q_d^*) = \begin{cases} (s, S_{max}^r/\beta_r, D_h + D_{nh} - S_{max}^r - \beta_f s) & (s,c_r) \in \Omega_1 \\ \left(\min(s, K_f, \frac{D_h+D_{nh}}{\beta_f}), (D_h + D_{nh} - \beta_f q_f^*)/\beta_r, 0\right) & (s, c_r) \in \Omega_2 \bigcup \Omega_6 \\ \left(\frac{D_h+D_{nh}-S_{max}^r}{\beta_f}, S_{max}^r/\beta_r, 0\right) & (s, c_r) \in \Omega_3 \bigcup \Omega_4 \\ (s - K_f, (D_h + D_{nh} - \beta_f(s - K_f))/\beta_r, 0) & (s, c_r) \in \Omega_5 \end{cases}$$

with

- $\Omega_1 = \{(s, c_r) : s \leq \tau_1(K_r), c_r \geq \underline{c}_r\}$
- $\Omega_2 = \{(s, c_r) : s > \tau_1(K_r), c_r \geq c_f \frac{\beta_r}{\beta_f}\}$
- $\Omega_3 = \{(s, c_r) : \tau_1(K_r) < s \leq \tau_3(K_r), c_r < c_f \frac{\beta_r}{\beta_f}\}$
- $\Omega_4 = \{(s, c_r) : \tau_3(K_r) < s, \underline{c}_r \leq c_r \leq (c_f - o_f)\frac{\beta_r}{\beta_f}\}$
- $\Omega_5 = \{(s, c_r) : \tau_3(K_r) < s \leq \tau_4, (c_f - o_f)\frac{\beta_r}{\beta_f} \leq c_r \leq c_f \frac{\beta_r}{\beta_f}\}$
- $\Omega_6 = \{(s, c_r) : s > \tau_4, (c_f - o_f)\frac{\beta_r}{\beta_f} \leq c_r \leq c_f \frac{\beta_r}{\beta_f}\}$

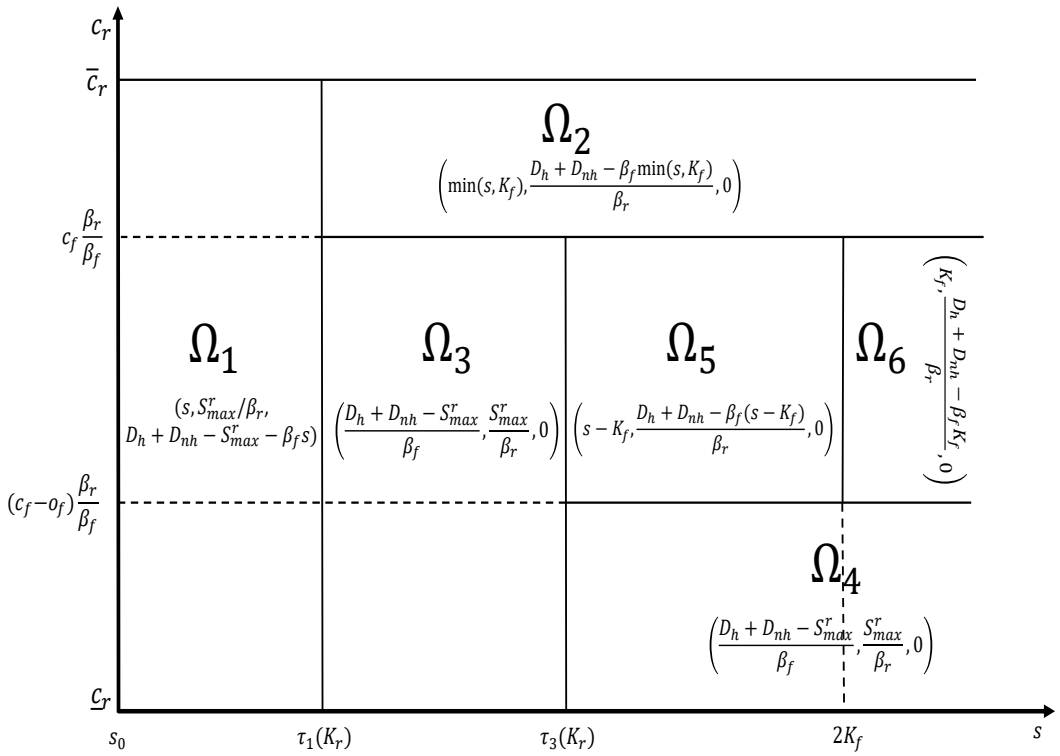

Figure 2.2: Second Stage Solutions

When $K_f < \tau_1(K_r)$, freshwater capacity is sufficiently small such that the water demand cannot be satisfied without desalinated water for all realizations of rainfall. When $K_f > \tau_1(K_r)$, there is enough freshwater capacity to satisfy demand together with the recycled water; hence desalinated water is only necessary when the rainfall is small (i.e., when $s < \tau_1(K_r)$ as in region Ω_1 in Figure 2.2). In both cases, it is optimal to supply the maximum quantity of freshwater (i.e., $\min(s, K_f)$) and recycled water available to meet the demand as they are cheaper sources compared to desalinated water. The rest of the demand (i.e., $D_h + D_{nh} - S^r_{max} - S^f_{max}$) is satisfied by desalinated water.

When both the freshwater capacity and the rainfall are sufficiently large (i.e., $K_f \geq \tau_1(K_r)$ and $s \geq \tau_1(K_r)$, respectively), the use of desalinated water is avoided. In this case, when the recycling cost is high (i.e., $c_r > c_f\frac{\beta_r}{\beta_f}$ as in region Ω_2 in Figure 2.2), the priority to satisfy the non-household demand is given to freshwater. The

rest of the demand (if there is any) is satisfied by recycled water. The amount of freshwater dispatched to meet household and non-household demands is limited by the amount of freshwater available (s) and the freshwater capacity (K_f).

When the recycling cost is moderate (i.e., $c_r \leq c_f \frac{\beta_r}{\beta_f}$), the priority to satisfy the non-household demand is given to recycled water as long as there is no risk of overflow in the reservoir ($s \leq \tau_3(K_r)$ as in region Ω_3 in Figure 2.2). In this case, recycled water is used as much as available ($\frac{S^r_{max}}{\beta_r}$) and the rest of the demand is satisfied by freshwater ($\frac{D_h+D_{nh}-S^r_{max}}{\beta_f}$). The same resource allocation is observed even if the risk of overflow arises with the maximum usage of recycled water available as long as the recycling cost is smaller than the marginal benefit of using freshwater to meet non-household demand when there is an overflow (i.e., $c_r \leq (c_f - o_f)\frac{\beta_r}{\beta_f}$ as in region Ω_4 in Figure 2.2). However, if the recycling cost is larger than this marginal benefit (i.e., $(c_f - o_f)\frac{\beta_r}{\beta_f} < c_r \leq c_f \frac{\beta_r}{\beta_f}$) and if the overflow can be prevented with the usage of freshwater to satisfy non-household demand (i.e., $\tau_3(K_r) < s \leq \tau_4$ as in region Ω_5 in Figure 2.2), then the priority to satisfy non-household demand is given to freshwater to an extent to prevent overflow (i.e., $q_f^* = s - K_f$) and the rest of the demand is satisfied by recycled water (i.e., $D_h + D_{nh} - \beta_f q_f^*$). If the overflow cannot be prevented even with the maximum usage of freshwater (i.e., $s \geq \tau_4$ as in region Ω_6 in Figure 2.2), then it is optimal to use freshwater as much as possible. The rest of the demand (if there is any) is satisfied by recycled water.

In stage 1, the urban water utility chooses the optimal recycling capacity K_r^* under rainfall and recycling cost uncertainties so as to minimize the expected cost $V(K_r)$, where

$$V(K_r) \doteq \underset{\tilde{c}_r, \tilde{s}}{\mathbb{E}} \left(Z^*(K_r, q_f, q_r; \tilde{s}, \tilde{c}_r) + \omega_r K_r \right)$$

and $Z^*(K_r, q_f, q_r; s, c_r)$ denotes the optimal stage 2 cost for a given recycling capacity K_r. The second stage results show that it is never optimal to set the recycling capacity larger than $\min\left(\beta_h D_h + \beta_{nh} D_{nh}, \frac{D_{nh}}{\beta_r}\right)$, thus I focus on the case

where $K_r \leq \min\left(\beta_h D_h + \beta_{nh} D_{nh}, \frac{D_{nh}}{\beta_r}\right)$. To rule out uninteresting cases, I assume that $\frac{D_h + D_{nh} - \beta_f K_f}{\beta_r} \leq \min\left(\beta_h D_h + \beta_{nh} D_{nh}, \frac{D_{nh}}{\beta_r}\right)$[3], which implies that $K_f \geq \underline{K}_f = (D_h + D_{nh} - \min\left(\beta_r(\beta_h D_h + \beta_{nh} D_{nh}), D_{nh}\right))/\beta_f$.

Let

$$
\begin{aligned}
m_d &\doteq \frac{\tilde{c}_r}{\beta_r} - c_d, \\
m_f^{no} &\doteq \frac{\tilde{c}_r}{\beta_r} - \frac{c_f}{\beta_f}, \\
m_f^{o} &\doteq \frac{\tilde{c}_r}{\beta_r} - \frac{c_f - o_f}{\beta_f}
\end{aligned}
$$

where m_d, m_f^{no} and m_f^o denote the unit marginal benefit/cost (a negative value means benefit) of recycling and the unit marginal benefit of recycling when the recycled unit replaces desalinated water, freshwater in the case of no overflow and freshwater in the case of overflow respectively.

Proposition 2.2 characterizes the optimal recycling capacity.

Proposition 2.2.

There exist three thresholds $\omega_r^0, \omega_r^1, \omega_r^2$ with $\omega_r^0 \leq \omega_r^1 < \omega_r^2$ such that

(i) if $\omega_r > \omega_r^2$, then $K_r^* = 0$;

(ii) if $\omega_r^1 < \omega_r \leq \omega_r^2$, then $K_r^* = \frac{D_h + D_{nh} - \beta_f K_f}{\beta_r}$

(iii) if $\omega_r^0 < \omega_r \leq \omega_r^1$, then K_r^* solves $\left.\frac{\partial V(K_r)}{\partial K_r}\right|_{K_r^*} = M(K_r)|_{K_r^*} + \omega_r = 0$;

(iv) if $\omega_r \leq \omega_r^0$, then $K_r^* = \min\left(\beta_h D_h + \beta_{nh} D_{nh}, \frac{D_{nh}}{\beta_r}\right)$.

where

$$
\begin{aligned}
M(K_r) =& \mathbb{E}[(m_d \beta_r) | (\tilde{s}, \tilde{c}_r) \in \Omega_1] \mathbf{Pr}((\tilde{s}, \tilde{c}_r) \in \Omega_1) \\
&+ \mathbb{E}[(m_f^{no} \beta_r) | (\tilde{s}, \tilde{c}_r) \in \Omega_3] \mathbf{Pr}((\tilde{s}, \tilde{c}_r) \in \Omega_3) \\
&+ \mathbb{E}[(m_f^{o} \beta_r) | (\tilde{s}, \tilde{c}_r) \in \Omega_4] \mathbf{Pr}((\tilde{s}, \tilde{c}_r) \in \Omega_4)
\end{aligned} \tag{2.6}
$$

is the expected marginal benefit of installing an additional unit of recycling capacity for $K_r \in \left[\frac{D_h + D_{nh} - \beta_f K_f}{\beta_r}, \min\left(\beta_h D_h + \beta_{nh} D_{nh}, \frac{D_{nh}}{\beta_r}\right)\right]$, and $\omega_r^2 = -\mathbb{E}_{\tilde{c}_r, \tilde{s}}[m_d \beta_r]$, $\omega_r^1 =$

[3]If $\frac{D_h + D_{nh} - \beta_f K_f}{\beta_r} > \min\left(\beta_h D_h + \beta_{nh} D_{nh}, \frac{D_{nh}}{\beta_r}\right)$, the optimal recycling capacity $K_r^* = 0$ if $\omega_r \geq \omega_r^0$ (ω_r^0 is defined in Proposition 2.2) and $K_r^* = \min\left(\beta_h D_h + \beta_{nh} D_{nh}, \frac{D_{nh}}{\beta_r}\right)$ otherwise.

$-M\left(\frac{D_h+D_{nh}-\beta_f K_f}{\beta_r}\right)$, *and* $\omega_r^0 = -M\left(\min\left(\beta_h D_h + \beta_{nh} D_{nh}, \frac{D_{nh}}{\beta_r}\right)\right)$.

The optimal recycling capacity K_r^* is characterized by comparing the unit capacity cost ω_r with the expected marginal benefit of an additional unit of capacity. In stage 2, the marginal benefit takes different forms as it depends on the rainfall and recycling cost realizations. When $K_r \in \left[\frac{D_h+D_{nh}-\beta_f K_f}{\beta_r}, \min\left(\beta_h D_h + \beta_{nh} D_{nh}, \frac{D_{nh}}{\beta_r}\right)\right]$, the unit marginal benefit depends on whether the additional unit of capacity replaces desalinated water, freshwater in the case of no overflow and freshwater in the case of overflow. For this case, we have $K_f \geq \tau_1(K_r)$, then, for $(s, c_r) \in \Omega_1$, the additional unit of recycling capacity, being a cheaper alternative, helps to replace β_r units of desalinated water, hence the marginal benefit is given by $m_d\beta_r$. For $(s, c_r) \in \Omega_3$ and $(s, c_r) \in \Omega_4$, the additional unit of recycling capacity helps to replace β_r units of freshwater as it has the priority, hence the marginal benefit is given by $m_f^{no}\beta_r$ and $m_f^{o}\beta_r$ as there is no overflow in region Ω_3 and there is overflow in region Ω_4, respectively. For the other regions (i.e., Ω_2, Ω_5 and Ω_6), the freshwater has priority over recycled water, hence the marginal benefit is zero.

When $K_r \in \left[0, \frac{D_h+D_{nh}-\beta_f K_f}{\beta_r}\right)$, we have $K_f < \tau_1(K_r)$. Then, as total demand cannot be met without desalinated water, the additional unit of recycling capacity replaces β_r units of desalinated water for all realizations of $\tilde{s}$ and $\tilde{c}_r$. Thus, the marginal benefit is given by $m_d\beta_r$, which is the same for all $K_r \in \left[0, \frac{D_h+D_{nh}-\beta_f K_f}{\beta_r}\right]$. Hence, $K_r^* = \frac{D_h+D_{nh}-\beta_f K_f}{\beta_r}$ if $\omega_r^1 < \omega_r \leq \omega_r^2$, and $K_r^* = 0$ if $\omega_r > \omega_r^2$.

Remark 1. *The intuition is very similar when* $K_f > \tau_2 = \frac{D_h+D_{nh}}{\beta_f}$ *with one particular exception. In this case, as* $K_f > \tau_2$*, we never have the situation where the total demand cannot be met without desalinated water for all realizations of* s *and* c_r*, thus the discontinuity in the marginal benefit at* $K_r = \frac{D_h+D_{nh}-\beta_f K_f}{\beta_r}$ *is not observed, hence* K_r^* *smoothly decreases with* ω_r*.*

Figure 2.3 illustrates the optimal recycling capacity K_r^*.

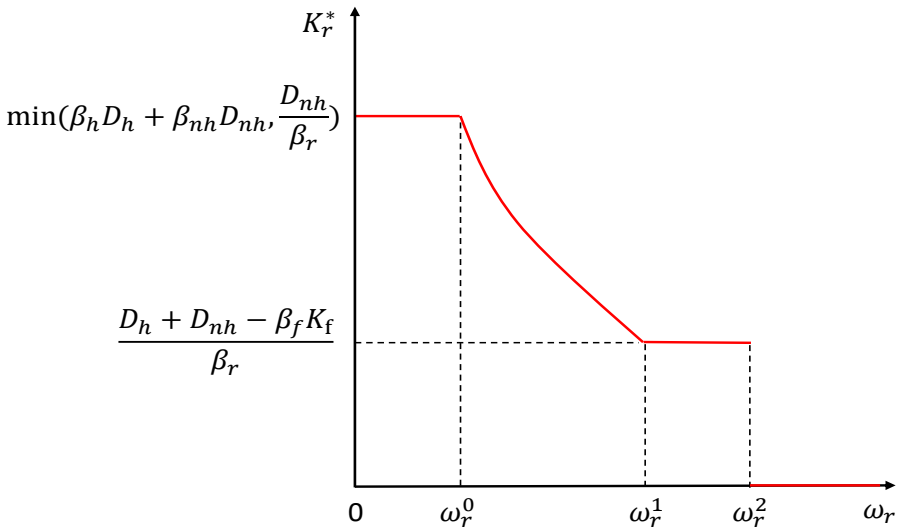

Figure 2.3: Optimal Recycling Capacity

I make an interesting observation about the behavior of K_r with respect to K_f for a given $\omega_r \in (\omega_r^0, \omega_r^2)$ in Corollary 2.1 and Figure 2.4.

Corollary 2.1. *Considering* $\omega_r^0 < \omega_r < \omega_r^2$, K_r^* *linearly decreases in* K_f *if* $\omega_r^1 \leq \omega_r < \omega_r^2$ *and increases in* K_f *if* $\omega_r^0 \leq \omega_r < \omega_r^1$.

Common wisdom may suggest that the optimal recycling capacity K_r^* and freshwater capacity K_f are substitutes. I prove this intuition is correct when K_f is relatively small (i.e., the optimal recycling capacity is set such that the total freshwater and recycling capacity is just enough to meet total demand and hence K_r^* decreases in K_f) by Corollary 2.1. Surprisingly, I also find that these two capacities can be complements when K_f becomes large. This is because, when K_f increases and becomes relatively large, the total freshwater and recycling capacity exceed the total demand. In this regard, which water source should be prioritized to serve the demand affects the capacity investment. Specifically, a larger freshwater capacity implies that the reservoirs' capability of holding the excess rainfall also increases; hence, the risk of overflow decreases. Thus the recycled water can be dispatched as the priority resource to meet the non-household demand in a larger range of rainfall realizations; hence it becomes optimal to increase K_r^* when K_f increases.

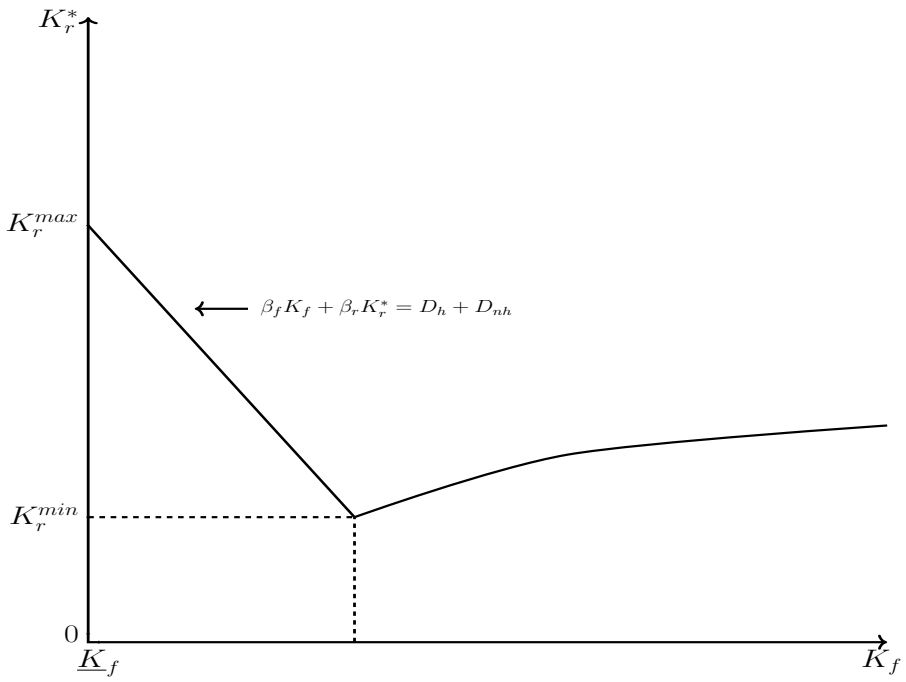

Note: $K_r^{max} = \frac{D_h + D_{nh} - \beta_f \underline{K}_f}{\beta_r}$ and K_r^{min} is the K_r^* when K_f makes $\omega_r = \omega_r^1$, respectively.

Figure 2.4: Impact of Freshwater Capacity On the Optimal Recycling Capacity

2.3.3 The Impacts of the Uncertainties

In this section, I investigate how the rainfall and recycling cost variabilities (σ_s and σ_c) and their correlation (ρ) affect the optimal expected cost V^* and the optimal recycling capacity K_r^*. Throughout this section, I assume $(\tilde{s}, \tilde{c}_r)$ follow a bivariate Normal distribution. I also assume that the freshwater capacity is larger than the expected amount of freshwater (i.e., $K_f \geq \mu_s$) and the expected amount of freshwater is insufficient to satisfy all household demand on expectation, i.e., $D_h \geq \beta_f \mu_s$. These assumptions are reasonable and validated by the practical data presented in Chapter 3.

I first characterize how the thresholds ω_r^0, ω_r^1 and ω_r^2 change with the variabilities and correlation in Lemma 2.1.

Lemma 2.1. *(1) ω_r^2 is independent of σ_s, σ_c and ρ;*

(2) ω_r^0 and ω_r^1 increase in ρ and decrease in σ_s;

(3) ω_0 and ω_1 increase in σ_c if $\mu_c \leq (c_f - o_f)\frac{\beta_r}{\beta_f}$ or $\rho \geq 0$; otherwise, there exists a threshold $\hat{\sigma}_c(K_f)$ such that the thresholds decrease in σ_c on $(0, \hat{\sigma}_c(K_f))$ and increase in σ_c on $[\hat{\sigma}_c(K_f), +\infty)$.

Following the results in Lemma 2.1, I show the global effects of ρ, σ_s and σ_c on the optimal expected cost in Proposition 2.3.

Proposition 2.3.A (Rainfall Variability)**.** *V^* increases in σ_s.*

Proposition 2.3.B (Cost Variability)**.**
(1) If $\rho \geq 0$, V^* decreases in σ_c;
(2) Otherwise, (i) if $\mu_c \leq (c_f - o_f)\frac{\beta_r}{\beta_f}$, V^* decreases in σ_c; (ii) if $\mu_c > (c_f - o_f)\frac{\beta_r}{\beta_f}$, there exists a threshold $\bar{\sigma}_c(K_f)$ such that V^* increases in σ_c for $\sigma_c \in (0, \bar{\sigma}_c(K_f))$ and decreases in σ_c for $\sigma_c \in [\bar{\sigma}_c(K_f), +\infty)$.

Proposition 2.3.C (Correlation)**.** *V^* decreases in ρ.*

Proposition 2.3.C demonstrates that a higher correlation is always (weakly) beneficial as it reduces the optimal expected cost. When the investment cost is high (e.g., $\omega_r \geq \omega_r^1$), the optimal recycling capacity is either $\frac{D_h + D_{nh} - \beta_f K_f}{\beta_r}$ or 0, which implies that either the recycling capacity is fully utilized or recycling is not used at all. In both cases, the optimal water allocation and the optimal expected cost are independent of the correlation ρ. If the unit recycling capacity cost is moderate, e.g., $\omega_r \in (\omega_r^0, \omega_r^1)$, the optimal expected cost decreases in ρ. The intuition is as follow: a higher ρ makes it more likely for the rainfall to be small (large) when the recycling cost c_r is low (high). Recycled water becomes more likely to be the priority resource to be dispatched when the recycling cost is low, resulting in the negative impact of the small rainfall to be mitigated. Similarly, freshwater becomes more likely to be the priority resource to be dispatched when the recycling cost is high, resulting in the negative impact of a high recycling cost to be mitigated as the amount of recycled

water dispatched is low. This also helps to reduce the overflow cost as the amount of freshwater dispatched will more likely be high when the rainfall is also large.

Proposition 2.3.A shows that a higher rainfall variability (σ_s) is undesirable as it may increase the optimal expected cost. High and low rainfall realizations become more likely with an increase in σ_s. A low rainfall realization is always detrimental (i.e., the expected cost is higher), while a high rainfall realization could be beneficial as long as it does not result in overflow. Specifically, with an increase in σ_s, the expected overflow cost and the expected cost of replacing recycled water with freshwater to prevent overflow increases as it is more likely to have high rainfall realizations; In addition, the expected amount of desalinated water used, hence, the expected cost increases as well because it is also more likely to have low rainfall realizations.

Proposition 2.3.B demonstrates that the impacts of recycling cost variability (σ_c) on the optimal expected cost depends on the average recycling cost (μ_c) and the correlation (ρ). High and low recycling cost realizations become more likely with an increase in σ_c. A lower recycling cost (c_r) is always beneficial as it reduces the expected cost and a higher c_r is undesirable as it increases the expected cost. However, when the correlation ρ is positive, a high c_r realization is more likely to be associated with a high rainfall realization, indicating that the likelihood of using recycled water as the priority source decreases and hence weakens the negative effect on the expected cost. Therefore, the optimal expected cost decreases. When the correlation is negative, a high (low) c_r is more likely to be associated with a low (high) rainfall realization. In this case, when the rainfall realization is low, recycled water is more likely to be prioritized to meet the demand. As c_r is high, the expected cost increases. When the rainfall realization is high, it is more likely to have a low c_r, which is beneficial. Moreover, if c_r is sufficiently small to make the recycling water as the priority source (i.e., the likelihood of being in region Ω_4 is high enough), the benefit from a lower c_r is sufficiently large and tends to dominate the negative effect from a higher c_r. In this

regard, the optimal expected cost decreases in the recycling cost variability. Moreover, I identify that the likelihood of being in region Ω_4 is high enough if $\mu_c \leq (c_f - o_f)\frac{\beta_r}{\beta_f}$ or if $\mu_c > (c_f - o_f)\frac{\beta_r}{\beta_f}$ and σ_c is high enough, i.e., $\sigma_c \in [\bar{\sigma}_c(K_f), +\infty)$. Otherwise, if $\mu_c > (c_f - o_f)\frac{\beta_r}{\beta_f}$ and σ_c is low, i.e., $\sigma_c \in [0, \bar{\sigma}_c(K_f))$, the likelihood of being in region Ω_4 is low, thus the optimal expected cost increases in the recycling cost variability.

I also characterize the impacts of variabilities and correlation on the optimal recycling capacity in Proposition 2.4.

Proposition 2.4.A (Rainfall Variability)**.** *K_r^* decreases in σ_s.*

Proposition 2.4.B (Cost Variability)**.**

(1) If $\rho \geq 0$, K_r^* increases in σ_c;

(2) Otherwise, (i) if $\mu_c \leq (c_f - o_f)\frac{\beta_r}{\beta_f}$, K_r^* increases in σ_c; (ii) if $\mu_c > (c_f - o_f)\frac{\beta_r}{\beta_f}$, there exists a threshold $\hat{\sigma}_c(K_f)$ such that K_r^* decreases in σ_c for $\sigma_c \in (0, \hat{\sigma}_c(K_f))$ and increases in σ_c for $\sigma_c \in [\hat{\sigma}_c(K_f), +\infty)$.

Proposition 2.4.C (Correlation)**.** *K_r^* increases in ρ.*

Proposition 2.4.A shows that the optimal recycling capacity decreases in the rainfall variability (σ_s). The influence of σ_s on K_r^* is determined by its effect on the expected marginal cost $M(K_r)$. Marginal cost of an additional unit of recycling capacity is nonzero only in regions Ω_1, Ω_3 and Ω_4. Remember that I assume $D_h \geq \beta_f \mu_s$ in this section, which implies that $\tau_1(K_r) > \mu_s$. An increase in the rainfall variability σ_s would make low and high rainfall realizations more likely. As $\tau_1(K_r) > \mu_s$, it is less likely to have rainfall realizations smaller than $\tau_1(K_r)$ and more likely to have rainfall realizations larger than $\tau_1(K_r)$. This means that probability of having a rainfall realization in region Ω_1 decreases and probability of having a rainfall realization in all the other regions increases. This increases the likelihood of using freshwater as the priority source when the recycling cost is larger than $(c_f - o_f)\frac{\beta_r}{\beta_f}$ ($c_f \frac{\beta_r}{\beta_f}$) when there is

(no) risk of overflow. As a result, with a higher σ_s, the expected marginal cost $M(K_r)$ increases and thus, the optimal recycling capacity decreases in the rainfall variability.

Structurally similar to the results characterized in Proposition 2.3.B, Proposition 2.4.B shows that the impact of recycling cost variability (σ_c) on the optimal recycling capacity (K_r^*) also depends on the correlation (ρ) and the average recycling cost (μ_c). To provide the intuition, we know that a higher σ_c implies that it is more likely to have high and low recycling cost realizations (c_r). A low c_r is beneficial as it decreases the marginal cost. A high c_r is undesirable as it increases the marginal cost but it is less consequential because a high c_r is more likely to be associated with a high rainfall when the correlation ρ is positive, and thus the likelihood of using recycled water as the priority source decreases. Hence, the marginal cost decreases and then the recycling capacity increases as σ_c increases when the correlation is positive. When the correlation coefficient ρ is negative, the impact of recycling cost variability (σ_c) on the optimal recycling capacity can be explained following the intuitions that used to explain Proposition 2.3.B.

Proposition 2.4.C shows that the optimal recycling capacity increases in the correlation coefficient. As discussed earlier, a high ρ makes it more likely that when the rainfall s is low (high), the recycling cost c_r is low (high). When the rainfall s is low, recycled water becomes more likely to be the priority resource to be dispatched and as the recycling cost is also low, the expected marginal cost decreases. When the amount of rainfall s is high, the likelihood of using recycled water as the priority source decreases thus a high recycling cost is less consequential. As a result, the expected marginal cost $M(K_r)$ decreases in the correlation; hence, the optimal recycling capacity increases in the correlation.

2.3.4 Water Leakage Reduction

In practice, in addition to treatment losses, a significant amount of water is lost in urban water supply systems through leakage. There are above 32 billion cubic meters of water leak from the urban water systems annually worldwide (Liemberger et al. 2006). Water leakage has been a critical issue for sustainable urban water management. The model in this work can incorporate leakage through the recovery ratios; hence, throughout this text, I use $1-\beta_f$, $1-\beta_r$ and $1-\beta_d$ to denote the effective freshwater, recycled water and desalinated water leakage ratios, respectively. In this section, my objective is to understand how leakage ratios affect the optimal expected cost. This analysis can provide urban water utilities insightful knowledge on which leakage ratio should be reduced in priority under limited maintenance resources. Without loss of generality, I normalize the costs of reducing the recycled water leakage ratio (i.e., $(1-\beta_r)$) and the potable water leakage ratio (i.e., $(1-\beta_f)$) to zero in this section. To characterize the global effects of reducing leakage ratios on the optimal expected cost, I first present the following results.

Lemma 2.2.

(1) ω_r^2 is independent of β_f and increases in β_r;

(2) ω_r^1 increases in β_r and decreases in β_f.

Based on the results in Lemma 2.2, I then characterize the global effects in Proposition 2.5.

Proposition 2.5.

(1) V^* decreases in β_f and β_r;

(2) If $\omega_r \geq \omega_r^2$, V^* is independent of β_r and it is always more beneficial to increase β_f in priority;

(3) If $\omega_r^1 \leq \omega_r < \omega_r^2$, it is better to increase β_f in priority if $\beta_f \geq C(\beta_r)$ and to

increase β_r in priority otherwise, where

$$C(\beta_r) = \frac{D_h + D_{nh}}{K_f} - \frac{(\omega_r - \omega_r^2)\beta_r}{\mu_c + \omega_r} - \frac{\underset{\tilde{c}_r,\tilde{s}}{\mathbb{E}}[\min(K_f, \tilde{s})]c_d\beta_r^2}{K_f(\mu_c + \omega_r)}$$

Proposition 2.5 shows that reducing the freshwater and recycled water leakage ratios (i.e., increasing β_f and β_r) is always (weakly) beneficial to the urban water utility as it reduces the expected cost. However, interestingly, Proposition 2.5 also shows that reducing water leakage can be inconsequential. Specifically, when the unit investment cost ω_r is very high (i.e., $\omega_r \geq \omega_r^2$), the optimal expected cost is independent of β_r and decreasing in β_f. In this case, no recycled water is dispatched; hence, the optimal expected cost is independent of β_r. As β_f increases, the effective amount of freshwater dispatched (i.e., $\beta_f q_r^*$) increases and then the expected amount of desalinated water decreases; hence, the optimal expected cost decreases. When ω_r decreases (i.e., $\omega_r^1 \leq \omega_r < \omega_r^2$), recall that under this case, the effective capacities $\beta_f K_f$ and $\beta_r K_r$ are enough to meet the total demand. As β_r and β_f increase, the effective amounts of both freshwater and recycled water increase; hence, less desalinated water is supplied, which reduces the cost.

When ω_r becomes even smaller (i.e., $\omega_r < \omega_r^1$), as β_f increases, less freshwater and less desalinated water are expected to be dispatched, which reduces the expected cost. Although the expected overflow cost may increase, the total expected cost decreases if the unit overflow cost is less than the unit freshwater treatment cost ($o_f \leq c_f$). If $o_f > c_f$, then the region Ω_4 in Figure 2.2 does not exist; thus, the freshwater is always prioritized when there is overflow, suggesting that overflow cost does not change; hence, the total expected cost decreases as less recycled water is expected to be used when β_f increases. Similarly, as β_r increases, less desalinated water is expected to be dispatched, which then reduces the total expected cost. On the other hand, less recycled water is expected to be used when freshwater is prioritized (i.e., freshwater is more beneficial), which also reduces the total expected cost. If the recycled water is prioritized (i.e., recycled water is more beneficial), less freshwater is

expected; moreover, the potential increase of overflow cost (if any) is offset by the cost reduction, which follows from the discussions above. Therefore, the optimal expected cost decreases as β_r increases. From these discussions, I can explain why the optimal expected cost V^* decreases in β_f and β_r in each piece. Although the cut-off points ω_r^2 and ω_r^1 may be affected by β_f and β_r, I find that the insights also hold globally.

In Proposition 2.5, I also find that, if $\omega_r \geq \omega_r^2$, it is always more beneficial to reduce freshwater leakage ratio in priority. If $\omega_r^1 \leq \omega_r < \omega_r^2$, given β_r, it is optimal to increase β_f in priority if β_f is larger than a certain threshold $C(\beta_r)$; otherwise, it is optimal to increase β_r in priority. These results provide managers with insights to prioritize water leakage reduction between potable water and recycled water. However, for the case that $\omega_r < \omega_r^1$, as the comparison between the benefits of reducing freshwater and recycled water leakage is too complex, I numerically characterize the priority on reducing water leakage ratios in Chapter 3.

2.3.5 Urban Water Vulnerability

Water supply vulnerability is a critical performance measure for urban water sustainability. The urban water vulnerability, in general, reflects the extent to which the water sources (the last resort is excluded) are failed to meet the urban water demand. Hence, it can be also seen as a measure of the service level of the urban water system. In my context, as the desalinated water/imported water serves as the last resort to satisfy the urban water demand, then the vulnerability can be measured by the expected amount of desalinated water used. The higher the expected amount of desalinated water is used, the higher the system vulnerability. Hence, understanding how the expected amount of desalinated water dispatched changes with the variabilities and other key factors is critical for urban water sustainability. I first characterize the expected amount of desalinated water dispatched (denoted by DW)

under different scenarios as follows.

$$\mathrm{DW}(\omega_r) = \mathop{\mathbb{E}}_{\tilde{c}_r,\tilde{s}}[D_h + D_{nh} - \beta_f q_f^* - \beta_r q_r^*]$$

$$= \begin{cases} D_h + D_{nh} - \beta_f \mathop{\mathbb{E}}_{\tilde{s}}[\min(\tilde{s}, K_f)], & \text{if } \omega_r \geq \omega_r^2 \\ \beta_f \mathop{\mathbb{E}}_{\tilde{s}}[(K_f - \tilde{s})^+], & \text{if } \omega_r^1 \leq \omega_r < \omega_r^2 \\ \mathop{\mathbb{E}}_{(\tilde{c}_r,\tilde{s})\in\Omega_1} \left[D_h + D_{nh} - \beta_f \tilde{s} - \beta_r K_r^*\right], & \text{if } \omega_r^0 \leq \omega_r < \omega_r^1 \\ \mathop{\mathbb{E}}_{(\tilde{c}_r,\tilde{s})\in\Omega_1} \left[D_h + D_{nh} - \beta_f \tilde{s} - \beta_r \min\left(\beta_h D_h + \beta_{nh} D_{nh}, \frac{D_{nh}}{\beta_r}\right)\right], & \text{if } \omega_r < \omega_r^0 \end{cases} \tag{2.7}$$

When the unit capacity investment cost is very large (i.e., $\omega_r \geq \omega_r^2$), the optimal recycling capacity is $K_r^* = 0$; hence, the expected amount of desalinated water dispatched is the remaining demand unfulfilled by freshwater. When $\omega_r^1 \leq \omega_r < \omega_r^2$, the optimal recycling capacity is set in such a way that K_r^* together with K_f is able to meet all demand (i.e., $K_r^* = \frac{D_h + D_{nh} - \beta_f K_f}{\beta_r}$). Therefore, DW is characterized by $\beta_f \mathop{\mathbb{E}}_{\tilde{s}}[(K_f - \tilde{s})^+]$. For other cases, depending on the value of the optimal recycling capacity, I derive DW accordingly.

Corollary 2.2. *$DW(\omega_r)$ increases in ω_r.*

Corollary 2.2 shows that the expected amount of desalinated water dispatched increases in the unit recycling capacity investment cost ω_r. This is because, as ω_r increases, the optimal recycling capacity decreases and the expected amount of recycled water dispatched decreases; hence, the expected amount of desalinated water dispatched increases.

In Proposition 2.6, I show how the freshwater capacity K_f affects DW globally. Before that, I characterize how the cut-off points ω_r^2, ω_r^1 and ω_r^0 change with K_f in Lemma 2.3.

Lemma 2.3.

(1) ω_2 is independent of K_f;

(2) ω_0 and ω_1 increase in K_f.

Proposition 2.6. *As K_f increases*

(1) If $\omega_r \geq \omega_r^2$, DW decreases;

(2) If $\omega_r^1 \leq \omega_r < \omega_r^2$, there exists a threshold $\bar{\omega}_r = \omega_r^1\Big|_{K_f=(D_h+D_{nh})/\beta_f}$ such that

(2.1) If $\bar{\omega}_r \leq \omega_r < \omega_r^2$, DW increases;

(2.2) Otherwise, there exists a threshold $\bar{K}_f$ such that DW increases on $(s_0, \bar{K}_f)$ and decreases on $[\bar{K}_f, (D_h + D_{nh})/\beta_f]$.

(3) Otherwise, DW decreases.

When the unit capacity investment cost is very large (i.e., $\omega_r \geq \omega_r^2$), no recycled water is dispatched to meet the demand. In this case, an increase in K_f implies that more freshwater is expected to be dispatched to meet the demand; hence, less desalinated water is required.

When the investment cost becomes relatively small (i.e., $\bar{\omega}_r \leq \omega_r < \omega_r^2$), interestingly, I find that DW increases in K_f. This is because, as K_f increases, more freshwater is expected to be dispatched; however, less recycled water is expected to be supplied as $K_r^* = \frac{D_h+D_{nh}-\beta_f K_f}{\beta_r}$ decreases. Specifically, since the realized rainfall may be less than the freshwater capacity, the increase in potable water does not exceed β_f units from an additional unit of freshwater capacity; however, each unit increase in freshwater capacity reduces β_f units of recycled water. Hence, the reduction of recycled water cannot be offset by the increased potable water, then more desalinated water is required. Although ω_r^1 increases in K_f, by the definition of $\bar{\omega}_r$, I know that $\omega_r < \omega_r^1$ is impossible as K_f increases. Hence, just as described in Proposition 2.6, I characterize the global effect for this case. However, when $\omega_r^1 \leq \omega_r < \bar{\omega}_r$, I find that DW first increases, which follows from the discussions above directly, and then decreases in K_f. The decreasing pattern is because, when K_f is sufficiently large, ω_r^1

becomes larger than ω_r such that the optimal recycling capacity becomes an interior solution. In this case, K_r^* increases in K_f; hence, less desalinated water is expected.

When the investment cost becomes further small (i.e., $\omega_r^0 \leq \omega_r < \omega_r^1$ initially), the optimal recycling capacity K_r^* is an interior solution. For this case, K_r^* increases in K_f. Hence, as I discussed, more potable water and recycled water are used and then DW decreases. As K_f increases, ω_r^0 increases, which may lead ω_r to be smaller than ω_r^0. Then, $K_r^* = \min\left(\beta_h D_h + \beta_{nh} D_{nh}, \frac{D_{nh}}{\beta_r}\right)$ is independent of K_f. Combining these cases and following the arguments above, more freshwater and recycled water are expected to be dispatched. Therefore, less desalinated water is needed.

In this section, I also investigate the impacts of variabilities and correlation on the expected amount of desalinated water dispatched. The global effects are characterized in Proposition 2.7.

Proposition 2.7.A (Correlation)**.** *DW decreases in ρ.*

Proposition 2.7.B (Rainfall Variability)**.** *DW increases in σ_s.*

Proposition 2.7.C (Cost Variability)**.**
(1) if $\mu_c \leq (c_f - c_o)\frac{\beta_r}{\beta_f}$ or $\rho \geq 0$, DW decreases in σ_c;
(2) otherwise, there exists a threshold $\hat{\sigma}_c$ such that DW increases in σ_c for $\sigma_c \in (0, \hat{\sigma}_c)$ and decreases in σ_c for $\sigma_c \in [\hat{\sigma}_c, +\infty)$.

When σ_s increases, it is more likely to have extremely high and low rainfall realizations, which implies that the probability of dispatching desalinated water increases. Then, more desalinated water is expected to be dispatched to satisfy demand.

I find that DW decreases in the correlation. First, the expected amount of freshwater dispatched is independent of the correlation. When $\omega_r \geq \omega_r^1$, $K_r^* = 0$ or $\frac{D_h + D_{nh} - \beta_f K_f}{\beta_r}$. In this regard, the amount of recycled water dispatched is also not affected by the correlation. Then, DW is independent of the correlation. As ρ increases, ω_r^1 and ω_r^0 become larger, leading ω_r to be less than ω_r^1 and even less than ω_r^0. If the

increase of ρ makes $\omega_r^0 \leq \omega_r < \omega_r^1$, K_r^* is then an interior solution and increases in the correlation coefficient; hence, more recycled water is expected to be dispatched, and less desalinated water is required. If $\omega_r < \omega_r^0$ happens, K_r^* is independent of the correlation such that the expected amount of recycled water and DW are also independent of the correlation. Then, I can conclude that DW decreases in ρ for this case. For the case that $\omega_r < \omega_r^1$, the decrease of DW in ρ can be explained similarly. Therefore, DW decreases in ρ globally.

Similarly, the impact of σ_c on DW is through the optimal recycling capacity. When σ_c increases, if K_r^* increases, more recycled water and less desalinated water are dispatched; otherwise, less recycled water and more desalinated water are expected to be dispatched. In Proposition 2.4.B, I characterize how the cost variability affects the optimal recycling capacity. Therefore, I derive the impact of cost variability on DW as characterized in Proposition 2.7.

2.3.6 Overflow Risk

Overflow risk is also an important criterion to measure the sustainability of urban water systems as it reflects the ability for the urban water system to adapt to extreme rainfall realizations. This section evaluates the overflow risk under the optimal framework and discusses how the overflow risk is affected by the key factors. Depending on the unit investment cost, the overflow risk PO is characterized as follows.

$$\mathrm{PO}(\omega_r) = \begin{cases} \mathbf{Pr}(\underline{c}_r \leq \tilde{c}_r \leq \bar{c}_r, \tilde{s} \geq 2K_f), & \text{if } \omega_r \geq \omega_r^1 \\ \mathbf{Pr}((c_f - o_f)\frac{\beta_r}{\beta_f} \leq \tilde{c}_r \leq \bar{c}_r, \tilde{s} \geq 2K_f) & \\ \quad + \mathbf{Pr}(\underline{c}_r \leq \tilde{c}_r < (c_f - o_f)\frac{\beta_r}{\beta_f}, \tilde{s} \geq K_f + \tau_1(K_r^*)), & \text{if } \omega_r < \omega_r^1 \end{cases}$$

This is because $K_r^* = 0$ or $\frac{D_h + D_{nh} - \beta_f K_f}{\beta_r}$ if $\omega_r \geq \omega_r^1$, K_r^* is an interior solution if $\omega_r^0 < \omega_r < \omega_r^1$ and $K_r^* = \min\left(\beta_h D_h + \beta_{nh} D_{nh}, \frac{D_{nh}}{\beta_r}\right)$ otherwise. Moreover, $\tau_1(K_r^*) = \frac{D_h + D_{nh} - \beta_r K_r^*}{\beta_f}$. It is easy to show that $\mathrm{PO}(\omega_r)$ decreases in ω_r as a larger ω_r leads to

a smaller recycling capacity; hence, more freshwater is expected to be used, which reduces the overflow risk. I show the global effect of the rainfall variability on the overflow risk in Proposition 2.8

Proposition 2.8 (Rainfall Variability)**.** *PO increases in* σ_s*.*

I find that, as the rainfall variability σ_s increases, the overflow risk increases as it is more likely to have extreme high amount of rainfall realization.

For the ease of exposition, I characterize the local effects of cost variability and freshwater capacity on the overflow risk in Proposition 2.9 (global effects are presented in Appendix B).

Proposition 2.9.A (Cost Variability)**.**

(1) If $\omega_r < \omega_r^0$*, PO increases in* σ_c *if* $\mu_c > (c_f - c_o)\frac{\beta_r}{\beta_f}$ *and decreases in* σ_c *otherwise;*

(2) If $\omega_r \geq \omega_r^1$*, PO is independent of* σ_c*;*

(3) Otherwise

(3.1) if $\mu_c \leq (c_f - c_o)\frac{\beta_r}{\beta_f}$*, PO increases in* σ_c *if* $\frac{dK_r^*}{d\sigma_c} \geq B$ *and decreases in* σ_c *otherwise;*

(3.2) if $\mu_c > (c_f - c_o)\frac{\beta_r}{\beta_f}$

(3.2.1) if $\rho \geq 0$*, PO increases in* σ_c*;*

(3.2.2) if $\rho < 0$*, (i) if* $\sigma_c > \hat{\sigma}_c$*, PO increases in* σ_c*; (ii) if* $\sigma_c \leq \hat{\sigma}_c$*, PO increases in* σ_c *if* $\frac{dK_r^*}{d\sigma_c} \geq B$ *and decreases in* σ_c *otherwise.*

where

$$B = \frac{\beta_f \sigma_s (B_2 - B_1)((c_f - o_f)\frac{\beta_r}{\beta_f} - \mu_c)}{\sigma_c^2 \beta_r B_3}$$

$$B_1 = \int_{\frac{2K_f - \mu_s}{\sigma_s}}^{+\infty} \phi\left(\frac{(c_f - o_f)\frac{\beta_r}{\beta_f} - \mu_c - \rho\sigma_c\tilde{z}_1}{\sigma_c\sqrt{1-\rho^2}}\right)\phi(\tilde{z}_1)d\tilde{z}_1$$

$$B_2 = \int_{\frac{K_f + \tau_1(K_r^*) - \mu_s}{\sigma_s}}^{+\infty} \phi\left(\frac{(c_f - o_f)\frac{\beta_r}{\beta_f} - \mu_c - \rho\sigma_c\tilde{z}_1}{\sigma_c\sqrt{1-\rho^2}}\right)\phi(\tilde{z}_1)d\tilde{z}_1$$

$$B_3 = \int_{-\infty}^{\frac{(c_f - o_f)\frac{\beta_r}{\beta_f} - \mu_c}{\sigma_c}} \phi\left(\frac{K_f + \tau_1(K_r^*) - \mu_s - \rho\sigma_s\tilde{z}_0}{\sigma\sqrt{1-\rho^2}}\right)\phi(\tilde{z}_0)d\tilde{z}_0$$

Proposition 2.9.B (Freshwater Capacity)**.**

(1) If $\omega_r \geq \omega_r^1$*, PO decreases in* K_f*;*

(2) If $\omega_r^0 < \omega_r < \omega_r^1$*, PO decreases in* K_f *if*

$$\frac{dK_r^*}{dK_f} \leq \frac{\beta_f}{\beta_r} + \frac{2\beta_f \int_{(c_f-o_f)\frac{\beta_r}{\beta_f}}^{\bar{c}_r} \psi(2K_f, \tilde{c}_r)d\tilde{c}_r}{\beta_r \int_{\underline{c}_r}^{(c_f-o_f)\frac{\beta_r}{\beta_f}} \psi(K_f + \tau_1(K_r^*), \tilde{c}_r)d\tilde{c}_r}$$

and increases otherwise;

(3) If $\omega_r < \omega_r^0$*, PO decreases in* K_f*.*

I find that, when ω_r is very large, PO is independent of σ_c. This is because, no matter what the recycling cost is, either no recycled water is dispatched or the recycling plant is operating under full capacity in this case; hence, the overflow risk is not affected by the cost variability. When the unit investment cost becomes smaller (i.e., $\omega_r^0 < \omega_r < \omega_r^1$), the optimal recycling capacity is an interior solution. Depending on the realization of the recycling cost, the optimal amount of recycled water dispatched may be different, which will affect the overflow cost. When $\mu_c \leq (c_f - c_o)\frac{\beta_r}{\beta_f}$, one the one hand, the optimal recycling capacity increases in σ_c; hence, less freshwater is expected to be dispatched and then the overflow risk increases; on the other hand, the probability that the recycling cost falls in the regions that recycled water is dispatched in priority decreases in σ_c, which implies that less recycled water and more freshwater are expected to be dispatched. Therefore, if the optimal recycling capacity increases fast enough, i.e., $\frac{dK_r^*}{d\sigma_c} \geq B$, PO increases in σ_c; otherwise, PO decreases in σ_c. If $\mu_c > (c_f - c_o)\frac{\beta_r}{\beta_f}$ and $\rho \geq 0$, the optimal recycling capacity increases in σ_c. In addition, the probability that the recycling cost falls in the regions in which recycled water is dispatched in priority increases in σ_c. As ρ is positive, a low recycling cost is more likely to be associated with a low rainfall; hence, more recycled water and less freshwater are expected to be dispatched. Then, the overflow risk increases as σ_c increases. If $\mu_c > (c_f - c_o)\frac{\beta_r}{\beta_f}$ and $\rho < 0$, the results can be explained similarly. When ω_r is very small, i.e., $\omega_r < \omega_r^0$, the optimal recycling capacity is independent of σ_c.

The results can also be explained by using the intuitions explained above.

I also find that PO decreases in K_f if $\omega_r \geq \omega_r^1$ or $\omega_r < \omega_r^0$ as a larger K_f implies that more freshwater is expected to be dispatched in this case. However, when $\omega_r^0 < \omega_r < \omega_r^1$, the change of K_f also affects the optimal recycling capacity, which then changes the expected amount of recycled water dispatched. Specifically, for this case, the optimal recycling capacity increases in K_f. On the one hand, a larger K_f implies that more freshwater is dispatched. Then, the overflow risk decreases; on the other hand, the increase of K_r^* implies that more recycled water is expected to be dispatched, then the overflow risk increases. Therefore, as K_f increases, if the optimal recycling capacity does not increase too much, i.e., $\frac{dK_r^*}{dK_f}$ is less than the threshold characterized, then PO decreases in K_f; otherwise, PO increases in K_f.

I numerically show the impact of ρ on the overflow risk under different cases and compare the overflow risk I obtained with the overflow risk under the benchmark case (the case that water recycling is unavailable) in Chapter 3.3.6.

2.4 Conclusion

Urban water scarcity becomes increasingly severe globally, which makes sustainable urban water management more imperative and critical. This chapter investigates the economic and sustainable implications of wastewater recycling capacity investment in an urban water system under rainfall and recycling cost uncertainties. Formulating the problem as a two-stage stochastic model, I characterize the most cost-effective water allocation scheme and the optimal recycling capacity. I show that the optimal recycling capacity and the freshwater treatment capacity could be substitutes or complements depending on the level of the freshwater treatment capacity. I also discuss the impacts of rainfall and recycling cost variabilities and their correlation on the optimal expected cost and recycling capacity in this chapter. My results show

that a larger correlation benefits the system, while increased rainfall variability is detrimental to the system. The impact of recycling cost variability depends on the mean value of recycling cost and the correlation. Moreover, in this chapter, I further investigate the sustainability of the integrated urban water system focusing on the vulnerability and the overflow risk, reflecting the reliability of hedging climate change risks. I discuss how the uncertainties and other key factors such as freshwater capacity affect the water supply vulnerability and the overflow risk in this chapter. These results are beneficial for an urban water utility that is interested in increasing water sustainability under uncertainties.

Nevertheless, this work does have few limitations, which suggest several future research directions. In this research, I consider a deterministic demand setting to derive the urban water management insights under supply uncertainty from climate change. In practice, the demand can also be affected by climate change and can be uncertain. Hence, capturing the demand uncertainty in the model and investigating how the demand uncertainty affects urban water operations can be an important and interesting research problem. Second, in some cities, wastewater has been recycled into potable water. It is interesting to investigate how incorporating this feature can affect the recycling decisions and the insights generated in future studies. Third, instead of optimizing the single wastewater recycling capacity, it would be interesting to consider the multiple water source portfolio optimization in the urban water context.

Chapter 3

Wastewater Recycling Capacity Investment In Urban Water Management: A Case Study

In this chapter, I discuss an application of my model in the context of urban water management. I calibrate the model parameters to represent the urban water management practice in Adelaide, the capital city of South Australia and conduct comprehensive numerical experiments to complement the analytical results presented in Chapter 2 and show additional managerial insights on urban water management. Specifically, in Section 3.1 and 3.2, I introduce the background and details of model calibration. Section 3.3 presents the numerical results and Section 3.4 concludes this chapter.

3.1 Practical Setting and Model Calibration

In this work, I apply the model to the urban water management in Adelaide to investigate the impacts of uncertainties on the optimal expected cost, optimal decisions and sustainability measures. I use publicly available data from annual National Performance Reports: Urban Water Utilities[1] and National Water Account published

[1]For the National Performance Reports: Urban Water Utilities, it should be noted that the data is reported for Adelaide only before the Year of 2013. After this year, the data is reported for entire South Australia. Hence, to exclude the potential heterogeneous effects from other regions of

by the Australia Bureau of Meteorology (ABM), complemented by the data obtained from the extant literature and technical reports. Before the estimation of parameters, I first introduce the urban water supply practice in Adelaide.

3.1.1 Adelaide Urban Water Supply Practice

In Adelaide, the urban water supply is managed by SA Water, which is a government-owned water utility. Multiple water sources, including surface water from reservoirs, recycled water and desalinated seawater, are supplied to meet the urban water demand. Specifically, ten major reservoirs supply water to urban areas in Adelaide with a total storage capacity of about 192.4 GL (billion litres). The total surface area of these reservoirs is 18.93 km^2 (square kilometer). Surface water from the reservoirs undergoes a series of treatments at water treatment plants and is distributed to customers. Six large conventional water treatment plants serve metropolitan Adelaide, with the largest one of treatment capacity more than 300 GL water per year. Water may also be imported from River Murray to the reservoirs under a certain contract if necessary.

In Adelaide, seawater may be desalinated and mixed with the treated freshwater to meet the urban demand. The desalination plant uses the reverse osmosis (RO) technique, and the capacity is 100 GL per year. Due to the high operating and energy costs, the plant works primarily as a backup supply during drought years with low rainfall and/or high demand.

Wastewater is also recycled to a high-quality level for non-household use in Adelaide. Sewerage is transported to and treated at three major metropolitan coastal wastewater treatment plants (WWTPs) at Bolivar, Glenelg and Christies Beach in Adelaide. At WWTPs, wastewater is treated via a multi-stage treatment process

South Australia, without other specifications, I use the data before 2013 when the data has to been extracted from the National Performance Reports, which is from Australia Bureau of Meteorology (2014).

before being discharged into the environment or further recycled. In Adelaide, this is generally a two-stage process involving primary and secondary treatments. Primary treatment removes most of the remaining particulate matter, involving comminution if necessary, followed by coagulation and/or flocculation before sedimentation. Secondary treatment involves a range of aerobic biological processes aiming to metabolize the dissolved or suspended organic matter microbially. Secondary treatment processes usually consist of aerated activated sludge basins with return activated sludge or fixed media filters with recycling flow, followed by solids separation via settling or membrane filtration and disinfection. After secondary treatment, wastewater can be discharged. The secondary effluent that is not discharged is diverted to wastewater recycling plants for tertiary treatment (in the main text, it is termed as recycling processes and I will use recycling and tertiary treatment interchangeably).

Tertiary treatment targets the further removal of nutrients and organic constituents, reducing total dissolved solids or salinity, and providing additional treatment barriers to pathogens. Approximately 30% of the wastewater treated at SA Water's WWTPs is used in recycled water applications. The current wastewater recycling capacity is 74 GL/year. In general practice, depending on the wastewater recycling criteria, budget, environmental standards and other factors, different technologies are applied in tertiary treatment, e.g., microfiltration (MF) and ultrafiltration (UF) membrane processes, ozone, nanofiltration (NF), and reverse osmosis (RO) technologies. In Adelaide, the Bolivar wastewater recycling plant introduces the Dissolved Air Flotation Filtration (DAFF) technology, which utilizes micro-filtration and floatation to produce Class A recycled water. In Glenelg and other recycling plants, ultrafiltration membrane technology is adopted. The recycled water from the Bolivar wastewater recycling plant is distributed through the Virginia Pipeline Scheme to the Adelaide Plains for unrestricted irrigation of vegetable and salad crops. In contrast, the recycled water from Glenelg is dispatched to irrigate parks, sports

playing fields and other industrial uses.

3.1.2 Parameter Estimation

In this part, I discuss the details about how I estimate the parameters in my model considering the wastewater recycling capacity investment is to be made at the beginning of year 2020 and the length of the single planning period is one year. Throughout this section, I use $\acute{x}$ to denote the calibrated value for parameter x, "NWI"to denote the net water inflow to reservoirs, "GL"to denote a billion litres, "mm"to denote millimeter, "km^2"to denote square kilometer, and "MD"to denote million dollars. I also note that the operating costs include treatment, transportation, labor and other costs.

Calibration for Desalination Cost. The operating cost for desalination is about 21.3 million dollars, and there was 4.23 GL desalinated water supplied in 2011 (Cardno 2013). Hence, the desalination operating cost in 2011 is 5.04 dollars/KL. The average inflation rate (IR) between 2011 and 2020 is about 1.83% per year. I estimate the IR adjusted unit desalination costs in 2020 as $\acute{c}_d = 5.93$ MD/GL[2].

Calibration for Basic Wastewater Treatment Cost. Recall that the basic wastewater treatment cost measures the cost of treated wastewater for disposal. From Australia Bureau of Meteorology (2014), I have the total sewage treatment cost in Adelaide from 2006 to 2012. As the total wastewater collected for treatment at WWTPs in Adelaide is also available, I estimate the basic wastewater treatment cost in Table 3.1

Taking the average of the IR adjusted operating cost in 2020 as the estimate of average basic wastewater treatment cost, I obtain $\acute{c}_b = 1.40$ MD/GL.

[2]I note that the desalination plant in Adelaide is fully completed in 2012; however, I do not have the direct operating cost data of other years. From ABCNEWS (2017), the energy cost of desalination is about 13.5 MD, and the amount of desalinated water dispatched is 4.1 GL. From the Australian Water Association, the energy cost can represent 50%-70% of total operating cost. Taking the average percentage, I then estimate the unit desalination cost in 2016 dollars as 5.48MD/GL, which is very close to 5.93 MD/GL and supports the estimation using data from year 2011.

Year	2006	2007	2008	2009	2010	2011	2012
Total Wastewater Treatment Cost (MD)	85.50	87.49	107.74	101.27	96.59	91.19	111.12
Total Wastewater Collected (GL)	88.96	83.50	83.38	85.12	89.69	88.57	88.49
Basic Wastewater Treatment Cost (MD/GL)	0.96	1.05	1.29	1.19	1.07	1.02	1.26
IR-Adjusted Operating Cost in 2020 (MD/GL)	1.31	1.40	1.64	1.49	1.30	1.20	1.46

Table 3.1: Basic Wastewater Treatment Cost

Calibration for the Amount of Available Freshwater and Recycling Cost Bivariate Distribution Parameters. The amount of available freshwater (AAF) (i.e., $\tilde{s}$) consists of two parts: the deterministic amount of freshwater from reservoirs (i.e., s_0) and the net water inflow (NWI), which is uncertain due to climate change. The variability of recycling cost is from fluctuating energy prices given that wastewater recycling is energy-intensive.

From the National Water Account 2020[3], I set the amount of freshwater available in reservoirs as 98.4 GL for 2020. The urban water management utility keeps the water storage above a minimum level for future consumption in practice. For Adelaide, I take the smallest amount of freshwater available in the past five years as the minimum level, which is about 81.3 GL [4]. In this regard, I estimate the deterministic amount of water available at the beginning of the period as $\acute{s}_0 = 98.4 - 81.3 = 17.1$ GL.

NWI is determined by three components: the direct rainfall precipitation, the rainfall run-off to the reservoirs and the evaporation. First, I estimate the reservoir rainfall precipitation. The annual precipitation to the reservoirs can be calculated by using the total size of reservoirs (denoted by SR km^2) times the annual rainfall amount (i.e., how many millimeters of annual rainfall, denoted by RP mm). I use the

[3] `http://www.bom.gov.au/water/nwa/2020/adelaide/`, accessed by 17/02/2021

[4] The data is retrieved from the website `https://theconversation.com/how-drought-is-affecting-water-supply-in-australias-capital-cities-127909`, accessed by 16/02/2021.

annual rainfall data recorded by ABM from 1884 to 2019. It should be noted that there are multiple weather observation stations in different areas in Adelaide, and the rainfall amount may be different from station to station. Due to the data availability issue, the data from North Adelaide station (represent North Adelaide), Second Valley (Poolamacca) station (represent south Adelaide) and Adelaide (Pooraka) station (represent central Adelaide) are obtained. The rainfall amount for Adelaide then is represented by the average of all the rainfall amounts observed at all stations for each year (see Figure 3.1).

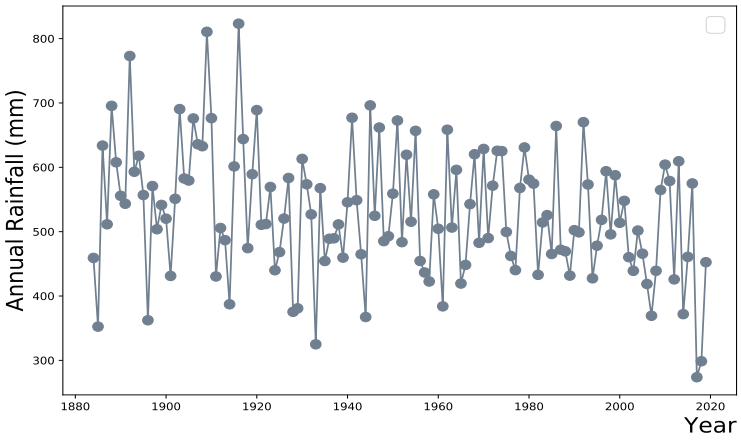

Figure 3.1: Adelaide Annual Rainfall Amount

I then use TRP to denote the annual total rainfall caught by the reservoirs with GL as the metric. Hence

$$\text{TRP(GL)} = \text{SR(km}^2\text{)} \times \text{RP} \times 10^{-6}\text{(km)} \times 10^3$$

In addition to the direct rainfall precipitation, reservoirs also receive surface rainfall run-off from the nearby rainfall catchment areas. Surface rainfall run-off is the flow of water occurring on the ground surface when excess rainwater can no longer sufficiently rapidly infiltrate the soil. According to Alcorn (2006), the relationship between the rainfall and the resultant run-off can be represented by the following formula:

Run-off Coefficient = Mean Annual Run-off (mm)/Mean Annual Rainfall (mm)

In Adelaide, the Run-off Coefficient is ranging from 0.1 to 0.25 (Alcorn 2006). I select

the Run-off Coefficient as 0.175, which is the mean value of 0.1 and 0.25. Therefore, I can derive the Mean Annual Run-off. As I described above, ten reservoirs supply water to urban areas in Adelaide. The catchment area size for Myponga reservoir is 124 km^2, for Mount Bold reservoir is 388 km^2, for (Happy Valley) Clarendon Weir is 54 km^2 (Paton et al. 2013), for Little Para reservoir is 82 km^2 (Hobson et al. 2010), for Kangaroo Creek and Hope Valley reservoir are 280 km^2 and 343 km^2, respectively [5]. The catchment area has a total size of 230 km^2 for Warren, Barossa and South Para reservoirs[6]. Millbrook reservoir has a catchment area of 36.1 km^2 (Nguyen et al. 2017). I then calculate the total size of all catchment areas as SC = 1537.1km^2. Therefore, the annual amount of run-off through catchment areas to the reservoirs (denoted by ROW) is derived by using the Mean Annual Run-off times the size of the water catchment areas, that is

$$\text{ROW(GL)} = \text{SC}(\text{km}^2) \times \text{Mean Annual Run-off} \times 10^{-6}(\text{km}) \times 10^3$$

As for the evaporation, due to data availability and completeness issue, I select the evaporation data from two weather observation stations: Adelaide Airport station and Loxton station. Adelaide Airport station has 35 years of data (from 1982 to 2016, data after 2016 is incomplete), and Loxton station has 32 years of data (from 1985 to 2016). Other stations usually have less than 20 years of data recorded before 2010. I then take the average between values of these two stations of each year to represent the annual evaporation amount (i.e., how many mm water evaporated, see Figure 3.2).

The total evaporation from reservoirs (TEV) is calculated by using the annual evaporation amount (AEA) times the size of the reservoirs (SR).

$$\text{TEV (GL)} = \text{SR}(\text{km}^2) \times \text{AEA} \times 10^{-6}(\text{km}) \times 10^3$$

[5]Retrieved from `http://www.bom.gov.au/water/about/waterResearch/document/torrens.pdf`, accessed by 14/02/2021

[6]Retrieved from `https://www.goyder.sa.gov.au/__data/assets/pdf_file/0019/263332/CLGR_Water_Supply_Project_Draft_Report_Part_1_of_2.pdf`, accessed by 14/02/2021

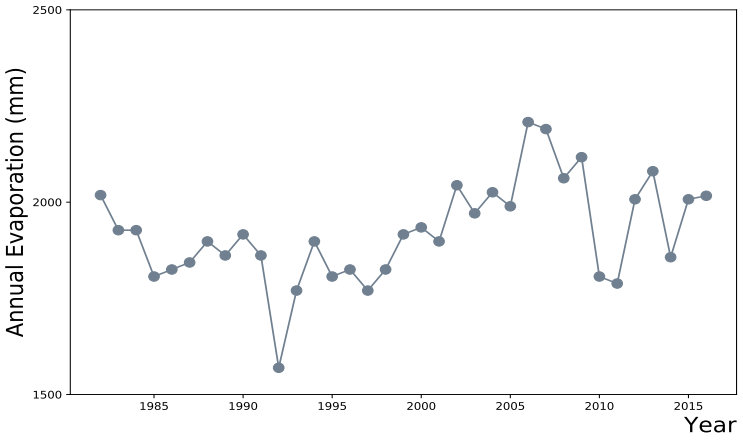

Figure 3.2: Adelaide Annual Evaporation

Combining the results above, I can derive the annual net water inflow to the reservoirs as

$$\text{NIW} = \text{TRP} + \text{ROW} - \text{TEV}$$

To estimate the bivariate distribution parameters, I also need to estimate the recycling cost. The wastewater recycling cost data is not directly available. As I described, wastewater recycling is energy-intensive, and the recycling cost uncertainty is linked to the energy price uncertainty. Let e_r denote the electricity consumption of the tertiary treatment/recycling process, p_e be the electricity price, and m be the other associated operating cost in tertiary treatment. Hence, the operating cost c_r in tertiary treatment/recycling process is

$$c_r = p_e e_r + m$$

Let $\bar{p}_e$ be the average electricity price over the periods and $\gamma = \frac{\bar{p}_e e_r}{\bar{p}_e e_r + m}$ denote the average percentage that the energy cost contributes to the total operating cost in tertiary treatment. Hence, I have

$$m = \frac{1-\gamma}{\gamma} \bar{p}_e e_r$$

In Adelaide, Short et al. (2014) show that the specific energy consumption for wastewater recycling (i.e., tertiary treatment) is estimated as 0.747 kWh/KL (Glenelg) and

2.4 kWh/KL (Aldinga). Then, I take the average energy consumption between these two plants as the tertiary treatment energy consumption in Adelaide and obtain $\acute{e}_r = 1.573$ kWh/KL.

From the Australian Energy Market Operator (AEMO), I can get the annual average electricity wholesale price from 1999 to 2020. The average Australian electricity bill is made up of four main components: wholesale price (34%), network (43%), retailing (16%) and environmental policy (6%)[7]. Hence, I can derive the retail price (see Figure 3.3).

Figure 3.3: Adelaide Annual Electricity Price

In general, the energy cost contributes to from 25% to 40% of the total operating cost in wastewater treatment (Panepinto et al. 2016, Gu et al. 2017). From Pearce (2008), I obtain that the energy cost contributes to 35% of the total operating cost in tertiary treatment processes for UF/MF technologies. Council et al. (2012) also show that the ratio (i.e., γ) can be as large as 35%. Based on these, we can obtain γ as $\acute{\gamma} = 0.35$. Hence, we can derive the recycling cost c_r (MD/GL) for each year.

Recall that the rainfall data is from 1884 to 2019, the evaporation data is from 1984 to 2016, and the electricity price data is from 1999 to 2020. Therefore, to calibrate

[7]The information is obtained from `https://www.climatecouncil.org.au/resources/electricity-prices-sorting-fact-from-fiction/`, accessed by 16/02/2021

the distribution parameters, I focus on data from overlapping years in these datasets and use data from 1999 to 2016. I test the bivariate Normality assumption of the data by using the Henze-Zirkler multivariate normality test, which is a common statistical method to test the normality of data. The p-value is about 0.1329, indicating no statistically significant evidence to reject the null hypothesis that the data is sampled from a bivariate Normal distribution. For a robustness check, I further use Royston's H test to test the Normality as it has better performance when the sample size is small (e.g., the sample size is around 25) (Farrell et al. 2007). The result shows that the p-value is 0.1353, which is consistent with the test result obtained under the Henze-Zirkler multivariate Normality test. Hence, I consider a bivariate Normal distribution and calibrate the parameters accordingly. Recall that $\acute{s}_0 = 17.1$ GL, then I estimate $\acute{\mu}_s = 122.2$(GL) and $\acute{\mu}_c = 0.88$(MD/GL)[8]. The correlation is $\acute{\rho} = 0.29$, the standard deviations are $\acute{\sigma}_s = 23.01$ and $\acute{\sigma}_c = 0.101$, respectively.

Calibration for Freshwater Operating Cost. From Australia Bureau of Meteorology (2014), I can get the total water supply cost in Adelaide from 2006 to 2010[9]. The total water supplied includes both surface water and recycled water. To obtain the unit freshwater operating cost, I use the total water supply cost subtract the total cost associated with recycled water and then divide the difference by the total surface water dispatched to the urban areas. The results are shown in Table 3.2.

Taking the average of the inflation rate adjusted unit freshwater operating cost, I estimate the unit freshwater operating cost in 2020 as $\acute{c}_f = 0.862$ MD/GL.

Calibration for The Unit Recycling Capacity Investment Cost. As the ultrafiltration (UF) membrane technology is adopted in Adelaide for water recycling, I focus on the investment in recycling capacity based on UF technology. For the

[8]When testing for the bivariate Normality and calculating the recycling cost, the electricity prices are adjusted by their corresponding inflation rates

[9]The ABM also provides the total water supply cost from 2013 to 2019; however, the data is for entire South Australia. To exclude the effect from desalination, I do not consider the data from 2011 and 2012. Hence, I use the data for Adelaide from 2005 to 2010 to do the estimation.

Year	2006	2007	2008	2009	2010
Total Water Supply Cost (MD)	122.95	122.37	159.93	145.75	139.23
Total Water Sourced (GL)	181.18	165.09	164.29	164.15	148.80
Recycled Water Supplied (GL)	25.05	25.26	25.50	24.39	19.80
Unit Cost of Recycled Water (MD/GL)	1.47	1.79	2.15	1.97	1.61
Freshwater Operating Cost (MD/GL)	0.55	0.54	0.76	0.69	0.83
IR-Adjusted Freshwater Operating Cost in 2020 (MD/GL)	0.75	0.72	0.97	0.86	1.01

Table 3.2: Freshwater Operating Costs

wastewater recycling plants at Glenelg and Aldinga, the capacities are 3.8 GL and 1.6 GL, and the capital costs are 88.27 MD and 73.71 MD (in 2020 dollars), respectively (Marchi et al. 2014). Assuming a 10-year lifetime (a 10-year lifetime is commonly used in the literature) for the wastewater recycling plant or the recycling technology used, I estimate the yearly-based capital costs for these two plants as 8.827 MD and 7.371 MD (i.e., considering the depreciation of the total capital cost over lifetime), respectively. Hence, the average unit capital cost is estimated as 3.47 MD/GL.

Calibration for Demand. The specific household and non-household demand data for Adelaide after 2013 are unavailable from the ABM. However, the residential and non-residential demand data for Adelaide can be obtained from 2005 to 2012. It should be noted that the recycled water is also supplied for residential uses such as toilet flushing. From Australia Bureau of Meteorology (2014), I find that the average percentage of the residential water demand that is satisfied by recycled water is about 0.2%. I can then use the residential demand (recycled water consumption excluded) to represent the household demand. I find that, on average, the household demand contributes to 68% of the total demand. As the total urban demand in 2020 is not publicly available, using the historic demand data and a simple exponential smoothing model, I project the total demand as 173.95 GL in 2020. Hence, I estimate the household demand as $\acute{D}_h = 173.95 * 0.68 = 118.29$ GL and the non-household demand as $\acute{D}_{nh} = 55.66$ GL.

Calibration for Leakage Ratios. From the National Water Account 2015-2019, I estimate the average urban freshwater leakage ratio (treatment losses included) as 0.107; hence, $\acute{\beta}_f = 0.893$. Similarly, from the National Water Account 2015-2019, the average loss ratio during wastewater basic treatment and recycling processes is estimated as 0.081; hence, $\acute{\beta}_r = 0.919$.

For the total volume of collected wastewater, I estimate that 72.5% of the used water (i.e., the total demand) is collected on average. Hence, the total wastewater collected is estimated as $\acute{q}_u = 173.95 \times 0.725 = 126.11$ GL.

3.2 Calibrated Parameters

Table 3.3 summarizes the calibrated parameter values representing the baseline scenario used in my numerical experiments.

Notation	Description	Value
$\acute{\mu}_s$, $\acute{\mu}_c$	Means of amount of available freshwater and recycling cost	122.2 GL, 0.88 MD/GL
$\acute{\sigma}_s$, $\acute{\sigma}_c$	Standard deviations of rainfall and recycling cost	23.01, 0.101
$\acute{\rho}$	Correlation between amount of available freshwater and recycling cost	0.29
$\acute{c}_f$	Unit freshwater treatment cost	0.862 MD/GL
$\acute{c}_d$	Effective unit desalination cost	5.93 MD/GL
$\acute{c}_b$	Average unit wastewater basic treatment cost	1.40 MD/GL
$\acute{\omega}_r$	Unit recycling capacity investment cost	3.47 MD/GL
$\acute{K}_f$	Freshwater storage and treatment capacity	192.4 GL
$\acute{D}_h$	Household demand	118.28 GL
$\acute{D}_{nh}$	Non-household demand	55.66 GL
$\acute{q}_u$	Volume of collected wastewater	126.11 GL
$\acute{\beta}_f$	the collection rate of freshwater	0.893
$\acute{\beta}_r$	the collection rate of recycled water	0.919

Table 3.3: Description of the Baseline Scenario Used in My Numerical Experiments. $\tilde{s}$ and $\tilde{c}_r$ are bivariate normally distributed.

For the overflow cost, due to the data availability issue, I failed to estimate the

unit overflow cost using real data. In this section, I set $\acute{o}_f = 0.5$ MD/GL (I conduct the sensitivity analysis by changing $\acute{o}_f$ from 0 to 10 and find that the optimal recycling capacity and optimal expected cost are barely affected). Based on these calibrated values, I find that $\acute{\mu}_s < \acute{K}_f < (\acute{D}_h + \acute{D}_{nh})/\acute{\beta}_f$. Moreover, I derive the cutoff points $\omega_r^2 = 4.57$, $\omega_r^1 = 4.56$ and $\omega_r^0 = 3.09$. Hence, I obtain that the estimated unit capacity cost $\acute{\omega}_r \in (\omega_r^0, \omega_r^1)$ and the optimal recycling capacity is an interior solution. I characterize the optimal recycling capacity and optimal expected cost as 55.02 GL per year and 620.27 MD, respectively.

3.3 Numerical Experiments

Based on the calibrated baseline scenario, I present the numerical results on sensitivity analysis, and implications of recycling capacity investment on urban water sustainability in this section.

3.3.1 Numerical Results: Sensitivity Analysis and The Value of Wastewater Recycling

As the calibration satisfies the bivariate normal distribution assumption made in Section 2.3.3, I first compare the numerical results with the characterized analytical results characterized in Chapter 2. Figure 3.4 plots the effects of changing variabilities (σ_s and σ_c) and correlation (ρ) on the optimal recycling capacity (panel a) and the optimal expected cost (panel b).

The insights obtained from Figure 3.4 parallel the ones from Proposition 2.3 and Proposition 2.4: i) the optimal recycling capacity increases in the correlation coefficient and the cost variability (as the estimated correlation is positive) and decreases in the rainfall variability; ii) the optimal expected cost decreases in the correlation coefficient and cost variability and increases in the rainfall variability. Hence, the

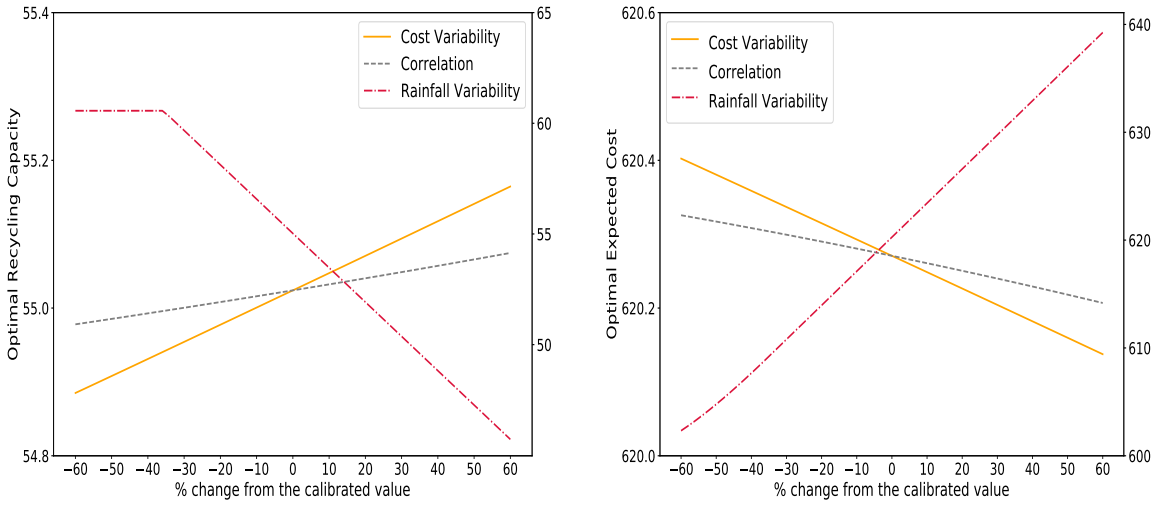

(a) (b)

Figure 3.4: Effects of rainfall and recycling cost variabilities and correlation on the optimal recycling capacity (Panel a) and optimal expected cost (Panel b). In the two panels, $\rho(\sigma_c, \sigma_s) \in [-60\%, 60\%]$ of the baseline value $\acute{\rho} = 0.29$ ($\acute{\sigma}_s = 23.01, \acute{\sigma}_c = 0.101$) with 2% increments.The dashed-dotted lines (represent the effects of rainfall variability) refer to the y-axis on the right.

numerical results further validate and complement the analytical sensitivity results.

In addition, I also numerically show the impact of freshwater capacity on the optimal wastewater recycling capacity in Figure 3.5. When the freshwater capacity (K_f) is relatively small, the optimal recycling capacity (K_r^*) is first independent of and then decreasing in the freshwater capacity. These observations are in line with the analytical characterizations. With the further increase of the freshwater capacity, although it is not obvious from the figure, I do find an increasing pattern. The reason for such an insignificant increasing effect is that the calibrated value for rainfall variability is not sufficiently high such that changing the freshwater capacity from the relatively high level does not significantly affect the marginal benefit of recycling capacity investment. These results further validate the substitute versus complement relationship between K_f and K_r^* characterized in Corollary 2.1 in Chapter 2.

I also investigate the value of wastewater recycling capacity optimization in this section. Recall that $V(K_r)$ is the expected cost for any given recycling capacity

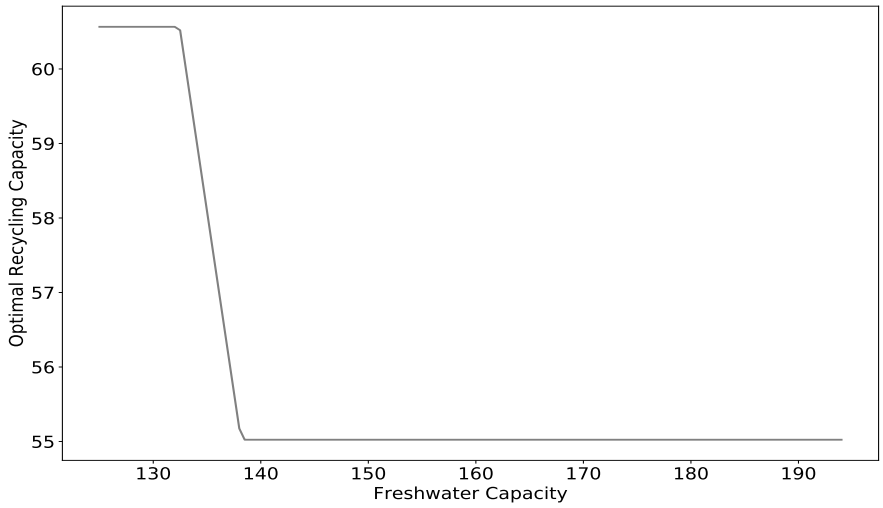

Figure 3.5: Effect of freshwater capacity on the optimal recycling capacity. The freshwater capacity changes with a stepsize equals to 1.

K_r and V^* is the optimal expected cost under the optimal recycling capacity K_r^*. I analyze how the difference between the expected cost for any given K_r and the optimal expected cost, i.e., $V(K_r) - V^*$, changes with K_r in Figure 3.6.

I next discuss the benefit of the investment on recycling by comparing my model with the benchmark model in which wastewater recycling is unavailable. The benchmark problem can be formulated as

$$\min_{q_f} Z^B(q_f)$$

$$s.t. \;\; 0 \leq q_f \leq \min(K_f, s, (D_h + D_{nh})/\beta_f)$$

with

$$Z^B(q_f) = o_f \left(s - q_f - K_f\right)^+ + c_f q_f + c_d(D_h + D_{nh} - \beta_f q_f) + c_b(\beta_h D_h + \beta_{nh} D_{nh})$$

Focusing on $K_f \leq \frac{D_h + D_{nh}}{\beta_f}$, the expected cost under the benchmark case is derived as

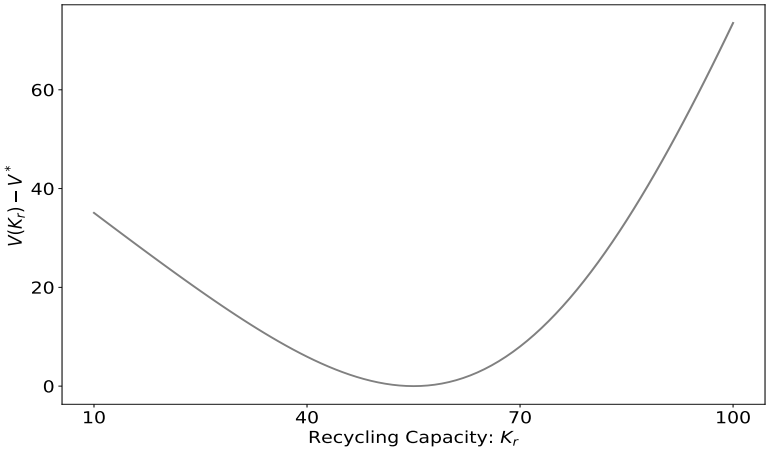

Figure 3.6: Value of wastewater recycling capacity optimization. The y-axis is the difference between the expected cost under any given recycling capacity K_r and the optimal expected cost. K_r is changing with a stepsize equals to 1.

follow.

$$
\begin{aligned}
V^B = & \int_{\underline{c}_r}^{\bar{c}_r} \int_{s_0}^{K_f} \left(c_f \tilde{s} + c_d(D_h + D_{nh} - \beta_f \tilde{s})\right) \psi(\tilde{s}, \tilde{c}_r) d\tilde{s} d\tilde{c}_r \\
& + \int_{\underline{c}_r}^{\bar{c}_r} \int_{K_f}^{+\infty} \left(c_f K_f + c_d(D_h + D_{nh} - \beta_f K_f)\right) \psi_f(\tilde{s}, \tilde{c}_r) d\tilde{s} d\tilde{c}_r \\
& + \int_{\underline{c}_r}^{\bar{c}_r} \int_{2K_f}^{+\infty} o_f(\tilde{s} - 2K_f) \psi_f(\tilde{s}, \tilde{c}_r) d\tilde{s} d\tilde{c}_r \\
& + \bar{c}_b(\beta_h D_h + \beta_{nh} D_{nh})
\end{aligned}
$$

The effects of uncertainties on V^B can be easily characterized in Corollary 3.1.

Corollary 3.1. *V^B is increasing in σ_s, and independent of σ_c and ρ.*

The benefit of wastewater recycling capacity investment is defined as $V^B - V^*$. As V^B is independent of σ_c and ρ, their effects on the benefit of recycling can be inferred from the effects on V^* (see Figure 3.4 Panel b). I focus on the rainfall variability here, and the results are shown in Figure 3.7. I find that, as the rainfall variability increases, the benefit of the investment decreases. This is because, as the rainfall variability increases, the optimal recycling capacity decreases and, hence, less recycled water is expected to be supplied. Therefore, the value of recycling decreases.

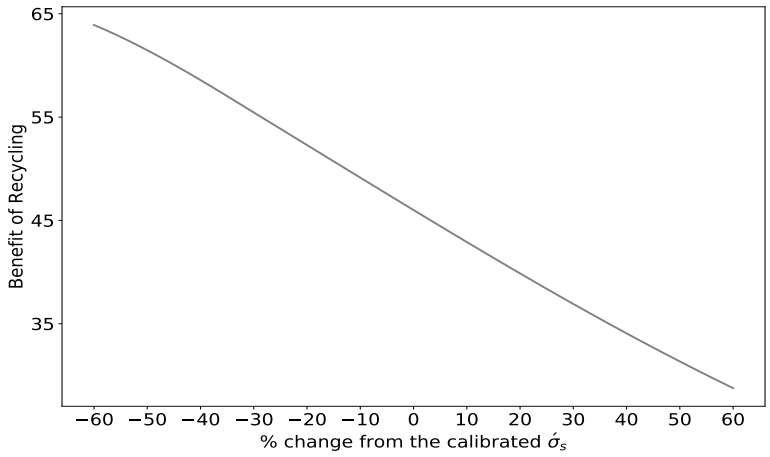

Figure 3.7: Effect of Rainfall Variability On The Benefit of The Investment On Recycling

I study the effect of changing demands (i.e., D_h and D_{nh}) on the benefit of wastewater recycling (i.e., $V^B - V^*$). From Figure 3.8, I observe that the benefit of wastewater recycling in household demand increases with decreasing marginal returns. However, as recycled water is only for non-household demand, I observe that the benefit of wastewater recycling in non-household demand increases almost linearly. Given that urban water demand is continuously increasing, these observations underline the importance of my work on wastewater recycling.

3.3.2 Numerical Results: Urban Water Vulnerability

I further numerically analyze the sustainability measures I discussed. For the overflow risk, as the calibrated rainfall variability $\acute{\sigma}_s = 23.01$ is not large enough in the sense that $\acute{\mu}_s + 5\acute{\sigma}_s$ is far less than $2\acute{K}_f$ and $\acute{K}_f + \tau_1(K_r^*)$, indicating that the overflow risk is very low in my calibration. Hence, I first focus on the vulnerability, which is denoted by the expected amount of desalinated water used.

I derive the expected amount of desalinated water supplied under the optimal framework and the benchmark case as DW = 16.94 GL and DW^B = 64.82 GL,

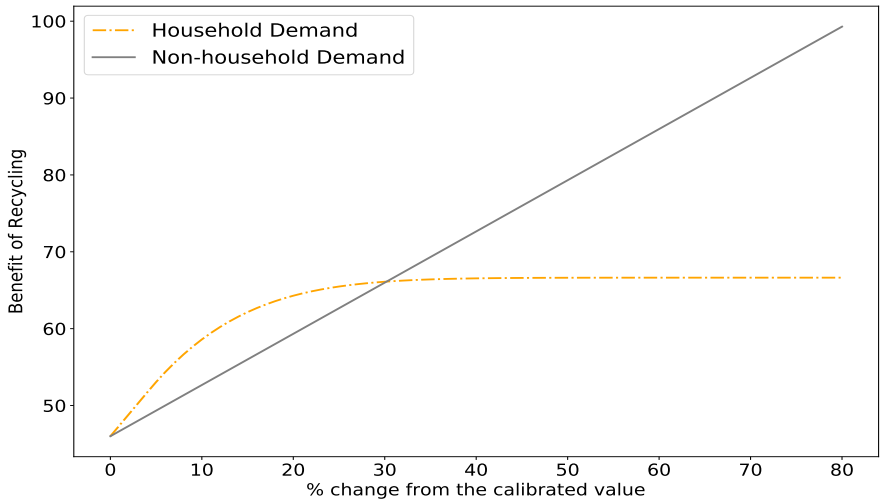

Figure 3.8: Effects of demands on the benefit of wastewater recycling. To study the effect of the household D_h (non-household D_{nh}) demand, I fix the non-household (household) demand at the calibrated baseline value, and then set $D_h(D_{nh})$ in $[0, 80\%]$ of the baseline value $\acute{D}_h$ ($\acute{D}_{nh}$) with a step size is 1% of the baseline value.

respectively, suggesting that the investment in wastewater recycling can greatly improve urban water sustainability, more specifically, reduce urban water vulnerability or increase the service level.

To further investigate the implications on sustainability, I examine how DW changes with the uncertainties and correlation and their effects on the difference between DW and DW^B (i.e., $\text{DW}^B - \text{DW}$). Figure 3.9 panel a shows that the expected amount of desalinated water used increases in the rainfall variability but decreases in the recycling cost variability and the correlation. These observations are in line with and further validate the analytical results characterized by Proposition 2.7. From Panel b, I observe that the difference $\text{DW}^B - \text{DW}$ decreases in the rainfall variability but increases in the recycling cost variability and the correlation, which implies that the additional benefits of the wastewater recycling in terms of reducing vulnerability decreases in the rainfall variability and increases in the recycling cost variability and correlation.

The effect of changing freshwater capacity on the vulnerability (i.e., the expected

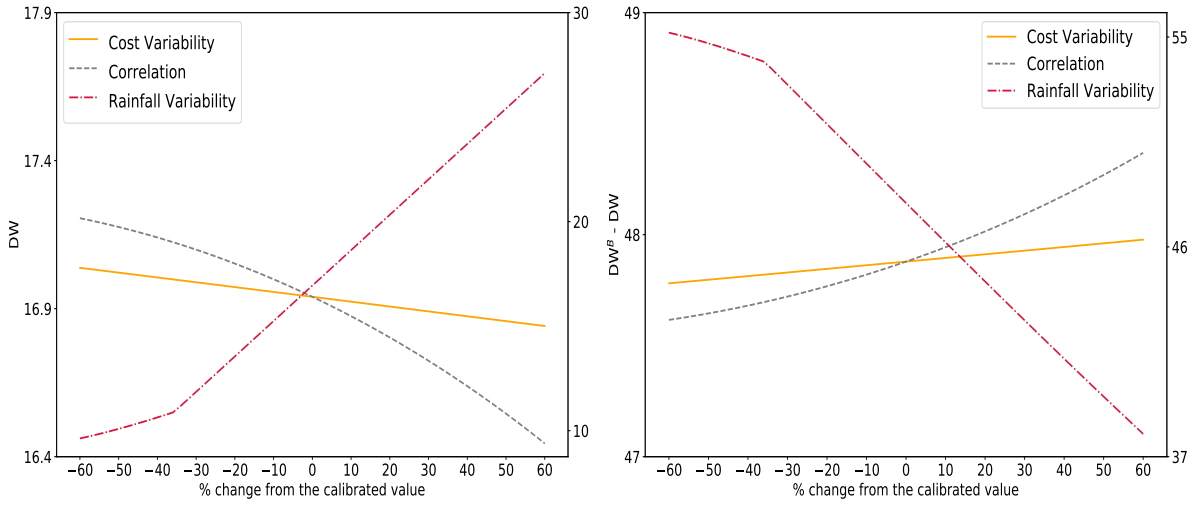

(a) (b)

Figure 3.9: Effects of rainfall and recycling cost variabilities and correlation on the expected amount of desalinated water supplied, i.e., DW (Panel a) and the difference $DW^B - DW$ (Panel b). In the two panels, the red lines (represent the effects of rainfall variability) refer to the y-axis on the right.

amount of desalinated water) is also discussed in this section. I show the numerical results in Figure 3.10. I observe that the expected amount of desalinated water used (DW) is non-decreasing in the freshwater capacity K_f in the characterized value region, which is the same as the results characterized by Proposition 2.6. On one hand, as the freshwater capacity increases, more freshwater and less desalinated water are expected to be dispatched. However, on the other hand, as I presented in Figure 3.5, the optimal recycling capacity is non-increasing in freshwater capacity, which implies that less recycled water and more desalinated water are expected to be used. The reduction of recycled water outweighs the increase in freshwater; hence, as presented by Figure 3.10, the expected amount of desalinated water is non-decreasing in K_f. These observations have important practical implications for the urban water utility in Adelaide to manage urban water shortage/vulnerability, that is, the expansion of freshwater capacity may further worsen urban water scarcity.

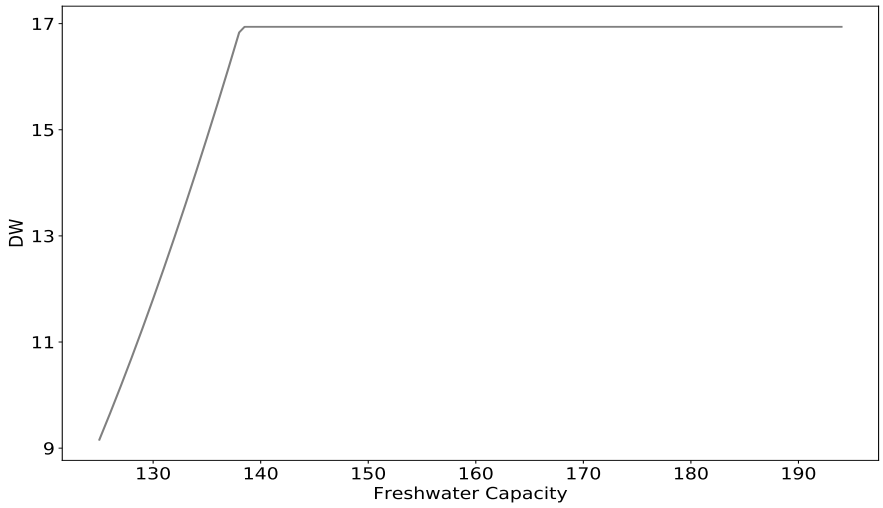

Figure 3.10: Effect of freshwater capacity on the expected amount of desalinated water used. The freshwater capacity K_f changes with a step size of 1.

3.3.3 Numerical Results: Value of Imported Water

In Adelaide, the freshwater can also be imported from River Murray and stored in the reservoirs for urban consumption. As importing freshwater is equivalent to increase the deterministic part of available freshwater (s_0), the value of an additional unit (GL) imported water can be characterized by $V^*(s_0+1)-V^*(s_0)$, which is the change of the optimal expected cost. Specifically, for given n units of imported water, I represent the value of an additional unit (GL) imported water by $V^*(\acute{s}_0 + n) - V^*(\acute{s}_0 + n + 1)$ (a positive value means the reduction of cost) and characterize the changes of the value in Figure 3.11. I find that, in general, importing an additional unit (GL) of freshwater results in a reduction of 3.36 MD/GL in the optimal expected cost (I also note that this benefit slightly decreases as the quantity of imported water increases), which suggests that, as long as the unit cost of importing freshwater is less than 3.36 MD/GL, it is beneficial for the water utility to import water.

I also analyze how the variabilities (σ_s and σ_c) and correlation (ρ) affect the value of importing an additional unit of water. As the imported freshwater can be a reliable water source to meet urban demand, common intuition may suggest that it is more

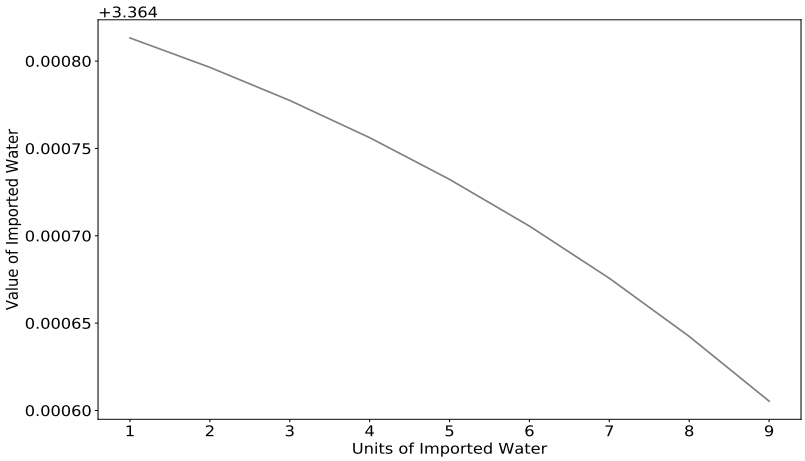

Figure 3.11: Value of an additional unit (GL) imported water: a positive value means that increasing the amount of imported water decreases the cost. The units of imported water changes with a step size of 1.

beneficial to import freshwater when the variabilities increase. However, Figure 3.12 shows that imported water becomes less beneficial when the variabilities and the correlation coefficient increase. Moreover, the rainfall variability has a larger impact on the benefit than recycling cost variability and the correlation.

In this section, for comparison, I further discuss the value of imported water under the benchmark case where wastewater recycling is unavailable. Similar to the case under the optimal framework with recycling, the value of imported water under the benchmark case is defined as $V^B(\acute{s}_0 + n) - V^B(\acute{s}_0 + n + 1)$ (recall that V^B is the expected cost of the benchmark case).

Comparing with the optimal framework that recycling is integrated, we can observe from Figure 3.13 that the water utility is willing to pay much higher (about 30% higher) for an additional unit of imported water. These results further highlight the value of wastewater recycling capacity investment and optimization.

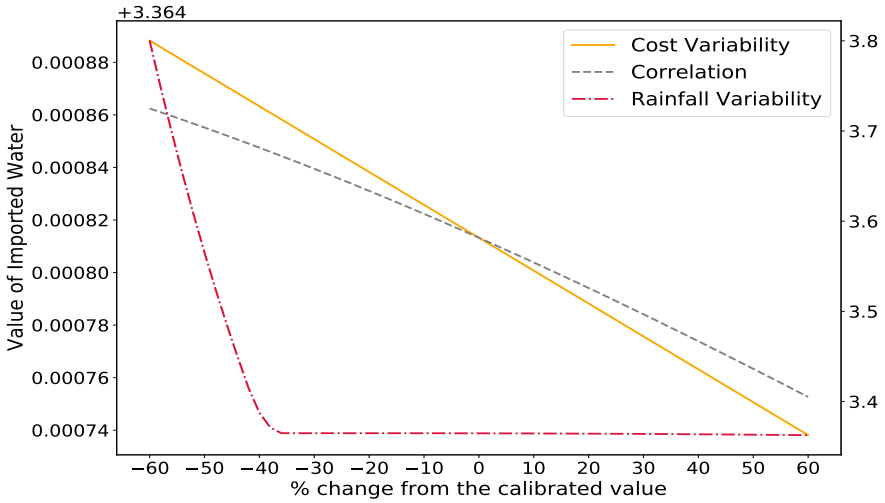

Figure 3.12: Sensitivity analysis with respect to the value of an additional unit (GL) imported water: a positive value means that an additional unit of imported water decreases the cost. The dashed-dotted line (represents the effects of rainfall variability) refers to the y-axis on the right.

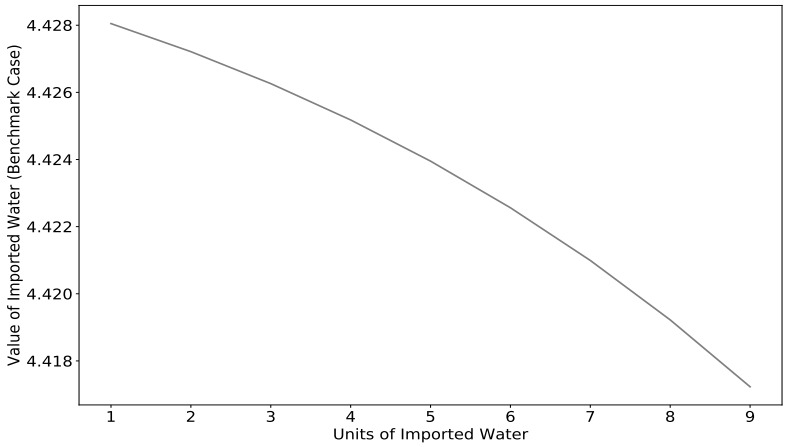

Figure 3.13: Value of an additional unit (GL) imported water (benchmark case): a positive value means increasing the amount of imported water decreases the cost. The units of imported water changes with a step size of 1.

3.3.4 Numerical Results: Unit Cost of Satisfying Demand

I also analyze the cost of satisfying a unit of household (non-household) demand under the optimal framework with wastewater recycling capacity investment. From the model, I first derive the analytical form of the unit household (non-household) demand cost. From the first stage objective function, I can derive the expected amount of recycled water used, which is denoted by EARW.

$$\begin{aligned}\text{EARW} = &\int\int_{\Omega_1 \bigcup \Omega_3 \bigcup \Omega_4} K_r \psi(\tilde{s}, \tilde{c}_r) d\tilde{s} d\tilde{c}_r \\ &+ \int\int_{\Omega_2 \bigcup \Omega_6} \Big[(D_h + D_{nh} - \beta_f \min(\tilde{s}, K_f))/\beta_r \Big] \psi(\tilde{s}, \tilde{c}_r) d\tilde{s} d\tilde{c}_r \\ &+ \int\int_{\Omega_5} \Big[(D_h + D_{nh} - \beta_f (\tilde{s} - K_f))/\beta_r \Big] \psi(\tilde{s}, \tilde{c}_r) d\tilde{s} d\tilde{c}_r\end{aligned}$$

Then, the expected amount of potable supplied for non-house demand is $D_{nh} -$ EARW. Hence, the total expected amount of potable water supplied is TPW $= D_h + D_{nh} -$ EARW. As the household demand can only be satisfied by the potable water (i.e., treated freshwater and/or desalinated water), the unit household demand cost is equal to the unit potable water cost. The total expected cost of producing potable water is

$$\begin{aligned}\text{ECPW} = &\int\int_{\Omega_1} \left[c_d (D_h + D_{nh} - \beta_r K_r - \beta_f \tilde{s}) + c_f \tilde{s} \right] \psi(\tilde{s}, \tilde{c}_r) d\tilde{s} d\tilde{c}_r \\ &+ \int\int_{\Omega_2 \bigcup \Omega_6} \Big[c_f \min(\tilde{s}, K_f) \Big] \psi(\tilde{s}, \tilde{c}_r) d\tilde{s} d\tilde{c}_r \\ &+ \int\int_{\Omega_3 \bigcup \Omega_4} \Big[\frac{c_f}{\beta_f} (D_h + D_{nh} - \beta_r K_r) \Big] \psi(\tilde{s}, \tilde{c}_r) d\tilde{s} d\tilde{c}_r \\ &+ \int\int_{\Omega_5} \Big[c_f (\tilde{s} - K_f) \Big] \psi(\tilde{s}, \tilde{c}_r) d\tilde{s} d\tilde{c}_r\end{aligned}$$

and the total expected cost of recycling is

$$\begin{aligned}\text{ECRW} = &\int\int_{\Omega_1 \bigcup \Omega_3 \bigcup \Omega_4} \tilde{c}_r K_r \psi(\tilde{s}, \tilde{c}_r) d\tilde{s} d\tilde{c}_r \\ &+ \int\int_{\Omega_2 \bigcup \Omega_6} \Big[\tilde{c}_r (D_h + D_{nh} - \beta_f \min(\tilde{s}, K_f))/\beta_r \Big] \psi(\tilde{s}, \tilde{c}_r) d\tilde{s} d\tilde{c}_r \\ &+ \int\int_{\Omega_5} \Big[\tilde{c}_r (D_h + D_{nh} - \beta_f (\tilde{s} - K_f))/\beta_r \Big] \psi(\tilde{s}, \tilde{c}_r) d\tilde{s} d\tilde{c}_r\end{aligned}$$

In addition to the potable water production cost, the unit household and non-household demand costs should also include the overflow cost and investment cost. The total expected overflow cost is

$$\begin{aligned}\mathrm{OC} = &\int\int_{\Omega_2 \bigcup \Omega_6} \left[o_f(\tilde{s} - \min(\tilde{s}, K_f) - K_f)^+\right] \psi(\tilde{s}, \tilde{c}_r) d\tilde{s} d\tilde{c}_r \\ &+ \int\int_{\Omega_4} \left[o_f(\tilde{s} - K_f - (D_h + D_{nh} - \beta_r K_r)/\beta_f)\right] \psi(\tilde{s}, \tilde{c}_r) d\tilde{s} d\tilde{c}_r\end{aligned}$$

and the total investment cost is $\mathrm{IC} = \omega_r K_r^*$. Hence, the unit household demand cost is

$$\mathrm{UHC} = \mathrm{ECPW}/\mathrm{TPW} + (\mathrm{OC} + \mathrm{IC})/(D_h + D_{nh})$$

and the unit non-household demand cost is

$$\mathrm{UNHC} = (\mathrm{ECRW} + (D_{nh} - \mathrm{EARW}) \times \mathrm{ECPW}/\mathrm{TPW})/D_{nh} + (\mathrm{OC} + \mathrm{IC})/(D_h + D_{nh})$$

For the given calibrated baseline values, the unit costs can be derived as UHC = 2.46 MD and UNHC = 3.25 MD. For the benchmark case in which wastewater recycling is unavailable, the unit cost of satisfying household (UHC^B) and non-household demand (UNHC^B) is equal to 3.83 MD. As we can see, the unit cost of satisfying household and non-household demands under the benchmark case is much higher than those under the framework with recycling, respectively.

I further investigate how $\mathrm{UHC} - \mathrm{UHC}^B$ ($\mathrm{UNHC} - \mathrm{UNHC}^B$), which is the difference between the unit costs of satisfying the household (non-household) demand under the optimal framework and the benchmark case, changes with the uncertainties and correlation. I find that, from Figure 3.14, the differences between the unit costs increase in the rainfall variability and decrease in the cost variability, which implies that, comparing with the benchmark case, the additional benefits of recycling decrease in the rainfall variability and increase in the cost variability in terms of the unit cost of satisfying household and non-household demands. These observations are in line with the insights from Figure 3.4b. However, as ρ increases, the additional benefits of

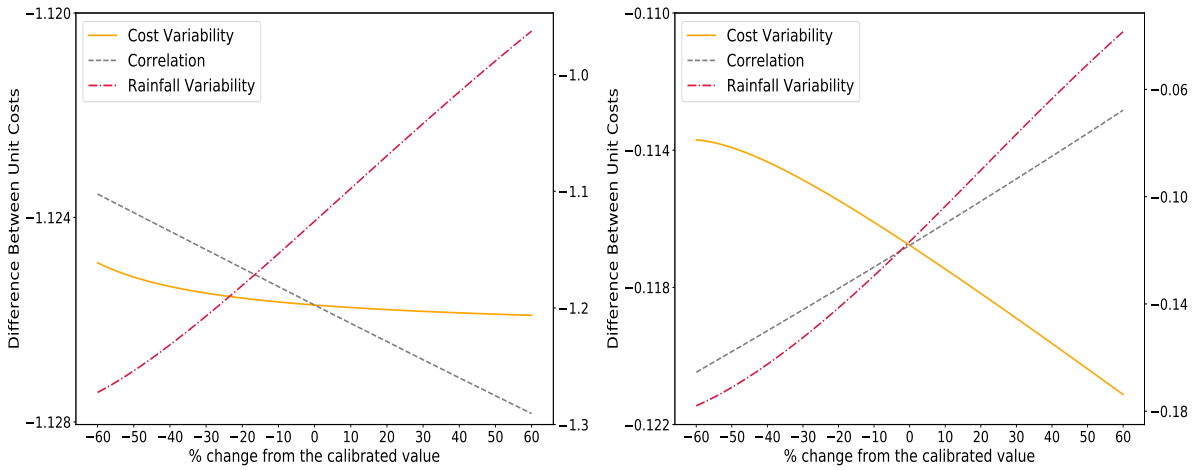

(a) (b)

Figure 3.14: Effects of rainfall and recycling cost variabilities and correlation on the unit cost differences: UHC − UHC^B (Panel a) and UNHC − UNHC^B (Panel b). A negative value implies that the unit cost under the optimal framework is smaller than that under the benchmark case. The dashed-dotted lines (represent the effects of rainfall variability) refer to the y-axis on the right.

satisfying a unit household demand (Panel a) increases, while the additional benefits of satisfying a unit non-household demand (Panel b) decreases.

3.3.5 Numerical Results: Value of Leakage Ratio Reduction

In this section, I also study the economic effects of changing the leakage ratios, or equivalently, recovery ratios (i.e., β_f and β_r) in Figure 3.15a. From Figure 3.15a, I observe that, given β_r (β_f), it is always beneficial to reduce the leakage ratio $1-\beta_f$ ($1-\beta_r$), which is in line with the results characterized in Section 2.3.4. In addition, I show in Figure 3.15b that, based on the calibrated baseline scenario, it is always better to prioritize the reduction of freshwater leakage, which has important practical implications for the urban water utility in Adelaide (i.e., SA Water) to manage the urban water leakage[10].

[10]I note that, in practice, there is leakage reduction associated cost. If the unit cost of freshwater leakage reduction is much more than that of the recycled water, then the priority and even the economic benefit should be adjusted accordingly.

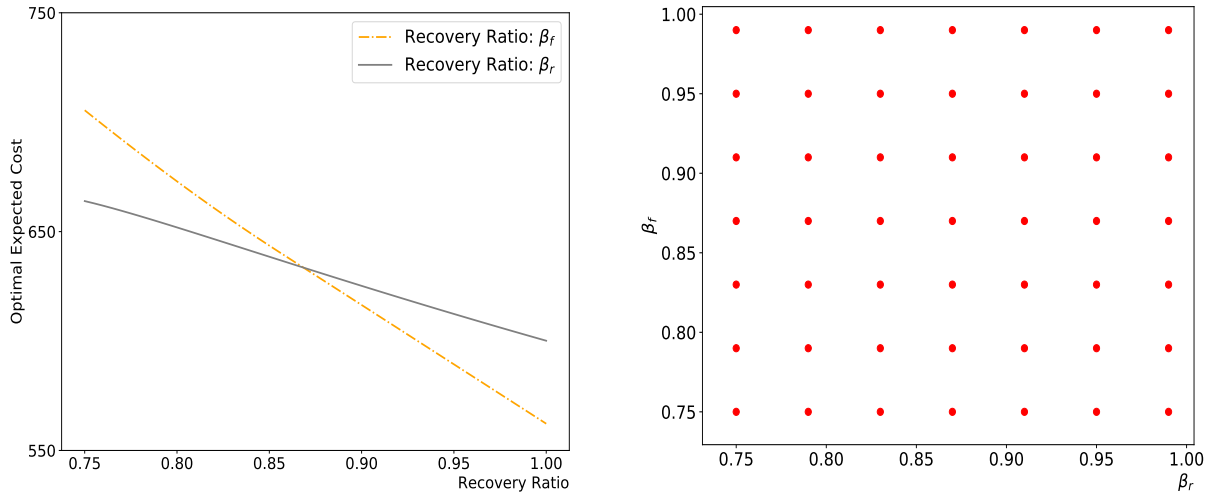

(a) (b)

Figure 3.15: Panel a: Economic effects of changing recovery ratios. The effect of $\beta_f(\beta_r)$ is characterized under $\beta_r = \acute{\beta}_r = 0.919$ ($\beta_f = \acute{\beta}_f = 0.893$). $\beta_f, \beta_r \in [0.75, 1]$ with a step size of 0.002. Panel b: marginal benefits comparison between reducing recycled water leakage and reducing freshwater leakage. The red dot indicates that reducing freshwater leakage is more beneficial than reducing recycled water leakage.

I also investigate the effects of reducing leakage ratios on the optimal recycling capacity in Figure 3.16. I find that reducing the freshwater leakage (i.e., increasing β_f) decreases the investment in recycling capacity, implying that leakage reduction could be a valuable hedge against the potential premature capacity expansion in light of urban water shortage, which is also in line with the insights obtained by Sahely and Kennedy (2007). However, I observe that the optimal recycling capacity increases as the recycled water leakage decreases (i.e., β_r increases). This is because a smaller leakage ratio makes the marginal benefit of the investment in recycling larger, and then the magnitude of the investment becomes larger.

To further complement the analysis above, I conduct numerical studies using a hypothetical case. Comparing with the baseline scenario calibrated by the practical data, I change the values of μ_s, σ_s, K_f, q_u, D_h and D_{nh} to characterize the hypothetical baseline scenario. Specifically, I set $\mu_s = 100$, $\sigma_s = 50$, $K_f = 110$, $q_u = 110$, $D_h = 95$ and $D_{nh} = 60$. Such changes (e.g., the values of μ_s and σ_s are changed from 122.2 and

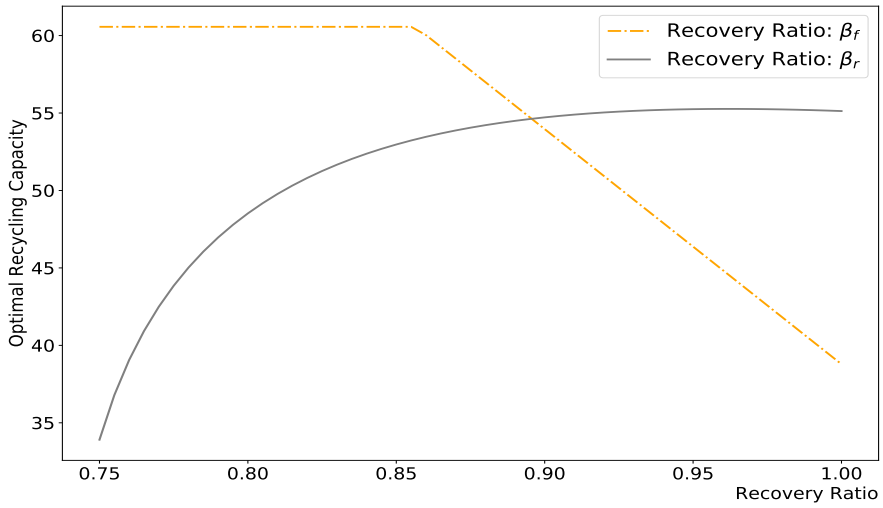

Figure 3.16: Effects of reducing recycled water leakage and reducing freshwater leakage on the optimal recycling capacity. The effect of $\beta_f(\beta_r)$ is characterized under $\beta_r = \acute{\beta}_r = 0.919$ ($\beta_f = \acute{\beta}_f = 0.893$). $\beta_f, \beta_r \in [0.75, 1]$ with a step size is 0.002.

23.02 (practical data-based) to 100 and 50 (hypothetical scenario), respectively) are reasonable given the global freshwater resources in distress and the increasing large impact of global climate change on freshwater availability.

Using this hypothetical case, I analyze the benefits of leakage reduction and which water pipeline leakage reduction gets the priority. I show the results in Figure 3.17.

For the hypothetical baseline scenario (i.e., $\sigma_s = 50$, Panel 3.17b), I find that it is better to reduce the recycled water leakage ratio (i.e., $1 - \beta_r$) when β_r and β_f are relatively small; otherwise, it is better to reduce the freshwater leakage ratio. I also observe from other panels that which leakage ratio gets priority may change when σ_s changes. For example, when the variability σ_s decreases (i.e., $\sigma_s = 20$), it becomes unlikely to prioritize reducing recycled water leakage in the given value regions. On the other hand, as σ_s increases, it is better to prioritize reducing the recycled water leakage in broader ranges of β_f and β_r.

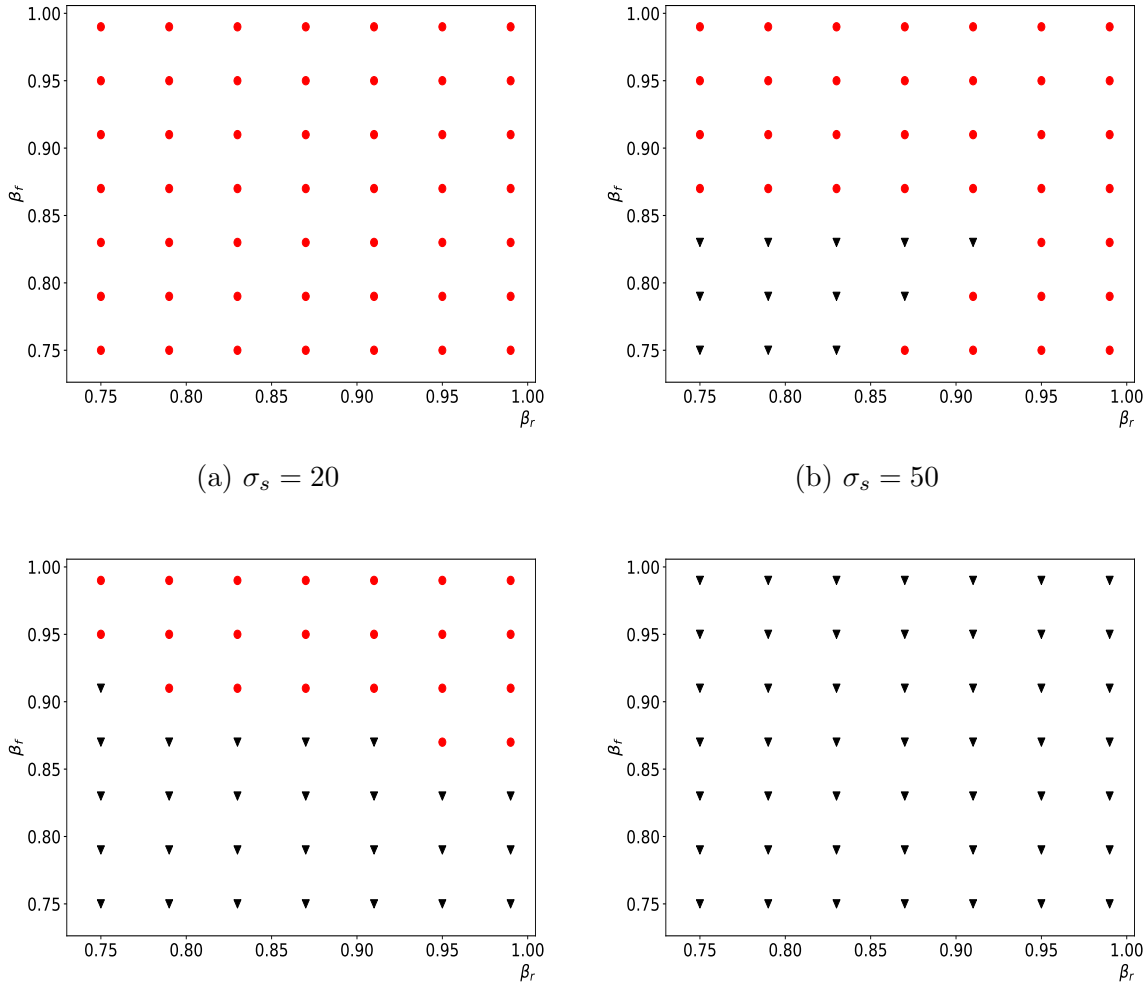

(a) $\sigma_s = 20$

(b) $\sigma_s = 50$

(c) $\sigma_s = 80$

(d) $\sigma_s = 110$

Figure 3.17: Marginal benefits comparison between reducing recycled water leakage and reducing freshwater leakage (hypothetical case) under different variabilities of available freshwater. The red (black) dot (triangle) indicates that reducing freshwater (recycled water) leakage is more beneficial.

3.3.6 Numerical Results: Overflow Risk

To complement the analysis on the overflow risk, I use the hypothetical scenario introduced in Section 3.3.5 to show the insights. Moreover, I set the baseline $\sigma_c = 5$ and $\rho = 0.5$ here to investigate the potential effects from recycling cost variability and correlation. Figure 3.18 characterizes the effects of uncertainties and their correlation on overflow risk.

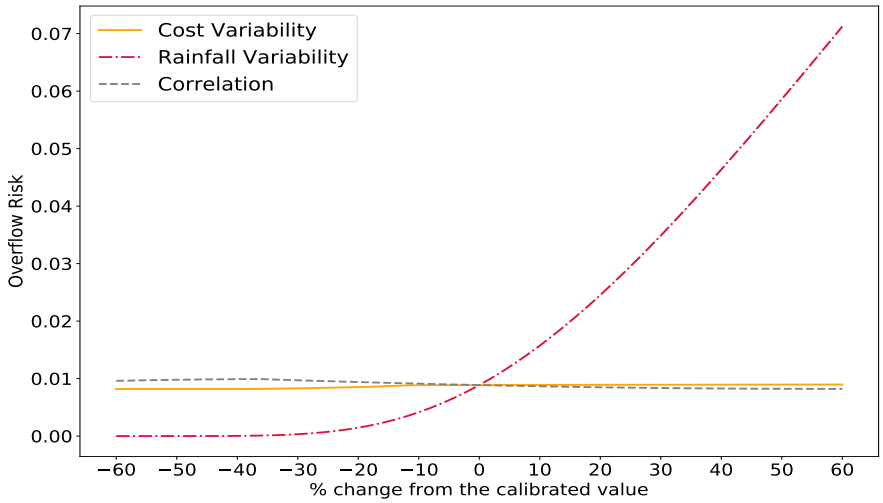

Figure 3.18: Effects of uncertainties and correlation on the overflow risk.

I find that the overflow risk increases in the rainfall and recycling cost variabilities, which are also characterized by the analytical results in Proposition 2.9.A. For effect of the correlation, Figure 3.18 shows that the overflow risk decreases as the correlation increases. A higher ρ makes it more likely that when the recycling cost is low (high), the amount of rainfall is low (high). Then, when the rainfall is heavy, it is more likely to dispatch freshwater in priority as ρ increases. Thus, the overflow risk decreases. I also note that compared with the impact from the rainfall variability, the impacts of cost variability and correlation are much less significant.

In addition, I also analytically compare the overflow risk under the optimal framework with that under the benchmark case. The overflow risk under the benchmark case is denoted by $\text{PO}^B = \mathbf{Pr}(\tilde{s} \geq 2K_f)$. Then the difference between PO^B and PO

is characterized as follows

$$\mathrm{PO}^B - \mathrm{PO} = \begin{cases} 0, & \text{if } \omega_r \geq \omega_r^1 \\ \mathbf{Pr}(\underline{c}_r \geq \tilde{c}_r \leq (c_f - o_f)\frac{\beta_r}{\beta_f}, \tilde{s} \geq 2K_f) & \\ \quad + \mathbf{Pr}(\underline{c}_r \leq \tilde{c}_r < (c_f - o_f)\frac{\beta_r}{\beta_f}, \tilde{s} \geq K_f + \tau_1(K_r^*)), & \text{if } \omega_r < \omega_r^1 \end{cases}$$

I show the sensitivity results in the following Corollary.

Corollary 3.2.

(1) PO^B is independent of σ_c and ρ, and increasing in σ_s;

(2) $PO^B - PO$ is non-positive;

(3) $PO^B - PO$ increases in σ_s;

(4) The impacts of σ_c can be directly obtained from Proposition 2.9.A.

3.4 Conclusion

In this chapter, using practical urban water system data from Adelaide, I conduct comprehensive numerical experiments to validate and complement the analytical results presented in Chapter 2. Specifically, I discuss how the rainfall and recycling cost variabilities and their correlation affect the optimal expected cost, optimal recycling capacity and the value of recycling. I characterize how the value of recycling changes with the increasing household and non-household demands and find the value increases in the household demand with decreasing marginal returns and increases in non-household demand almost linearly, respectively. In addition, I also study the benefit of importing water and the sustainability of urban water systems (e.g., the leakage reduction, the vulnerability, which is represented by the amount of desalinated water used, and the overflow risk). I find that it is always beneficial to reduce water leakage and, in the calibrated practical case, the freshwater leakage is prioritized to reduce; while in the hypothetical case, I develop more insights that the priority of reducing which leakage ratio depends on the leakage rations' ranges and also significantly af-

fected by the rainfall variability (e.g., a large rainfall variability makes reducing the recycled water leakage ratio more beneficial). From the numerical analysis, I further find that comparing with the recycling cost variability and the correlation, the rainfall variability has a much larger impact on the urban water system's economic and sustainable performances. These observations provide insightful implications for urban water utilities to manage the urban water systems under the challenge of rapid urbanization, population growth and climate change.

Bibliography

Aalen, O. O. and Johansen, S. (1978). An empirical transition matrix for non-homogeneous markov chains based on censored observations. *Scandinavian Journal of Statistics*, pages 141–150.

ABCNEWS (2017). Adelaide desalination plant too expensive, liberals say, despite falling electricity bill. `https://www.abc.net.au/news/2017-10-28/adelaide-desal-plant-too-big-and-too-expensive/9096046`. Accessed: 2021-02-15.

Agrawal, V. V., Ferguson, M., Toktay, L. B., and Thomas, V. M. (2012). Is leasing greener than selling? *Management Science*, 58(3):523–533.

Alagoz, O., Bryce, C., Schaefer, A., Angus, D., and Roberts, M. (2002). Predicting the future health states of liver disease patients using empirical stochastic models. *Medical Decision Making*, 22(6):541.

Alagoz, O., Maillart, L. M., Schaefer, A. J., and Roberts, M. S. (2004). The optimal timing of living-donor liver transplantation. *Management Science*, 50(10):1420–1430.

Alcorn, M. (2006). Surface water assessment of the currency creek catchment.

Angelus, A. and Özer, Ö. (2020). When variability trumps volatility: Optimal control and value of reverse logistics in supply chains with multiple flows of product. *Manufacturing & Service Operations Management*.

Armstrong, R. D. and Willis, C. E. (1977). Simultaneous investment and allocation decisions applied to water planning. *Management Science*, 23(10):1080–1088.

Asena, T. F. and Goshu, A. T. (2017). Comparison of sojourn time distributions in modeling hiv/aids disease progression. *Biometrical Letters*, 54(2):155–174.

Atasu, A., Guide Jr, V. D. R., and Van Wassenhove, L. N. (2008a). Product reuse economics in closed-loop supply chain research. *Production and Operations Management*, 17(5):483–496.

Atasu, A., Sarvary, M., and Van Wassenhove, L. N. (2008b). Remanufacturing as a marketing strategy. *Management Science*, 54(10):1731–1746.

Atasu, A. and Souza, G. C. (2013). How does product recovery affect quality choice? *Production and Operations Management*, 22(4):991–1010.

Atasu, A. and Subramanian, R. (2012). Extended producer responsibility for e-waste: Individual or collective producer responsibility? *Production and Operations Management*, 21(6):1042–1059.

Australia Bureau of Meteorology (2014). National performance report 2013–14: Urban water utilities, part b. `http://www.bom.gov.au/water/npr/npr_2013-14.shtml`. Accessed: 2021-02-15.

Avi-Itzhak, B. and Ben-Tuvia, S. (1963). A problem of optimizing a collecting reservoir system. *Operations Research*, 11(1):122–136.

Ayer, T., Alagoz, O., and Stout, N. K. (2012). Or forum—a pomdp approach to personalize mammography screening decisions. *Operations Research*, 60(5):1019–1034.

Ayer, T., Alagoz, O., Stout, N. K., and Burnside, E. S. (2016). Heterogeneity in

women's adherence and its role in optimal breast cancer screening policies. *Management Science*, 62(5):1339–1362.

Ban, G.-Y. (2020). Confidence intervals for data-driven inventory policies with demand censoring. *Operations Research*, 68(2):309–326.

Barrett, M., Smith, M., Elixhauser, A., Honigman, L., and Pines, J. (2014). Utilization of intensive care services, 2011. *Healthcare Cost and Utilization Project, Agency for Healthcare Research and Quality*.

Beh, E. H., Maier, H. R., and Dandy, G. C. (2015). Adaptive, multiobjective optimal sequencing approach for urban water supply augmentation under deep uncertainty. *Water Resources Research*, 51(3):1529–1551.

Bertsimas, D., Dunn, J., and Mundru, N. (2019a). Optimal prescriptive trees. *INFORMS Journal on Optimization*, 1(2):164–183.

Bertsimas, D., Kallus, N., Weinstein, A. M., and Zhuo, Y. D. (2017). Personalized diabetes management using electronic medical records. *Diabetes Care*, 40(2):210–217.

Bertsimas, D., Orfanoudaki, A., and Weiner, R. B. (2019b). Personalized treatment for coronary artery disease patients: A machine learning approach. *arXiv preprint arXiv:1910.08483*.

Bhushan, R. and Ng, T. L. (2016). Integrating desalination to reservoir operation to increase redundancy for more secure water supply. *Water Resources Research*, 52(8):6137–6155.

Boloori, A., Saghafian, S., Chakkera, H. A., and Cook, C. B. (2020). Data-driven management of post-transplant medications: an ambiguous partially observable

markov decision process approach. *Manufacturing & Service Operations Management*.

Boretti, A. and Rosa, L. (2019). Reassessing the projections of the world water development report. *NPJ Clean Water*, 2(1):1–6.

Calmon, A. P. and Graves, S. C. (2017). Inventory management in a consumer electronics closed-loop supply chain. *Manufacturing & Service Operations Management*, 19(4):568–585.

Cardno (2013). Review of capital and operating expenditure plans of sa water - 2013/14 to 2015/16 price determination. `https://www.escosa.sa.gov.au/ArticleDocuments/484/130207-ReviewofCapexOpexPlansofSAWa.pdf.aspx?Embed=Y`. Accessed: 2021-02-10.

Chan, C. W., Farias, V. F., Bambos, N., and Escobar, G. J. (2012). Optimizing intensive care unit discharge decisions with patient readmissions. *Operations Research*, 60(6):1323–1341.

Charitos, T., de Waal, P. R., and van der Gaag, L. C. (2008). Computing short-interval transition matrices of a discrete-time markov chain from partially observed data. *Statistics in Medicine*, 27(6):905–921.

Cheng, G., Xie, J., and Zheng, Z. (2019). Optimal stopping for medical treatment with predictive information: Theory and application in icu mechanical ventilation. *Available at SSRN 3397530*.

Chhatwal, J., Alagoz, O., and Burnside, E. S. (2010). Optimal breast biopsy decision-making based on mammographic features and demographic factors. *Operations Research*, 58(6):1577–1591.

Chhatwal, J., Jayasuriya, S., and Elbasha, E. H. (2016). Changing cycle lengths in state-transition models: challenges and solutions. *Medical Decision Making*, 36(8):952–964.

Chu, L. Y. and Lai, G. (2013). Salesforce contracting under demand censorship. *Manufacturing & Service Operations Management*, 15(2):320–334.

Clifton, L., Clifton, D. A., Pimentel, M. A., Watkinson, P. J., and Tarassenko, L. (2012). Gaussian processes for personalized e-health monitoring with wearable sensors. *IEEE Transactions on Biomedical Engineering*, 60(1):193–197.

Colopy, G. W., Roberts, S. J., and Clifton, D. A. (2017). Bayesian optimization of personalized models for patient vital-sign monitoring. *IEEE Journal of Biomedical and Health Informatics*, 22(2):301–310.

Council, N. R. et al. (2012). *Water reuse: potential for expanding the nation's water supply through reuse of municipal wastewater*. National Academies Press.

Cox, D. and Hinkley, D. (1979). Theoretical statistics. *CRC Press*.

Craig, B. A., Fryback, D. G., Klein, R., and Klein, B. E. (1999). A bayesian approach to modelling the natural history of a chronic condition from observations with intervention. *Statistics in Medicine*, 18(11):1355–1371.

Craig, B. A. and Sendi, P. P. (2002). Estimation of the transition matrix of a discrete-time markov chain. *Health Economics*, 11(1):33–42.

Dasbach, E. J., Fryback, D. G., Newcomb, P. A., Klein, R., and Klein, B. E. (1991). Cost-effectiveness of strategies for detecting diabetic retinopathy. *Medical Care*, pages 20–39.

Dasta, J. F., McLaughlin, T. P., Mody, S. H., and Piech, C. T. (2005). Daily cost

of an intensive care unit day: the contribution of mechanical ventilation. *Critical Care Medicine*, 33(6):1266–1271.

Debo, L. G., Toktay, L. B., and Van Wassenhove, L. N. (2005). Market segmentation and product technology selection for remanufacturable products. *Management Science*, 51(8):1193–1205.

Debo, L. G., Toktay, L. B., and Wassenhove, L. N. V. (2006). Joint life-cycle dynamics of new and remanufactured products. *Production and Operations Management*, 15(4):498–513.

DeCroix, G. A. and Zipkin, P. H. (2005). Inventory management for an assembly system with product or component returns. *Management Science*, 51(8):1250–1265.

Eijgenraam, C., Brekelmans, R., den Hertog, D., and Roos, K. (2017). Optimal strategies for flood prevention. *Management Science*, 63(5):1644–1656.

Erenay, F. S., Alagoz, O., and Said, A. (2014). Optimizing colonoscopy screening for colorectal cancer prevention and surveillance. *Manufacturing & Service Operations Management*, 16(3):381–400.

Erlenkotter, D., Sethi, S., and Okada, N. (1989). Planning for surprise: Water resources development under demand and supply uncertainty I. the general model. *Management Science*, 35(2):149–163.

Farrell, P. J., Salibian-Barrera, M., and Naczk, K. (2007). On tests for multivariate normality and associated simulation studies. *Journal of Statistical Computation and Simulation*, 77(12):1065–1080.

Feiler, D. C., Tong, J. D., and Larrick, R. P. (2013). Biased judgment in censored environments. *Management Science*, 59(3):573–591.

Ferguson, M., Guide Jr, V. D., Koca, E., and Souza, G. C. (2009). The value of quality grading in remanufacturing. *Production and Operations Management*, 18(3):300–314.

Ferrer, G. and Swaminathan, J. M. (2006). Managing new and remanufactured products. *Management Science*, 52(1):15–26.

Fiacco, A. V. and Ghaemi, A. (1982). Sensitivity analysis of a nonlinear water pollution control model using an upper hudson river data base. *Operations Research*, 30(1):1–28.

Fleischmann, M., Beullens, P., BLOEMHOF-RUWAARD, J. M., and Van Wassenhove, L. N. (2001). The impact of product recovery on logistics network design. *Production and Operations Management*, 10(2):156–173.

Fletcher, S. M., Miotti, M., Swaminathan, J., Klemun, M. M., Strzepek, K., and Siddiqi, A. (2017). Water supply infrastructure planning: decision-making framework to classify multiple uncertainties and evaluate flexible design. *Journal of Water Resources Planning and Management*, 143(10):04017061.

Flörke, M., Schneider, C., and McDonald, R. I. (2018). Water competition between cities and agriculture driven by climate change and urban growth. *Nature Sustainability*, 1(1):51–58.

Francas, D. and Minner, S. (2009). Manufacturing network configuration in supply chains with product recovery. *Omega*, 37(4):757–769.

Galbreth, M. R. and Blackburn, J. D. (2010). Optimal acquisition quantities in remanufacturing with condition uncertainty. *Production and Operations Management*, 19(1):61–69.

Georgiadis, P. and Athanasiou, E. (2010). The impact of two-product joint lifecycles on capacity planning of remanufacturing networks. *European Journal of Operational Research*, 202(2):420–433.

Georgiadis, P., Vlachos, D., and Tagaras, G. (2006). The impact of product lifecycle on capacity planning of closed-loop supply chains with remanufacturing. *Production and Operations management*, 15(4):514–527.

Goh, J., Bayati, M., Zenios, S. A., Singh, S., and Moore, D. (2018). Data uncertainty in markov chains: Application to cost-effectiveness analyses of medical innovations. *Operations Research*, 66(3):697–715.

Gu, Y., Li, Y., Li, X., Luo, P., Wang, H., Wang, X., Wu, J., and Li, F. (2017). Energy self-sufficient wastewater treatment plants: feasibilities and challenges. *Energy Procedia*, 105:3741–3751.

Guide Jr, V. D. R. and Van Wassenhove, L. N. (2009). Or forum—the evolution of closed-loop supply chain research. *Operations Research*, 57(1):10–18.

Gupta, V., Han, B. R., Kim, S.-H., and Paek, H. (2020). Maximizing intervention effectiveness. *Management Science*.

Ho, T.-H., Lim, N., Reza, S., and Xia, X. (2017). Om forum—causal inference models in operations management. *Manufacturing & Service Operations Management*, 19(4):509–525.

Hobson, P., Fabris, R., Develter, E., Linden, L. G., Burch, M. D., and Brookes, J. D. (2010). Reservoir inflow monitoring for improved management of treated water quality—a south australian experience. *Water Resources Management*, 24(14):4161–4174.

Hopp, W. J., Li, J., and Wang, G. (2018). Big data and the precision medicine revolution. *Production and Operations Management*, 27(9):1647–1664.

Huang, Y. (2009). Cost analysis with censored data. *Medical Care*, 47(Supplement):S115–S119.

Huh, W. T. and Lall, U. (2013). Optimal crop choice, irrigation allocation, and the impact of contract farming. *Production and Operations Management*, 22(5):1126–1143.

Ibrahim, R., Kucukyazici, B., Verter, V., Gendreau, M., and Blostein, M. (2016). Designing personalized treatment: An application to anticoagulation therapy. *Production and Operations Management*, 25(5):902–918.

Imbens, G. W. and Rubin, D. B. (2015). *Causal inference in statistics, social, and biomedical sciences*. Cambridge University Press.

Infante-Rivard, C. and Cusson, A. (2018). Reflection on modern methods: selection bias—a review of recent developments. *International Journal of Epidemiology*, 47(5):1714–1722.

Jain, A., Rudi, N., and Wang, T. (2015). Demand estimation and ordering under censoring: Stock-out timing is (almost) all you need. *Operations Research*, 63(1):134–150.

Jilkov, V. P. and Li, X. R. (2004). Online bayesian estimation of transition probabilities for markovian jump systems. *IEEE Transactions on Signal Processing*, 52(6):1620–1630.

Johnson, C. R., Šmigoc, H., and Yang, D. (2014). Solution theory for systems of bilinear equations. *Linear and Multilinear Algebra*, 62(12):1553–1566.

Kaynar, N. and Siddiq, A. (2019). Learning hidden action principal-agent models. *Available at SSRN 3431383*.

KC, D. S., Scholtes, S., and Terwiesch, C. (2020). Empirical research in healthcare operations: Past research, present understanding, and future opportunities. *Manufacturing & Service Operations Management*, 22(1):73–83.

Kendall, M. G. and Alan, S. (1961). The advanced theory of statistics. vols. ii and iii.

Keskinocak, P. and Savva, N. (2020). A review of the healthcare-management (modeling) literature published in manufacturing & service operations management. *Manufacturing & Service Operations Management*, 22(1):59–72.

Lagakos, S. W., Sommer, C. J., and Zelen, M. (1978). Semi-markov models for partially censored data. *Biometrika*, 65(2):311–317.

Leaf, D. E. (2017). Unified method for markov chain transition model estimation using incomplete survey data. *arXiv preprint arXiv:1707.02548*.

Lee, E. K., Wei, X., Baker-Witt, F., Wright, M. D., and Quarshie, A. (2018). Outcome-driven personalized treatment design for managing diabetes. *Interfaces*, 48(5):422–435.

Lee, S. (2006). Propensity score adjustment as a weighting scheme for volunteer panel web surveys. *Journal of Official Statistics*, 22(2):329.

Lee, T. C., Judge, G., and Zellner, A. (1968). Maximum likelihood and bayesian estimation of transition probabilities. *Journal of the American Statistical Association*, 63(324):1162–1179.

Lee, T.-C., Judge, G. G., and Zellner, A. (1970). Estimating the parameters of the markov probability model from aggregate time series data.

Liemberger, R., Marin, P., et al. (2006). The challenge of reducing non-revenue water (nrw) in developing countries-how the private sector can help: a look at performance-based service contracting. Technical report, The World Bank.

Madansky, A. (1959). Least squares estimation in finite markov processes. *Psychometrika*, 24(2):137–144.

Mannor, S., Mebel, O., and Xu, H. (2012). Lightning does not strike twice: Robust mdps with coupled uncertainty. *arXiv preprint arXiv:1206.4643*.

Marchi, A., Dandy, G., and Maier, H. (2014). Financial costs, energy consumption and greenhouse gas emissions for major supply water sources and demand management options for metropolitan adelaide. *Goyder Institute for Water Research Technical Report Series*, (14/12).

Martin, J. J. (1967). *Bayesian decision problems and Markov chains*. Wiley.

Meade, M., Guyatt, G., Cook, D., Griffith, L., Sinuff, T., Kergl, C., Mancebo, J., Esteban, A., and Epstein, S. (2001). Predicting success in weaning from mechanical ventilation. *Chest*, 120(6):400S–424S.

Meenaxi, D. S. and Singh, N. (2018). A reliability model for the progression of chronic heart failure. *International Journal of Applied Engineering Research*, 13(21):15351–15355.

Miller, G. A. (1952). Finite markov processes in psychology. *Psychometrika*, 17(2):149–167.

Miller, J. D. and Carlo, W. A. (2008). Pulmonary complications of mechanical ventilation in neonates. *Clinics in Perinatology*, 35(1):273–281.

Mulligan, A. E. and Ahlfeld, D. P. (2002). A new interior-point boundary projection

method for solving nonlinear groundwater pollution control problems. *Operations Research*, 50(4):636–644.

Mun, K. G., Zhao, Y., and Rafique, R. A. (2021). Designing hydro supply chains for energy, food, and flood. *Manufacturing & Service Operations Management*, 23(2):274–293.

Murali, K., Lim, M. K., and Petruzzi, N. C. (2015). Municipal groundwater management: Optimal allocation and control of a renewable natural resource. *Production and Operations Management*, 24(9):1453–1472.

Nguyen, H. H., Recknagel, F., Meyer, W., Frizenschaf, J., and Shrestha, M. K. (2017). Modelling the impacts of altered management practices, land use and climate changes on the water quality of the millbrook catchment-reservoir system in south australia. *Journal of Environmental Management*, 202:1–11.

Nilim, A. and Ghaoui, L. E. (2005). Robust control of markov decision processes with uncertain transition matrices. *Operations Research*, 53(5):780–798.

Oraiopoulos, N., Ferguson, M. E., and Toktay, L. B. (2012). Relicensing as a secondary market strategy. *Management Science*, 58(5):1022–1037.

Ouyang, H., Argon, N. T., and Ziya, S. (2020). Allocation of intensive care unit beds in periods of high demand. *Operations Research*, 68(2):591–608.

Panepinto, D., Fiore, S., Zappone, M., Genon, G., and Meucci, L. (2016). Evaluation of the energy efficiency of a large wastewater treatment plant in Italy. *Applied Energy*, 161:404–411.

Pasanisi, A., Fu, S., and Bousquet, N. (2012). Estimating discrete markov models from various incomplete data schemes. *Computational Statistics & Data Analysis*, 56(9):2609–2625.

Paton, F., Maier, H., and Dandy, G. (2013). Relative magnitudes of sources of uncertainty in assessing climate change impacts on water supply security for the Southern Adelaide water supply system. *Water Resources Research*, 49(3):1643–1667.

Pearce, G. (2008). Uf/mf pre-treatment to ro in seawater and wastewater reuse applications: a comparison of energy costs. *Desalination*, 222(1-3):66–73.

Rabinowitz, G., Mehrez, A., and Oron, G. (1988). A nonlinear optimization model of water allocation for hydroelectric energy production and irrigation. *Management Science*, 34(8):973–990.

Richey, A. S., Thomas, B. F., Lo, M.-H., Reager, J. T., Famiglietti, J. S., Voss, K., Swenson, S., and Rodell, M. (2015). Quantifying renewable groundwater stress with grace. *Water Resources Research*, 51(7):5217–5238.

Rivera, L. and Weissman, C. (1997). Dynamic ventilatory characteristics during weaning in postoperative critically III patients. *Anesthesia & Analgesia*, 84(6):1250–1255.

Rudi, N. and Drake, D. (2014). Observation bias: The impact of demand censoring on newsvendor level and adjustment behavior. *Management Science*, 60(5):1334–1345.

Rygaard, M., Binning, P. J., and Albrechtsen, H.-J. (2011). Increasing urban water self-sufficiency: New era, new challenges. *Journal of Environmental Management*, 92(1):185–194.

Sahely, H. R. and Kennedy, C. A. (2007). Water use model for quantifying environmental and economic sustainability indicators. *Journal of Water Resources Planning and Management*, 133(6):550–559.

Savaskan, R. C., Bhattacharya, S., and Van Wassenhove, L. N. (2004). Closed-loop supply chain models with product remanufacturing. *Management Science*, 50(2):239–252.

Savaskan, R. C. and Van Wassenhove, L. N. (2006). Reverse channel design: the case of competing retailers. *Management Science*, 52(1):1–14.

Schneider, M. H. and Zenios, S. A. (1990). A comparative study of algorithms for matrix balancing. *Operations Research*, 38(3):439–455.

Schork, N. J. (2015). Personalized medicine: time for one-person trials. *Nature*, 520(7549):609–611.

Shechter, S. M. (2006). *When to initiate, when to switch, and how to sequence HIV therapies: A Markov decision process approach.* PhD thesis, University of Pittsburgh.

Shechter, S. M., Bailey, M. D., Schaefer, A. J., and Roberts, M. S. (2008). The optimal time to initiate hiv therapy under ordered health states. *Operations Research*, 56(1):20–33.

Short, M., Saint, C., Regel, R., and van den Akker, B. (2014). *An integrated approach for performance benchmarking of water recycling operations.* Australian Water Recycling Centre of Excellence.

Skandari, M. R., Shechter, S. M., and Zalunardo, N. (2015). Optimal vascular access choice for patients on hemodialysis. *Manufacturing & Service Operations Management*, 17(4):608–619.

Sobel, M. J. (1971). Chebyshev optimal waste discharges. *Operations Research*, 19(2):308–322.

Souza, G. C. (2013). Closed-loop supply chains: A critical review, and future research. *Decision Sciences*, 44(1):7–38.

Srinivasan, V., Gorelick, S. M., and Goulder, L. (2010). Sustainable urban water supply in south india: Desalination, efficiency improvement, or rainwater harvesting? *Water Resources Research*, 46(10).

Stoecker, A., Seidmann, A., and Lloyd, G. (1985). A linear dynamic programming approach to irrigation system management with depleting groundwater. *Management Science*, 31(4):422–434.

Storm, H., Heckelei, T., and Mittelhammer, R. C. (2015). Bayesian estimation of non-stationary markov models combining micro and macro data. *European Review of Agricultural Economics*, 43(2):303–329.

Stukel, T. A., Fisher, E. S., Wennberg, D. E., Alter, D. A., Gottlieb, D. J., and Vermeulen, M. J. (2007). Analysis of observational studies in the presence of treatment selection bias: effects of invasive cardiac management on ami survival using propensity score and instrumental variable methods. *Jama*, 297(3):278–285.

Taylor, A. C. (1973). A planning model for a water quality management agency. *Management Science*, 20(4-part-ii):675–685.

Theil, H. and Rey, G. (1966). A quadratic programming approach to the estimation of transition probabilities. *Management Science*, 12(9):714–721.

Thille, A. W., Richard, J.-C. M., and Brochard, L. (2013). The decision to extubate in the intensive care unit. *American Journal of Respiratory and Critical Care Medicine*, 187(12):1294–1302.

Toktay, L. B., Wein, L. M., and Zenios, S. A. (2000). Inventory management of remanufacturable products. *Management Science*, 46(11):1412–1426.

Truog, R. D., Mitchell, C., and Daley, G. Q. (2020). The toughest triage—allocating ventilators in a pandemic. *New England Journal of Medicine*, 382(21):1973–1975.

Üster, H. and Hwang, S. O. (2017). Closed-loop supply chain network design under demand and return uncertainty. *Transportation Science*, 51(4):1063–1085.

Van der Laan, E., Salomon, M., Dekker, R., and Van Wassenhove, L. (1999). Inventory control in hybrid systems with remanufacturing. *Management Science*, 45(5):733–747.

Vincent, J.-L., Akça, S., de Mendonça, A., Haji-Michael, P., Sprung, C., Moreno, R., Antonelli, M., and Suter, P. M. (2002). The epidemiology of acute respiratory failure in critically ill patients. *Chest*, 121(5):1602–1609.

Vlachos, D., Georgiadis, P., and Iakovou, E. (2007). A system dynamics model for dynamic capacity planning of remanufacturing in closed-loop supply chains. *Computers & Operations Research*, 34(2):367–394.

Welton, N. J. and Ades, A. E. (2005). Estimation of markov chain transition probabilities and rates from fully and partially observed data: Uncertainty propagation, evidence synthesis, and model calibration. *Medical Decision Making*, 25(6):633–645.

Wiesemann, W., Kuhn, D., and Rustem, B. (2013). Robust markov decision processes. *Mathematics of Operations Research*, 38(1):153–183.

Woods, G. J., Kang, D., Quintanar, D. R., Curley, E. F., Davis, S. E., Lansey, K. E., and Arnold, R. G. (2013). Centralized versus decentralized wastewater reclamation in the houghton area of tucson, arizona. *Journal of Water Resources Planning and Management*, 139(3):313–324.

Wooldridge, J. M. (2010). *Econometric analysis of cross section and panel data*. MIT press.

Wu, H. and Noé, F. (2010). Maximum a posteriori estimation for markov chains based on gaussian markov random fields. *Procedia Computer Science*, 1(1):1665–1673.

Wu, W., Dandy, G. C., Maier, H. R., Maheepala, S., Marchi, A., and Mirza, F. (2017). Identification of optimal water supply portfolios for a major city. *Journal of Water Resources Planning and Management*, 143(9):05017007.

Zhang, H., Chao, X., and Shi, C. (2018). Technical note—perishable inventory systems: Convexity results for base-stock policies and learning algorithms under censored demand. *Operations Research*, 66(5):1276–1286.

Zhang, J., Denton, B. T., Balasubramanian, H., Shah, N. D., and Inman, B. A. (2012). Optimization of prostate biopsy referral decisions. *Manufacturing & Service Operations Management*, 14(4):529–547.

Zhang, W., Rahimian, H., and Bayraksan, G. (2016). Decomposition algorithms for risk-averse multistage stochastic programs with application to water allocation under uncertainty. *INFORMS Journal on Computing*, 28(3):385–404.

Zhang, Y., Steimle, L., and Denton, B. (2017). Robust markov decision processes for medical treatment decisions. *Optimization Online*.

Zhao, Y., Fang, X., and Simchi-Levi, D. (2017). Uplift modeling with multiple treatments and general response types. In *Proceedings of the 2017 SIAM International Conference on Data Mining*, pages 588–596. Society for Industrial and Applied Mathematics.

Appendix A

Appendix of Chapter 1

A.1 Technical Proofs

Proof of Theorem 1.1. Define

$$\bar{A}_i = \sum_{z=1}^{N} P_{iz}^{a=1} \left(p_i^{te} \sum_{k=z-\bar{\delta}(i)}^{N} P_{ik}^{a=0} \right)$$

$$\tilde{A}_i = \sum_{z=1}^{N} P_{iz}^{a=0} \left(p_i^{te} \sum_{k=\max(z+\bar{\delta}(i)+1,1)}^{N} P_{ik}^{a=1} \right)$$

$$\bar{B}_i = p_i^{se} \sum_{k=1}^{N} q_k^{se} \mathbb{I}_{i \geq k}$$

$$\tilde{B}_i = p_i^{se} \sum_{k=1}^{N} q_k^{se} (1 - \mathbb{I}_{i \geq k})$$

I have

$$\sum_{z=1}^{N} P_{iz}^{a=1} \left(p_i^{te} \sum_{k=z-\bar{\delta}(i)}^{N} P_{ik}^{a=0} + p_i^{se} \sum_{k=1}^{N} q_k^{se} \mathbb{I}_{i \geq k} \right) = \bar{A}_i + \bar{B}_i$$

$$\sum_{z=1}^{N} P_{iz}^{a=0} \left(p_i^{se} \sum_{k=1}^{N} q_k^{se} (1 - \mathbb{I}_{i \geq k}) + p_i^{te} \sum_{k=\max(z+\bar{\delta}(i)+1,1)}^{N} P_{ik}^{a=1} \right) = \tilde{A}_i + \tilde{B}_i$$

It is easy to show $\bar{A}_i + \tilde{A}_i = p_i^{te}$. Assume there are two different solutions $(\mathbf{P}_i^{a=1(1)}, \mathbf{P}_i^{a=0(1)})$ and $(\mathbf{P}_i^{a=1(2)}, \mathbf{P}_i^{a=0(2)})$, then $(\bar{A}_i^{(1)}, \tilde{A}_i^{(1)})$ and $(\bar{A}_i^{(2)}, \tilde{A}_i^{(2)})$ are the corresponding values under the two solutions respectively. Without lose of generality, I assume $\bar{A}_i^{(1)} \leq \bar{A}_i^{(2)}$,

then I have $\bar{A}_i^{(1)} + \bar{B}_i \leq \bar{A}_i^{(2)} + \bar{B}_i$ and $\tilde{A}_i^{(1)} \geq \tilde{A}_i^{(2)}$, which implies $\tilde{A}_i^{(1)} + \tilde{B}_i \geq \tilde{A}_i^{(2)} + \tilde{B}_i$. Furthermore, because solution (1) and solution (2) are both solutions to the equation system. Then I have

$$\frac{P_{ij}^{a=1(1)}\left(p_i^{te}\sum_{k=j-\bar{\delta}(i)}^{N}P_{ik}^{a=0(1)}+\bar{B}_i\right)}{\bar{A}_i^{(1)}+\bar{B}_i}=\frac{P_{ij}^{a=1(2)}\left(p_i^{te}\sum_{k=j-\bar{\delta}(i)}^{N}P_{ik}^{a=0(2)}+\bar{B}_i\right)}{\bar{A}_i^{(2)}+\bar{B}_i} \tag{A.1}$$

$$\frac{P_{ij}^{a=0(1)}\left(\tilde{B}_i+p_i^{te}\sum_{k=\max(j+\bar{\delta}(i)+1,1)}^{N}P_{ik}^{a=1(1)}\right)}{\tilde{A}_i^{(1)}+\tilde{B}_i}=\frac{P_{ij}^{a=0(2)}\left(\tilde{B}_i+p_i^{te}\sum_{k=\max(j+\bar{\delta}(i)+1,1)}^{N}P_{ik}^{a=1(2)}\right)}{\tilde{A}_i^{(2)}+\tilde{B}_i} \tag{A.2}$$

Moreover, from assumption $q_{i1}^s > 0$ and $p_i^s > 0$, I have $\bar{B}_i > 0$. Therefore, $\bar{A}_i^{(1)} \leq \bar{A}_i^{(2)} \Longrightarrow P_{i,(N+\bar{\delta}(i)+1)}^{a=1(1)} \leq P_{i,(N+\bar{\delta}(i)+1)}^{a=1(2)}, ..., P_{iN}^{a=1(1)} \leq P_{iN}^{a=1(2)}$ (Note that here I assume $\bar{\delta}(i) < 0$, for the case with $\bar{\delta}(i) \geq 0$, the analysis is similar by starting from equation A.2), which can further generate $\sum_{k=\max(j+\bar{\delta}(i)+1,1)}^{N} P_{ik}^{a=1(1)} \leq \sum_{k=\max(j+\bar{\delta}(i)+1,1)}^{N} P_{ik}^{a=1(2)}$. This is because, e.g., let $j = N + \bar{\delta}(i) + 1$, then I have

$$\frac{P_{i,(N+\bar{\delta}(i)+1)}^{a=1(1)}\left(\bar{B}_i\right)}{\bar{A}_i^{(1)}+\bar{B}_i}=\frac{P_{i(N+\bar{\delta}(i)+1)}^{a=1(2)}\left(\bar{B}_i\right)}{\bar{A}_i^{(2)}+\bar{B}_i}$$

since $\bar{A}_i^{(1)} \leq \bar{A}_i^{(2)}$ and $\bar{B}_i > 0$, I must have $P_{i,(N+\bar{\delta}(i)+1)}^{a=1(1)} \leq P_{i,(N+\bar{\delta}(i)+1)}^{a=1(2)}$, following the same reasoning process, I can derive $P_{i,(N+\bar{\delta}(i)+1)}^{a=1(1)} \leq P_{i,(N+\bar{\delta}(i)+1)}^{a=1(2)}, ..., P_{iN}^{a=1(1)} \leq P_{iN}^{a=1(2)}$. Similarly, I have $\tilde{A}_i^{(1)} + \tilde{B}_i \geq \tilde{A}_i^{(2)} + \tilde{B}_i$, then I can immediately have $P_{iN}^{a=0(1)} \geq P_{iN}^{a=0(2)}$ based on Equation A.2. Moreover, from Equation A.1, I know

$$\frac{P_{i,(N+\bar{\delta}(i))}^{a=1(1)}\left(p_i^{te}\sum_{k=N}^{N}P_{ik}^{a=0(1)}+\bar{B}_i\right)}{\bar{A}_i^{(1)}+\bar{B}_i}=\frac{P_{i,(N+\bar{\delta}(i))}^{a=1(2)}\left(p_i^{te}\sum_{k=N}^{N}P_{ik}^{a=0(2)}+\bar{B}_i\right)}{\bar{A}_i^{(2)}+\bar{B}_i}$$

then, $\bar{A}_i^{(1)} \leq \bar{A}_i^{(2)}$, $\bar{B}_i > 0$, and $P_{iN}^{a=0(1)} \geq P_{iN}^{a=0(2)}$ can derive $P_{i,(N+\bar{\delta}(i))}^{a=1(1)} \leq P_{i,(N+\bar{\delta}(i))}^{a=1(2)}$, combining with $\sum_{k=\max(N+\bar{\delta}(i)+1,1)}^{N} P_{ik}^{a=1(1)} \leq \sum_{k=\max(N+\bar{\delta}(i)+1,1)}^{N} P_{ik}^{a=1(2)}$, I can derive $\sum_{k=\max(N+\bar{\delta}(i),1)}^{N} P_{ik}^{a=1(1)} \leq \sum_{k=\max(N+\bar{\delta}(i),1)}^{N} P_{ik}^{a=1(2)}$, from which I can show $P_{i,(N-1)}^{a=0(1)} \geq P_{i,(N-1)}^{a=0(2)}$ in equation A.2. By

doing such reasoning process repeatedly, I can show $P_{ij}^{a=1(1)} \leq P_{ij}^{a=1(2)}$ and $P_{ij}^{a=0(1)} \geq P_{ij}^{a=0(2)}$ for all $j \in S$. As solution (1) and solution (2) are different, then there is at least one $P_{ij}^{a=1(1)} < P_{ij}^{a=1(2)}$ and one $P_{ij}^{a=0(1)} > P_{ij}^{a=0(2)}$, then, I have

$$1 = \sum_{j=1}^{N} P_{ij}^{a=1(1)} < \sum_{j=1}^{N} P_{ij}^{a=1(2)} = 1$$

$$1 = \sum_{j=1}^{N} P_{ij}^{a=0(1)} > \sum_{j=1}^{N} P_{ij}^{a=0(2)} = 1$$

which cannot be true. Then I can conclude that two different solution is impossible, which means the solution is unique to the system. □

Proof of Theorem 1.2. (1) The probabilistic convergence of $\hat{\Pi}^a(n)$ is obvious because I assume a multinomial distribution for the transitions.

(2)I know that $\mathbf{G}_i$ is a continuous one to one mapping on open set, then the inverse mapping $\mathbf{G}_i^{-1}$ exists and continuous. Since I have $\mathbb{P}(||\hat{\mathbf{\Pi}}_i^a(n) - \mathbf{\Pi}_i^a|| > \epsilon) \to 0$, then $\exists \lambda > 0$ such that $\mathbb{P}(||\hat{\mathbf{\Pi}}_i^a(n) - \mathbf{\Pi}_i^a|| \leq \lambda) \to 1$, with the condition that $\mathbf{G}_i^{-1}$ is continuous, I can generate $\mathbb{P}(||\boldsymbol{G}_i^{-1}(\hat{\mathbf{\Pi}}_i^a(n)) - \boldsymbol{G}_i^{-1}(\mathbf{\Pi}_i^a)|| \leq \epsilon) \to 1$, then $\mathbb{P}(||\hat{\boldsymbol{P}}_i^a(n) - \boldsymbol{P}_i^a|| > \epsilon) \to 0$. (Continuous Mapping Theorem)

(3) I know $\mathbf{G}_i$ is continuously differentiable, assume $\det(J_{\mathbf{G}_i}) \neq 0$, where $J_{\mathbf{G}_i}$ is the Jacobian matrix. Then $\boldsymbol{G}_i^{-1}$ is also continuously differentiable. Therefore, following Lemma 3.9 from Wooldridge (2010), I have $\sqrt{n}[\mathbf{G}_i^{-1}(\hat{\mathbf{\Pi}}_i^a) - \mathbf{G}_i^{-1}(\mathbf{\Pi}_i^a)] \overset{d}{\sim} \mathcal{N}(0, \mathbf{\Delta} \boldsymbol{V}^{-1} \mathbf{\Delta}')$ as $\sqrt{n}[\hat{\mathbf{\Pi}}_i^a - \mathbf{\Pi}_i^a] \overset{d}{\sim} \mathcal{N}(0, \boldsymbol{V}^{-1})$ following from Cox and Hinkley (1979). □

Proof of Theorem 1.3. In the system of equations, $(\hat{\Pi}_{ij}^{a=1}, \hat{\Pi}_{ij}^{a=1}) = (\frac{\hat{Y}_{ij}}{\hat{K}_i^{a=1}}, \frac{\hat{X}_{ij}}{\hat{K}_i^{a=0}})$, which is the maximum likelihood estimator derived from the following log-likelihood function with constraints $\sum_{j=1}^{N} \hat{\Pi}_{ij}^a = 1$ for $a = 0, 1$.

$$\log(L(\Pi_{ij}^{a=0}, \Pi_{ij}^{a=1})) = \log(\frac{K_i^{a=1}!}{Y_{i1}!...Y_{iN}!}) + \log(\frac{K_i^{a=0}!}{X_{i1}!...X_{iN}!}) + \sum_{j=1}^{N} \left(Y_{ij} \log(\Pi_{ij}^{a=1})\right) + \sum_{j=1}^{N} \left(Y_{ij} \log(\Pi_{ij}^{a=0})\right)$$

As $g_{ij}^a(\boldsymbol{P}_i^{a=0}, \boldsymbol{P}_i^{a=1}) = \Pi_{ij}^a$ for any well defined i, j,and a, and the mapping is one-to-

one, then by definition, I have $\left(g_{ij}^{a=1}((\hat{\mathbf{P}}_i^{a=1}, \hat{\mathbf{P}}_i^{a=0})), g_{ij}^{a=0}((\hat{\mathbf{P}}_i^{a=1}, \hat{\mathbf{P}}_i^{a=0}))\right) = (\frac{\hat{Y}_{ij}}{\hat{K}_i^{a=1}}, \frac{\hat{X}_{ij}}{\hat{K}_i^{a=0}})$, then $(\hat{\mathbf{P}}_i^{a=1}, \hat{\mathbf{P}}_i^{a=0})$ maximizes

$$\begin{aligned}\log(L(\boldsymbol{P}_i^{a=0}, \boldsymbol{P}_i^{a=1})) = \log(\frac{K_i^{a=1}!}{Y_{i1}!...Y_{iN}!}) + \log(\frac{K_i^{a=0}!}{X_{i1}!...X_{iN}!}) + \\ + \sum_{j=1}^{N} \left(y_{ij} \log(g_{ij}^{a=1}(\boldsymbol{P}_i^{a=0}, \boldsymbol{P}_i^{a=1}))\right) \\ + \sum_{j=1}^{N} \left(x_{ij} \log(g_{ij}^{a=0}(\boldsymbol{P}_i^{a=0}, \boldsymbol{P}_i^{a=1}))\right)\end{aligned}$$

which by definition is a direct ML estimator. □

A.2 Model with Multiple Treatment-Effect Thresholds Setting

Let q_{il}^{te} be the probability that l is selected as the threshold under treatment-effect-based policy for state i patients. As the state space $\mathcal{S} = \{1, 2, ..., N\}$; hence, the treatment-effect threshold candidate set is $\{2-2N, 1-2N, ..., 2N-2\}$. Therefore, the structural model with multiple treatment-effect threshold is as follow.

$$\hat{\Pi}_{ij}^{a=1} = \frac{P_{ij}^{a=1}\left(p_i^{te}\sum_{l=2-2N}^{2N-2} q_{il}^{te}\sum_{k=j-l}^{N} P_{ik}^{a=0} + p_i^{se}\sum_{k=1}^{N} q_k^{se}\mathbb{I}_{i\geq k}\right)}{\sum_{z=1}^{N} P_{iz}^{a=1}\left(p_i^{te}\sum_{l=2-2N}^{2N-2} q_{il}^{te}\sum_{k=z-l}^{N} P_{ik}^{a=0} + p_i^{se}\sum_{k=1}^{N} q_k^{se}\mathbb{I}_{i\geq k}\right)}$$

$$\hat{\Pi}_{ij}^{a=0} = \frac{P_{ij}^{a=0}\left(p_i^{se}\sum_{k=1}^{N} q_k^{se}(1-\mathbb{I}_{i\geq k}) + p_i^{te}\sum_{l=2-2N}^{2N-2} q_{il}^{te}\sum_{k=\max(j+l+1,1)}^{N} P_{ik}^{a=1}\right)}{\sum_{z=1}^{N} P_{iz}^{a=0}\left(p_i^{se}\sum_{k=1}^{N} q_k^{se}(1-\mathbb{I}_{i\geq k}) + p_i^{te}\sum_{l=2-2N}^{2N-2} q_{il}^{te}\sum_{k=\max(z+l+1,1)}^{N} P_{ik}^{a=1}\right)}$$

A.3 Supplementary Simulation Settings

A.3.1 Predictive Models in Simulations

To build the predictive models in the simulation, I separate $\mathcal{D}$ into two subsets, $\mathcal{D}_1$ and $\mathcal{D}_0$, by action $a = 1$ and $a = 0$, respectively. For the dataset $\mathcal{D}_0$ ($\mathcal{D}_1$), I train predictive model $Mod0(Mod1)$ base on pv^0 and RR^0(pv^1 and RR^1), and then I apply $Mod0(Mod1)$ to dataset $\mathcal{D}_1(\mathcal{D}_0)$ to predict the censored RR values with $pv^0(pv^1)$ as the input under $a = 0(a = 1)$. The predicted RR values are classified into different states, and then all data (predicted and observed) are combined to derive $\tilde{\mathbf{P}}^a$ with MLE by assuming a multinomial prior distribution. The prediction accuracy of $Mod0$ and $Mod1$ are denoted by β^0 and β^1, respectively.

A.3.2 Two-Stage Estimation

For the estimation of p and $\boldsymbol{q}^{se}$, as I mentioned, I employ an ensembling method with maximizing the MLE to select the parameters. Specifically, let DCM_k (DCM_{te}) be the severity-based (treatment-effect-based) decision classification model such that, for any patient at period t, s/he will be extubated (i.e., $a = 0$) if $s_t < k$ ($\delta_t \geq 0$) and continue the ventilation otherwise. Then, the probability that patients with state s and treatment effect δ will continue the ventilation (i.e., $a = 1$) at time t can be represented by

$$Pr_{s,\delta}(a = 1|t) = \sum_{k=1}^{4} q_k^{se}(1 - p) \times (\mathbb{I}_{s\geq k}|t, DCM_K) + p \times (\mathbb{I}_{\delta<0}|t, DCM^{te})$$

Then, for each data point j, I can derive the probability that a patient will continue the ventilation $p(a_j = 1)$, where a_j is the action of data point j. Let ven_j be the indicator that $a_j = 1$ if $ven_j = 1$ and $a_j = 0$ otherwise. Subsequently, I can write the likelihood function for data point j as

$$\mathcal{L}_j(p, \boldsymbol{q}^{se}) = p(a_j = 1)^{ven_j}(1 - p(a_j = 1))^{1-ven_j}$$

The log-likelihood on the selected sample can then be obtained. I then select the $\hat{p}$ and $\hat{\mathbf{q}}^{se}$ that maximize the sample log-likelihood as the estimated parameters. As the ensembling model depends on the treatment effect, which is derived by the predictive models, then the two-stage estimator depends on the prediction accuracy.

A.4 Simulation Results

A.4.1 Error-Free Structural Model: Additional Results

The performance comparison with matrices distance is measured by 2-norm is presented in Figure A.1. and the performance comparison with matrices distance is

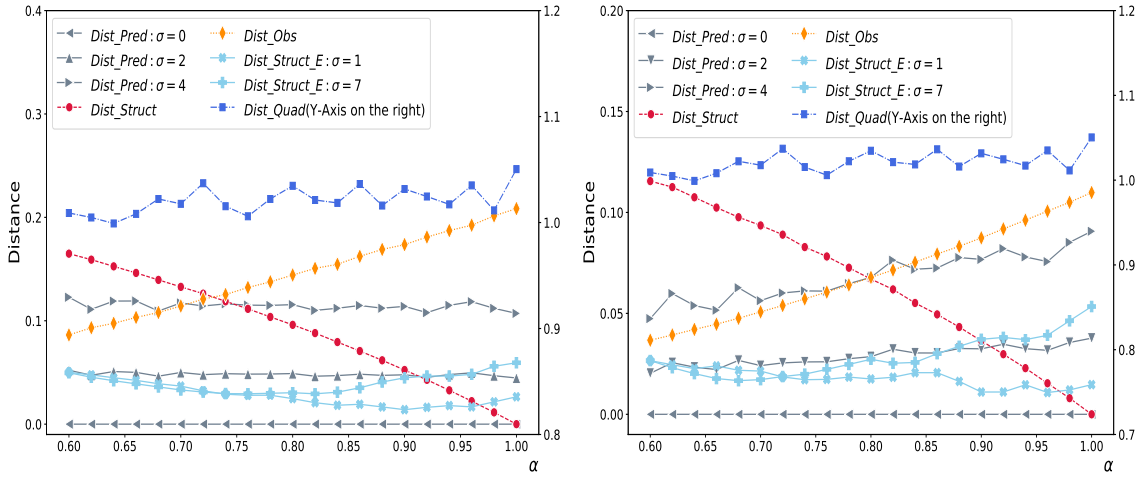

(a) Action $a = 0$ (b) Action $a = 1$

Figure A.1: Performances Comparison 2-Norm

measured by Frobenius norm (F-norm) is presented in Figure A.2.

In the simulation, I know that the ground truth value of the probability of using treatment-effect-based policy is $p = 0.45$. In the two-stage estimation, the first stage MLE estimation tends to underestimate p. Moreover, for the two-stage estimators, the estimated values of p (i.e., $\hat{p}$) may be different under different values of α. To validate the insights I obtained by the curves of *Dist_Struct_E* in Section **??**, I

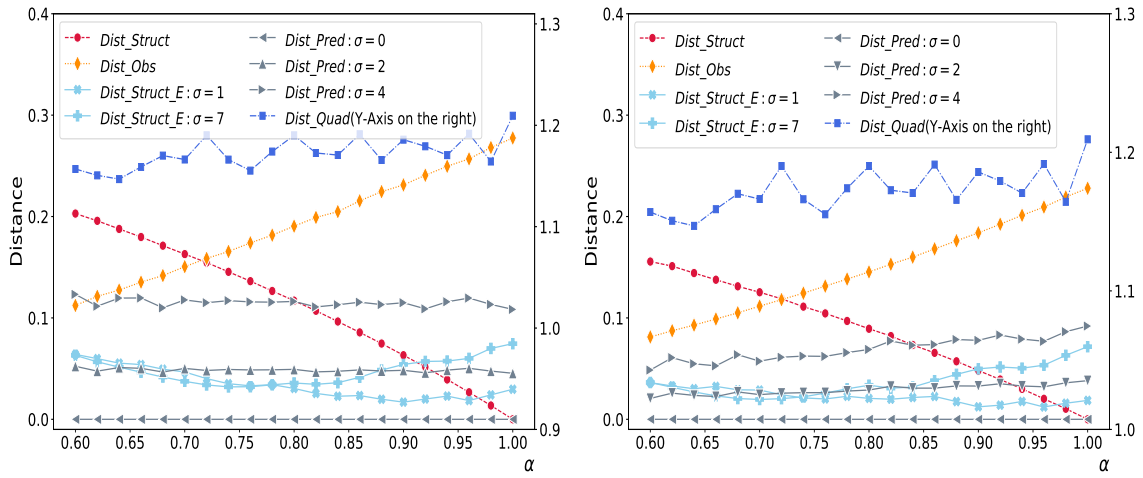

(a) Action $a = 0$ (b) Action $a = 1$

Figure A.2: Performances Comparison Frobenius-Norm

conduct sensitivity analysis and force $\hat{p} = 0.4, 0.3, 0.2$ and then use these values in the error-free model to derive the estimators with keeping $\boldsymbol{q}^{se}$ as the ground truth value. The results under the max-norm (same insights can be observed under 2-norm and F-norm) are shown in Figure A.3. From Figure A.3, I find that given $\hat{p} \in (0, p)$,

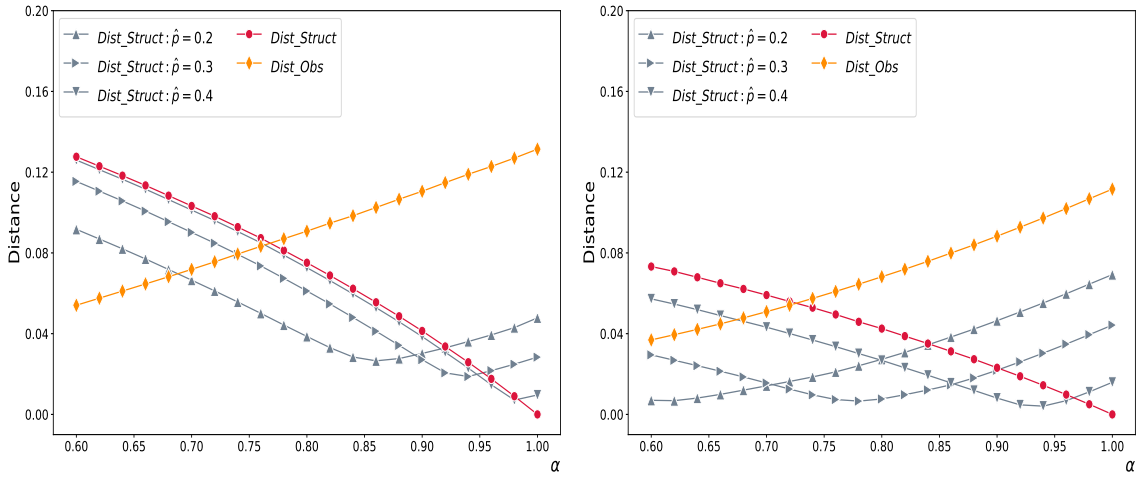

(a) Action $a = 0$ (b) Action $a = 1$

Figure A.3: Sensitivity Analysis to $\boldsymbol{p}^{te}$

and estimate the TPMs using $\hat{p}$ and the error-free model, the performance (i.e., Max-norm distance here) of the estimated TPM presents a U-shaped curve such that the

distance first decreases and then increases in α. These observations further validate the insights that I obtained from *Dist_Struct_E* in the main text. I may note that there are fluctuations for *Dist_Struct_E* in Figure 1.4, but in Figure A.3, the curves behave much more smooth. The reason is, as I mentioned, the first stage estimators are not necessarily the same for different values of α in Figure 1.4; moreover, the estimated $\hat{\mathbf{q}}^{se}$ are also different from the ground truth values. Hence, *Dist_Struct_E* in Figure 1.4 is not necessarily behaves exactly the same with the corresponding curves in A.3.

A.4.2 Correlation and Prediction Accuracy

The correlation coefficients between pv^0 and RR^0(pv^1 and RR^1) is denoted by $\rho_0(\rho_1)$. Figure A.4 uses the cases with $\alpha = 0.96, 0.9, 0.86$, and 0.8 to illustrate the relationship between $\rho_0(\rho_1)$ and the prediction accuracy of $Mod0(Mod1)$, respectively. I can see that β^0 and β^1 are increasing in ρ_0 and ρ_1. Moreover, with the perfect linear correlation ($\sigma_0 = \sigma_1 = 0$), $\beta^0 = \beta^1 = 1$. However, the accurate rates drop dramatically

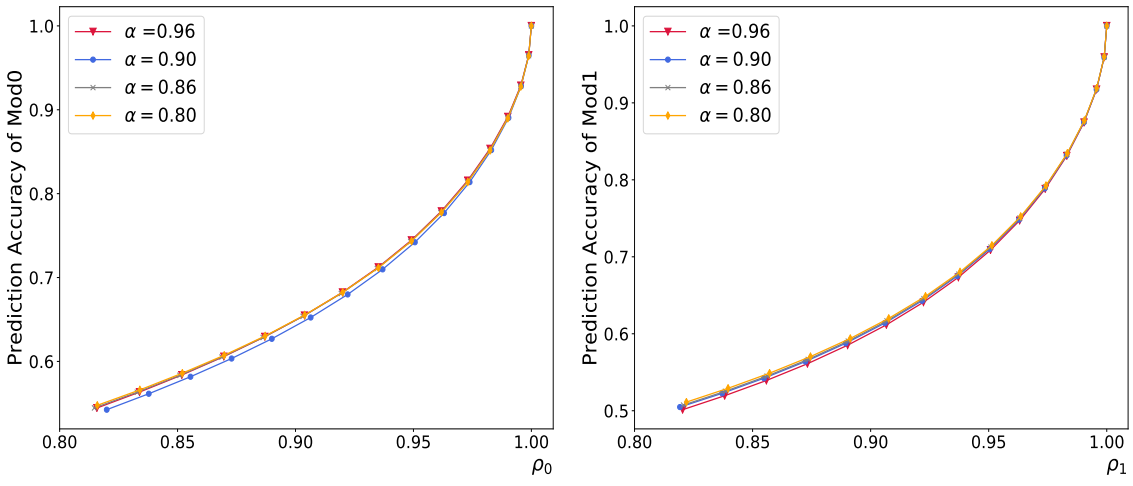

(a) Action $a = 0$ (b) Action $a = 1$

Figure A.4: Relationship Between Correlation and Prediction Accuracy

with the reduction of correlation. When ρ_0 and ρ_1 are approaching 0.8, β^0 and β^1

are approaching 0.5. The reason for this is as follow: given ρ_0 and ρ_1 in dataset $\mathcal{D}$, after the split of $\mathcal{D}$, I observe that ρ_{00} and ρ_{11} tend to be much larger than ρ_{01} and ρ_{10}, respectively, which suggests that $Mod0$ and $Mod1$ may have very high in-sample accuracy on datasets $\mathcal{D}_0$ and $\mathcal{D}_1$ but low out-of-sample accuracy on datasets $\mathcal{D}_1$ and $\mathcal{D}_0$. Therefore, I can observe the patterns in Figure A.4. These observations indicate that data noise resulted from treatment-effect-based censoring has significantly negative impacts on the performances of predictive models.

A.4.3 Simulation: Additional Supports

I derive the deviation matrices $\hat{\boldsymbol{\Delta}}_E^a = \hat{\mathbf{P}}_E^a - \boldsymbol{P}^a$, $\hat{\boldsymbol{\Delta}}^a = \hat{\mathbf{P}}^a - \boldsymbol{P}^a$, $\tilde{\boldsymbol{\Delta}}^a = \tilde{\mathbf{P}}^a - \boldsymbol{P}^a$ and $\bar{\boldsymbol{\Delta}}^a = \hat{\boldsymbol{\Pi}}^a - \boldsymbol{P}^a$ and use the case that $\alpha = 0.78$ and $\sigma = 7$ (these two representative values are selected base on the results in the case study) as the representative to illustrate the average results.

$$\hat{\boldsymbol{\Delta}}_E^{a=1} = \begin{pmatrix} 0.019 & -0.011 & -0.006 & -0.001 \\ 0.008 & 0.002 & -0.007 & -0.003 \\ 0.002 & 0.005 & 0.001 & -0.007 \\ 0.001 & 0.004 & 0.006 & -0.010 \end{pmatrix} \quad \hat{\boldsymbol{\Delta}}_E^{a=0} = \begin{pmatrix} 0.001 & 0.000 & -0.001 & -0.000 \\ 0.007 & 0.000 & -0.005 & -0.003 \\ 0.004 & 0.010 & -0.002 & -0.012 \\ 0.000 & -0.002 & -0.018 & 0.020 \end{pmatrix}$$

$$\hat{\boldsymbol{\Delta}}^{a=1} = \begin{pmatrix} -0.006 & 0.006 & 0.001 & 0 \\ -0.016 & 0.002 & 0.011 & 0.003 \\ -0.007 & -0.011 & 0 & 0.018 \\ -0.002 & -0.008 & -0.018 & 0.028 \end{pmatrix} \quad \hat{\boldsymbol{\Delta}}^{a=0} = \begin{pmatrix} -0.044 & 0.03 & 0.01 & 0.004 \\ -0.035 & -0.01 & 0.025 & 0.02 \\ -0.013 & -0.037 & -0.024 & 0.073 \\ 0.001 & 0 & -0.009 & 0.008 \end{pmatrix}$$

$$\tilde{\boldsymbol{\Delta}}^{a=1} = \begin{pmatrix} 0.043 & -0.035 & -0.006 & -0.001 \\ 0.007 & -0.003 & -0.003 & -0.001 \\ 0.003 & 0.005 & 0.001 & -0.009 \\ 0.001 & 0.003 & 0.025 & -0.029 \end{pmatrix} \quad \tilde{\boldsymbol{\Delta}}^{a=0} = \begin{pmatrix} 0.039 & -0.033 & -0.005 & -0.001 \\ 0.009 & -0.006 & -0.002 & -0.001 \\ 0.003 & 0.012 & -0.002 & -0.012 \\ 0.001 & 0.002 & 0.053 & -0.056 \end{pmatrix}$$

$$\bar{\mathbf{\Delta}}^{a=1} = \begin{pmatrix} 0.015 & -0.01 & -0.004 & -0.001 \\ 0.039 & -0.008 & -0.022 & -0.01 \\ 0.02 & 0.023 & -0.012 & -0.03 \\ 0.004 & 0.016 & 0.027 & -0.047 \end{pmatrix} \quad \bar{\mathbf{\Delta}}^{a=0} = \begin{pmatrix} 0.061 & -0.044 & -0.015 & -0.003 \\ 0.091 & -0.007 & -0.057 & -0.027 \\ 0.04 & 0.065 & -0.013 & -0.091 \\ 0.008 & 0.025 & 0.038 & -0.072 \end{pmatrix}$$

From the deviation matrices, I can see that, on average sense, $\hat{\mathbf{P}}_E^a$ is much closer to $\boldsymbol{P}^a$ when compared with $\tilde{\mathbf{P}}^a$ and $\hat{\mathbf{\Pi}}^a$. Hence, it also supports the conclusion that the proposed structural model outperforms other estimation methods. Moreover, from the deviation matrices, I can see that the observed TPMs tend to overestimate the effects of both ventilation and extubation, which validate the results of Proposition 1.1. For the structural model, the estimated TPM $\hat{\mathbf{P}}^a$ tends to underestimate the effects of actions. This is because the error-free model assumes that all predictions are correct, which means the model potentially treats every observed transition as the one with better outcome (the censored transition has worse outcome). However, when I have prediction errors, the observed outcomes are not necessarily better; hence, under wrong predictions, censored transitions with better outcomes are recovered as transitions with worse outcomes. Therefore, $\hat{\mathbf{P}}^a$ tends to underestimate the effect of action a.

As the supplement results, I compare the absolute value of each entry of the deviation matrices. These comparisons can also reflect the performance of each estimation method. Specifically, I investigate the percentages of negative entries in the matrices $|\hat{\mathbf{\Delta}}_E^a| - |\bar{\mathbf{\Delta}}^a|$ (for illustration, $\hat{\mathbf{\Delta}}_E^a$ is selected under $\sigma = 7$) and $|\hat{\mathbf{\Delta}}_E^a| - |\tilde{\mathbf{\Delta}}^a|$ under different α and σ for $a = 0, 1$. The results are shown in Figure A.5. From Figure A.5, I can see that more than 90% entries of $\hat{\mathbf{P}}_E^a$ (again, under $\sigma = 7$) is closer to the ground truth when compared with $\hat{\mathbf{\Pi}}^{a=1}$ under almost all α. When compared with $\tilde{\mathbf{P}}^a$, I find that, when the predictive models are not very accurate (i.e., σ is not very small), over 50% entries of $|\hat{\mathbf{\Delta}}_E^a| - |\tilde{\mathbf{\Delta}}^a|$ is negative under most values of α, which

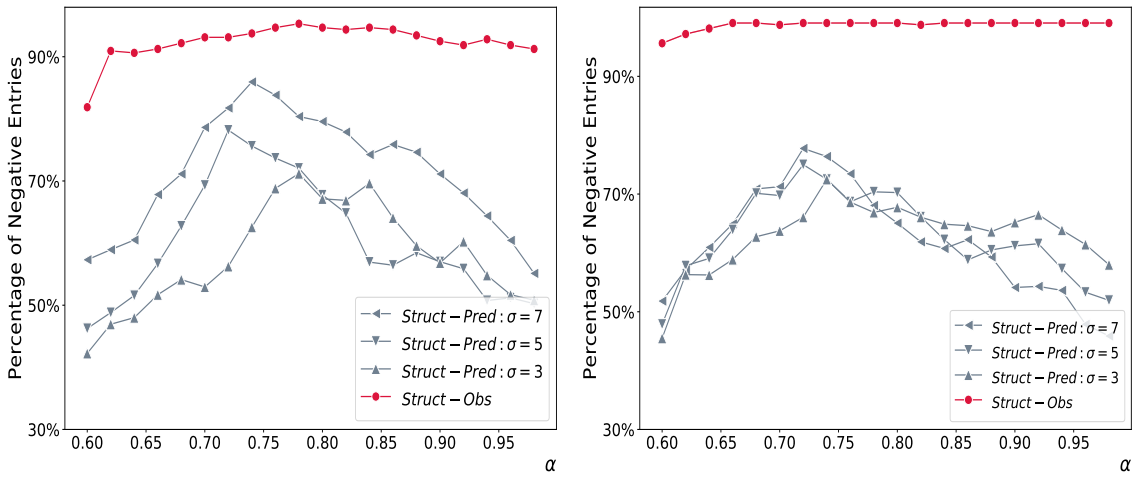

(a) Action $a = 0$ (b) Action $a = 1$

$\sigma = 3$: $\beta^0 \in (0.881, 0.887)$, $\beta^1 \in (0.869, 0.874)$; $\sigma = 5$: $\beta^0 \in (0.800, 0.809)$, $\beta^1 \in (0.781, 0.789)$;
$\sigma = 7$: $\beta^0 \in (0.726, 0.733)$, $\beta^1 \in (0.680, 0.687)$;

Figure A.5: Performances Comparison: Percentage of Entries Closer to Ground Truth

also suggests that $\hat{\mathbf{P}}_E^a$, in overall, is closer to $\boldsymbol{P}^a$. Therefore, these findings further support the use of the proposed structural model to recover the underlying TPMs.

A.4.4 Performance Comparison: Structural Models with and without Prediction Errors

I compare the structural model with prognostic errors incorporated with the error-free structural model in this section by investigating the distance between the estimation and ground truth TPM. As I defined in the main text, *Dist_Struct_E* denotes the norm distance between the estimated underlying TPM from the error-free model and the corresponding ground truth TPM. Under the structural model with prognostic error incorporated, I consider the two-stage estimation with the ground truth prognostic information is used (as this information is available in the simulation). I then term $Dist\_Struct\_E(GT)$ (i.e., the ground truth accuracy information is used) as the norm distances from the corresponding estimators under these two cases to $\boldsymbol{P}^a$, respectively. Using the max-norm as the representation, I show that the performance of

the error-free structural model, in general, is better than that of the structural model with prognostic errors incorporated in Figure A.6. When the prognostic accuracy is low (e.g., $\alpha < 0.65$), the performance of the prognostic-error embedded model tends to outperform the error model. I claim that the insights also hold under 2-norm and F-norm specifications. When the ground truth prognostic accuracy information is

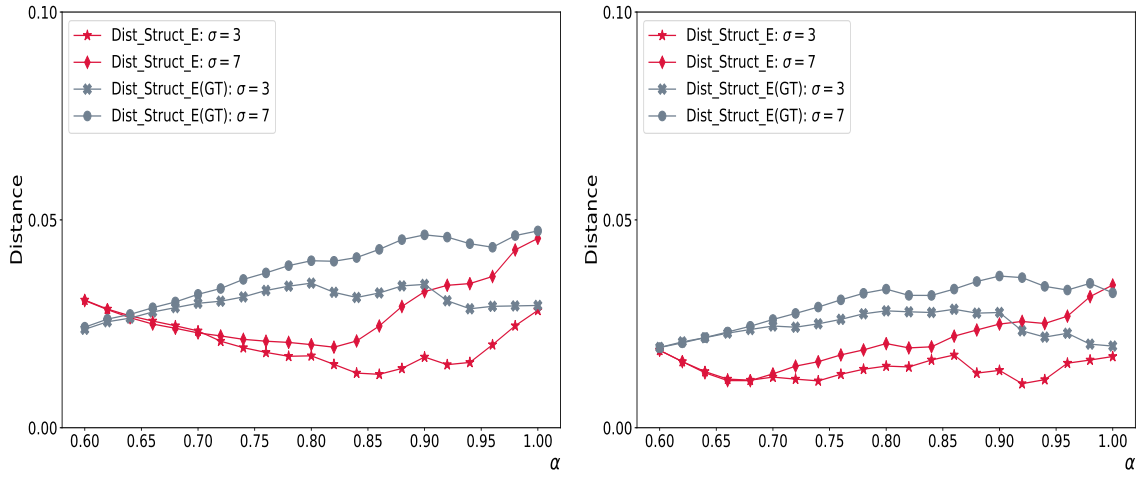

(a) Action $a = 0$ (b) Action $a = 1$

Figure A.6: Comparison Between Two Models:Max-Norm

used (i.e., $Dist\_Struct\_E(GT)$), under two-stage estimation, there is no error in the second stage, but the error from the first stage estimation may distort the estimators. On the contrary, for the error-free model, the first stage estimation error may mitigate the second stage error such that the performance of the estimator can be even better. In summary, these results support the conclusion that an error-free model is better for the estimation.

A.5 Case Study: Predictive Models

I train the predictive models $Mod0(Mod1)$ with XGBoost(Extreme Gradient Boosting) methods to predict the censored outcomes under $a = 0(a = 1)$ on the dataset $\mathcal{D}_1(\mathcal{D}_0)$. Recall that $\mathcal{D}_1(\mathcal{D}_0)$ only contains the observations under action $a = 1(a = 0)$.

Specifically, we build the predictive models following the similar logic that I train the predictive models adopted in the simulations. I use all relevant physiological data and demographics to predict the RR values with multiple methods, including linear model, classification and regression tree model, random forest model and XGBoost(Extreme Gradient Boosting) model. I split the data into two sets with 75% data in the training set, and the remaining is in the test set. I train the predictive models with the mentioned methods on the training set with 10-fold cross-validation and comprehensive parameter tuning (random forest model and XGBoost model). Based on the prediction accuracy of each model, I select the XGBoost model as the final predictive model. The parameters of the model are presented in Table A.1.

Parameters	$Mod0$	$Mod1$
learning_rate	0.07	0.07
n_estimator	1000	1000
max_depth	6	2
min_child_weight	5	5
gamma	0.01	0.08
subsample	0.81	0.55
colsample_bytree	0.5	0.58
reg_alpha	0.011	0.011
objective	multi:softmax	multi:softmax
nthread	4	4
scale_pos_weight	1	1
num_class	4	4
seed	123	271
out-of-sample accuracy	0.685	0.601

Table A.1: Parameters of Predictive Models

A.6 Quadratic Programming Method

I present the quadratic programming method discussed in Theil and Rey (1966) and Schneider and Zenios (1990) in this section. Let x_{it} denote the probability of state i observed in period t and $\boldsymbol{A}$ be the transition matrix and a_{ij} is the transition prob-

ability from i to j. Then they solve the following quadratic problem to derive the estimator.

$$\min_{\boldsymbol{A}} \sum_{t=1}^{T} (x_{t+1} - \boldsymbol{A}' x_t)' \boldsymbol{D} (x_{t+1} - \boldsymbol{A}' x_t)$$

$$s.t\ a_{ij} \geq 0, \quad \sum_j a_{ij} = 1 \quad \forall i$$

where $\boldsymbol{D}$ is a weighting matrix. I use $\boldsymbol{D} = \boldsymbol{I}$, which is adopted in the literature, as the representatives.

Appendix B

Appendix of Chapter 2

B.1 Sensitivity Analysis: Global Effects On The Overflow Risk

Proposition B.1.A (Freshwater Capacity)**.**

(1) If

$$\frac{dK_r^*}{dK_f} \leq \frac{\beta_f}{\beta_r} + \frac{2\beta_f \int_{(c_f-o_f)\frac{\beta_r}{\beta_f}}^{\bar{c}_r} \psi(2K_f, \tilde{c}_r)d\tilde{c}_r}{\beta_r \int_{\underline{c}_r}^{(c_f-o_f)\frac{\beta_r}{\beta_f}} \psi(K_f + \tau_1(K_r^*), \tilde{c}_r)d\tilde{c}_r}$$

PO decreases in K_f;

(2) Otherwise, I have two thresholds $\bar{\omega}_r = \omega_r^1\left((D_h + D_{nh})/\beta_f\right)$ and $\hat{\omega}_r = \omega_r^0\left((D_h + D_{nh})/\beta_f\right)$ such that

(2.1) If $\omega_r < \omega_r^0$, PO decreases in K_f;

(2.2) If $\omega_r^0 < \omega_r < \min(\omega_r^1, \hat{\omega}_r)$, there exists a threshold $\hat{K}_f^0$ such that PO increases in K_f on $(0, \hat{K}_f^0)$ and decreases otherwise;

(2.3) If $\hat{\omega}_r < \omega_r < \omega_r^1$, PO increases in K_f;

(2.4) If $\omega_r^1 < \omega_r < \hat{\omega}_r$, there exist two thresholds $\hat{K}_f^1$ and $\hat{K}_f^2$ such that PO decreases on $(0, \hat{K}_f^1)$, increases on $[\hat{K}_f^1, \hat{K}_f^2)$ and decreases on $[\hat{K}_f^2, (D_h + D_{nh})/\beta_f]$;

(2.5) If $\max(\omega_r^1, \hat{\omega}_r) < \omega_r < \bar{\omega}_r$, PO decreases on $(0, \hat{K}_f^1)$ and increases on

$[\hat{K}_f^1, (D_h + D_{nh})/\beta_f]$;

(2.6) If $\omega_r \geq \bar{\omega}_r$, PO decreases in K_f.

In terms of the impact from the cost variability, for simplicity, I assume $\mu_c > (c_f - c_o)\frac{\beta_r}{\beta_f}$ and $\rho \geq 0$.

Proposition B.2 (Cost Variability)**.** *PO increases in σ_c.*

B.2 Proofs

Proof of Proposition 2.1: The proof is omitted. □

Proof of Proposition 2.2: Considering two cases: (1) $K_f \leq \frac{D_h+D_{nh}}{\beta_f}$ and (2) $K_f > \frac{D_h+D_{nh}}{\beta_f}$.

Considering case (1), I have two subcases (1.1) $K_r \in [0, \frac{D_h+D_{nh}-\beta_f K_f}{\beta_r}]$ and (1.2) $K_r \in [\frac{D_h+D_{nh}-\beta_f K_f}{\beta_r}, \min(\beta^U q_u, \frac{D_{nh}}{\beta_r})]$[1].

Case 1.1: $K_r \in [0, \frac{D_h+D_{nh}-\beta_f K_f}{\beta_r}]$

Under this case, I have

$$
\begin{aligned}
V(K_r) &= \underset{\tilde{c}_r,\tilde{s}}{E}\left(\min_{q_f,q_r} z(K_r;\tilde{s},\tilde{c}_r) + \omega_r K_r\right) \\
&= \int_{\underline{c}_r}^{\bar{c}_r}\int_{s_0}^{K_f}\Big[\tilde{c}_r K_r + c_f\tilde{s} + c_d(D_h + D_{nh} - \beta_r K_r - \beta_f\tilde{s})\Big]\psi(\tilde{s},\tilde{c}_r)d\tilde{s}d\tilde{c}_r \\
&+ \int_{\underline{c}_r}^{\bar{c}_r}\int_{K_f}^{+\infty}\Big[\tilde{c}_r K_r + c_f K_f + c_d(D_h + D_{nh} - \beta_r K_r - \beta_f K_f) \\
&+ o_f(\tilde{s} - 2K_f)^+\Big]\psi(\tilde{s},\tilde{c}_r)d\tilde{s}d\tilde{c}_r + \bar{c}_b(\beta_h D_h + \beta_{nh} D_{nh}) + \omega_r K_r \\
&= (\mu_c - \beta_r c_d)K_r + \bar{c}_b(\beta_h D_h + \beta_{nh} D_{nh}) + c_d(D_h + D_{nh}) + \omega_r K_r \\
&+ \int_{\underline{c}_r}^{\bar{c}_r}\int_{s_0}^{K_f}(c_f - \beta_f c_d)\tilde{s}\psi(\tilde{s},\tilde{c}_r)d\tilde{s}d\tilde{c}_r + \int_{\underline{c}_r}^{\bar{c}_r}\int_{K_f}^{+\infty}(c_f - \beta_f c_d)K_f\psi(\tilde{s},\tilde{c}_r)d\tilde{s}d\tilde{c}_r \\
&+ \int_{\underline{c}_r}^{\bar{c}_r}\int_{2K_f}^{+\infty} o_f(\tilde{s} - 2K_f)\psi(\tilde{s},\tilde{c}_r)d\tilde{s}d\tilde{c}_r
\end{aligned}
$$

Then I have

$$\frac{dV(K_r)}{dK_r} = \underset{\tilde{c}_r,\tilde{s}}{E}[m_d\beta_r] + \omega_r$$

[1] If $\frac{D_h+D_{nh}-\beta_f K_f}{\beta_r} > \min(\beta^U q_u, \frac{D_{nh}}{\beta_r})$, I do not have case (1.2)

Then I know, if $\omega_r \leq \omega_r^2 = -\underset{\tilde{c}_r,\tilde{s}}{E}[m_d\beta_r]$, the optimal capacity to invest is $K_r^* = \frac{D_h+D_{nh}-\beta_f K_f}{\beta_r}$; Otherwise, $K_r^* = 0$.

Case (1.2): $K_r \in [\frac{D_h+D_{nh}-\beta_f K_f}{\beta_r}, \min(\beta^U q_u, \frac{D_{nh}}{\beta_r})]$

The expected cost function is

$$
\begin{aligned}
V(K_r) &= \underset{\tilde{c}_r,\tilde{s}}{E}\left(\min_{q_f,h} z(K_r;\tilde{s},\tilde{c}_r) + \omega_r K_r\right) \\
&= \underset{\tilde{c}_r,\tilde{s}}{E}\left(\tilde{c}_r q_r^* + c_b(\beta_h D_h + \beta_{nh} D_{nh} - q_r^*) + c_f q_f^* + o_f(\tilde{s} - q_f^* - K_f)^+ + c_d q_d^*\right) + \omega_r K_r \\
&= \int\int_{\Omega_1} \left[(\tilde{c}_r - \beta_r c_d)K_r + c_d(D_h + D_{nh}) + (c_f - \beta_f c_d)\tilde{s}\right]\psi(\tilde{s},\tilde{c}_r)d\tilde{s}d\tilde{c}_r \\
&+ \int\int_{\Omega_2 \bigcup \Omega_6} \Bigg[(\frac{\tilde{c}_r}{\beta_r})(D_h + D_{nh}) - (\frac{\tilde{c}_r\beta_f}{\beta_r} - c_f)\min(\tilde{s}, K_f, \frac{D_h + D_{nh}}{\beta_f}) \\
&+ o_f(\tilde{s} - \min(\tilde{s}, K_f, \frac{D_h + D_{nh}}{\beta_f}) - K_f)^+\Bigg]\psi(\tilde{s},\tilde{c}_r)d\tilde{s}d\tilde{c}_r \\
&+ \int\int_{\Omega_3} \left[(\tilde{c}_r - \frac{\beta_r c_f}{\beta_f})K_r + \frac{c_f}{\beta_f}(D_h + D_{nh})\right]\psi(\tilde{s},\tilde{c}_r)d\tilde{s}d\tilde{c}_r \\
&+ \int\int_{\Omega_4} \left[(\tilde{c}_r - \frac{\beta_r(c_f - o_f)}{\beta_f})K_r + \frac{c_f - o_f}{\beta_f}(D_h + D_{nh}) + o_f(\tilde{s} - K_f)\right]\psi(\tilde{s},\tilde{c}_r)d\tilde{s}d\tilde{c}_r \\
&+ \int\int_{\Omega_5} \left[\frac{\tilde{c}_r}{\beta_r}(D_h + D_{nh}) + (c_f - \frac{(\tilde{c}_r)\beta_f}{\beta_r})(\tilde{s} - K_f)\right]\psi(\tilde{s},\tilde{c}_r)d\tilde{s}d\tilde{c}_r + c_b(\beta_h D_h + \beta_{nh} D_{nh}) + \omega_r K_r
\end{aligned}
$$

The first order derivative is $\frac{dV(K_r)}{dK_r} = M(K_r) + \omega_r$, where

$$
\begin{aligned}
M(K_r) = &\int\int_{\Omega_1} (m_d\beta_r)\psi(\tilde{s},\tilde{c}_r)d\tilde{s}d\tilde{c}_r + \int\int_{\Omega_3} (m_f^{no}\beta_r)\psi(\tilde{s},\tilde{c}_r)d\tilde{s}d\tilde{c}_r \\
&+ \int\int_{\Omega_4} (m_f^{o}\beta_r)\psi(\tilde{s},\tilde{c}_r)d\tilde{s}d\tilde{c}_r
\end{aligned} \tag{B.1}
$$

Let $c_1 = (c_f - o_f)\frac{\beta_r}{\beta_f}$ and $c_2 = c_f\frac{\beta_r}{\beta_f}$. Then the second order derivative is

$$
\begin{aligned}
\frac{d^2V(K_r)}{dK_r^2} = &\int_{\underline{c}_r}^{\bar{c}_r} (-\frac{\beta_r}{\beta_f})m_d\beta_r\psi(\tau_1(K_r),\tilde{c}_r)d\tilde{c}_r \\
&+ \int_{\underline{c}_r}^{c_2} \frac{\beta_r}{\beta_f} m_f^{no}\beta_r\psi(\tau_1(K_r),\tilde{c}_r)d\tilde{c}_r \\
&- \int_{\underline{c}_r}^{c_2} \frac{\beta_r}{\beta_f} m_f^{no}\beta_r\psi(\tau_3(K_r),\tilde{c}_r)d\tilde{c}_r \\
&+ \int_{\underline{c}_r}^{c_1} \frac{\beta_r}{\beta_f} m_f^{o}\beta_r\psi(\tau_3(K_r),\tilde{c}_r)d\tilde{c}_r \geq 0
\end{aligned}
$$

Hence, $V(K_r)$ is convex in K_r. Let

$$\omega_r^0 = -M(\min(\beta_h D_h + \beta_{nh} D_{nh}, \frac{D_{nh}}{\beta_r}))$$
$$\omega_r^1 = -M(\frac{D_h + D_{nh} - \beta_f K_f}{\beta_r})$$

Then, $\omega_r^0 \leq \omega_r^1 \leq \omega_r^2$. If $\omega_r \in (\omega_r^1, \omega_r^2)$, $\frac{dV(K_r)}{dK_r} > 0$, the optimal recycling capacity to invest is $K_r^* = \frac{D_h + D_{nh} - \beta_f K_f}{\beta_r}$; if $\omega_r \in (\omega_r^0, \omega_r^1]$, K_r^* satisfies $M(K_r^*) + \omega_r = 0$; otherwise, $\frac{dV(K_r)}{dK_r} < 0$ and $K_r^* = \min(\beta_h D_h + \beta_{nh} D_{nh}, \frac{D_{nh}}{\beta_r})$.

Case (2): $K_f > \frac{D_h + D_{nh}}{\beta_f}$

Similarly, I can show the second order derivative is positive. ω_r^0 remains as the same definition, in addition, let $\omega_r^3 = -M(0)$, where $M(K_r)$ is as defined in equation B.1 when $K_r \in [0, \min(\beta_h D_h + \beta_{nh} D_{nh}, \frac{D_{nh}}{\beta_r})]$. Hence, I have $K_r* = 0$ if $\omega_r > \omega_r^3$, K_r^* solves $M(K_r^*) + \omega_r = 0$ if $\omega_r \in (\omega_r^0, \omega_3]$ and $K_r^* = \min(\beta_h D_h + \beta_{nh} D_{nh}, \frac{D_{nh}}{\beta_r})$ otherwise. □

Proof of Lemma 2.1: I assume that $(\tilde{s}, \tilde{c}_r)$ is a bivariate normal random variable. I let $\phi(\cdot)$ and $\Phi(\cdot)$ denote the pdf and cdf of standard normal distribution and define the following standard normal random variables.

$$\tilde{z}_0 \stackrel{d}{=} \frac{\tilde{c}_r - \mu_c}{\sigma_c}$$
$$\tilde{z}_1 \stackrel{d}{=} \frac{\tilde{s} - \mu_s}{\sigma_s}$$
$$\tilde{z}_2 \stackrel{d}{=} \frac{\tilde{c}_r - \mu_c - \rho\frac{\sigma_c}{\sigma_s}(s_1 - \mu_s)}{\sigma_c\sqrt{1-\rho^2}}\Big|\tilde{s}$$
$$\tilde{z}_3 \stackrel{d}{=} \frac{\tilde{s} - \mu_s - \rho\frac{\sigma_s}{\sigma_c}(c_{wr}^h - \mu_c)}{\sigma_s\sqrt{1-\rho^2}}\Big|\tilde{c}_r$$

As $\omega_r^2 = -\underset{\tilde{c}_r, \tilde{s}}{E}[m_d \beta_r]$, obviously it is independent of σ_s, σ_c and ρ. I then show the impacts of σ_s, σ_c and ρ on the thresholds ω_r^0 and ω_r^1 below. As I defined, I have

$$\omega_r^0 = -M(\min(\beta_h D_h + \beta_{nh} D_{nh}, \frac{D_{nh}}{\beta_r}))$$
$$\omega_r^1 = -M(\frac{D_h + D_{nh} - \beta_f K_f}{\beta_r})$$

Recall that function $M(K_r)$ represents the first-order derivative function. Hence, to show the effects of variabilities and correlation on ω_r^0 and ω_r^1, it is sufficient to show

the impacts on $M(K_r)$ for any given K_r. First, I have

$$\frac{\partial M(\sigma_s,\sigma_c,\rho;K_r)}{\partial \sigma_s} =$$

$$-\frac{\tau_1(K_r)-\mu_s}{\sigma_s^2\sqrt{1-\rho^2}}\int_{-\infty}^{+\infty}(\sigma_c\tilde{z}_0+\mu_c-\beta_f c_d)\phi(\frac{\tau_1(K_r)-\mu_s-\rho\sigma_s\tilde{z}_0}{\sigma_s\sqrt{1-\rho^2}})\phi(\tilde{z}_0)d\tilde{z}_0 \tag{B.2}$$

$$+\frac{\tau_1(K_r)-\mu_s}{\sigma_s^2\sqrt{1-\rho^2}}\int_{-\infty}^{\frac{c_2-\mu_c}{\sigma_c}}(\sigma_c\tilde{z}_0+\mu_c-\beta_f\frac{c_f}{\beta_r})\phi(\frac{\tau_1(K_r)-\mu_s-\rho\sigma_s\tilde{z}_0}{\sigma_s\sqrt{1-\rho^2}})\phi(\tilde{z}_0)d\tilde{z}_0 \tag{B.3}$$

$$-\frac{\tau_3(K_r)-\mu_s}{\sigma_s^2\sqrt{1-\rho^2}}\int_{-\infty}^{\frac{c_2-\mu_c}{\sigma_c}}(\sigma_c\tilde{z}_0+\mu_c-\beta_f\frac{c_f}{\beta_r})\phi(\frac{\tau_3(K_r)-\mu_s-\rho\sigma_s\tilde{z}_0}{\sigma_s\sqrt{1-\rho^2}})\phi(\tilde{z}_0)d\tilde{z}_0 \tag{B.4}$$

$$+\frac{\tau_3(K_r)-\mu_s}{\sigma_s^2\sqrt{1-\rho^2}}\int_{-\infty}^{\frac{c_1-\mu_c}{\sigma_c}}(\sigma_c\tilde{z}_0+\mu_c-\beta_f\frac{c_f-o_f}{\beta_r})\phi(\frac{\tau_3(K_r)-\mu_s-\rho\sigma_s\tilde{z}_0}{\sigma_s\sqrt{1-\rho^2}})\phi(\tilde{z}_0)d\tilde{z}_0 \tag{B.5}$$

I have the summation of (B.4) and (B.5) is positive. If the summation of (B.2) and (B.3) is also positive, then $\frac{\partial M(\sigma_s,\sigma_c,\rho;K_r)}{\partial \sigma_s}$ is positive. If the summation of (B.2) and (B.3) is negative, as $\frac{\partial M(\sigma_s,\sigma_c,\rho;K_r)}{\partial K_r}>0$, then

$$\frac{\partial M(\sigma_s,\sigma_c,\rho;K_r)}{\partial \sigma_s} \geq \frac{\tau_1(K_r)-\mu_s}{\sigma_s^2\sqrt{1-\rho^2}}\frac{\beta_f}{\beta_r}\frac{\partial M(\sigma_s,\sigma_c,\rho;K_r)}{\partial K_r}>0$$

Then, I show that $M(K_r)$ increases and hence ω_r^0 and ω_r^1 decrease in σ_s.

Similarly, I have

$$\begin{aligned}\frac{\partial M(\sigma_s,\sigma_c,\rho;K_r)}{\partial \sigma_c} &= \int_{-\infty}^{+\infty}\tilde{z}_0\Phi(\frac{\tau_1(K_r)-\mu_s-\rho\sigma_s\tilde{z}_0}{\sigma_s\sqrt{1-\rho^2}})\phi(\tilde{z}_0)d\tilde{z}_0\\ &+\int_{-\infty}^{\frac{c_2-\mu_c}{\sigma_c}}\tilde{z}_0\Phi(\frac{\tau_3(K_r)-\mu_s-\rho\sigma_s\tilde{z}_0}{\sigma_s\sqrt{1-\rho^2}})\phi(\tilde{z}_0)d\tilde{z}_0\\ &-\int_{-\infty}^{\frac{c_2-\mu_c}{\sigma_c}}\tilde{z}_0\Phi(\frac{\tau_1(K_r)-\mu_s-\rho\sigma_s\tilde{z}_0}{\sigma_s\sqrt{1-\rho^2}})\phi(\tilde{z}_0)d\tilde{z}_0\\ &+\int_{-\infty}^{\frac{c_1-\mu_c}{\sigma_c}}\tilde{z}_0(1-\Phi(\frac{\tau_1(K_r)-\mu_s-\rho\sigma_s\tilde{z}_0}{\sigma_s\sqrt{1-\rho^2}}))\phi(\tilde{z}_0)d\tilde{z}_0\end{aligned}$$

Let $L = \frac{\partial M(\sigma_s,\sigma_c,\rho;K_r)}{\partial \sigma_c}$, then

$$\begin{aligned}\frac{dL}{d\sigma_c} &= -\frac{(c_2-\mu_c)^2}{\sigma_c^3}\Phi(\frac{\tau_3(K_r)-\mu_s-\rho\sigma_s\tilde{z}_0}{\sigma_s\sqrt{1-\rho^2}})\phi(\frac{c_2-\mu_c}{\sigma_c}) \\ &+ \frac{(c_2-\mu_c)^2}{\sigma_c^3}\Phi(\frac{\tau_1(K_r)-\mu_s-\rho\sigma_s\tilde{z}_0}{\sigma_s\sqrt{1-\rho^2}})\phi(\frac{c_2-\mu_c}{\sigma_c}) \\ &- \frac{(c_1-\mu_c)^2}{\sigma_c^3}(1-\Phi(\frac{\tau_1(K_r)-\mu_s-\rho\sigma_s\tilde{z}_0}{\sigma_s\sqrt{1-\rho^2}}))\phi(\frac{c_1-\mu_c}{\sigma_c}) < 0\end{aligned}$$

thus, $\frac{\partial M(\sigma_s,\sigma_c,\rho;K_r)}{\partial \sigma_c}$ decreases in σ_c. Moreover, following the Stein's lemma that $\mathbb{E}[h(\tilde{z})\tilde{z}] = \mathbb{E}[h^{'}(\tilde{z})]$ for any differentiable function $h(\cdot)$ and normal random variable $\tilde{z}$, I can derive

$$\frac{\partial M(\sigma_s,\sigma_c,\rho;K_r)}{\partial \sigma_c}\Big|_{\sigma_c\to 0} = \begin{cases} 0 & \text{If } \mu_c \le c_1 \\ > 0 & \text{If } \mu_c > c_1 \text{ and } \rho < 0 \\ < 0 & \text{Otherwise} \end{cases}$$

Therefore, if $\mu_c \le c_1$ or $\rho \ge 0$, $\frac{\partial M(\sigma_s,\sigma_c,\rho;K_r)}{\partial \sigma_c} < 0$. Now for the case $\mu_c > c_1$ and $\rho < 0$,

$$L\Big|_{\sigma_c\to+\infty} = \int_0^{+\infty}\tilde{z}_0\Phi(\frac{\tau_1(K_r)-\mu_s-\rho\sigma_s\tilde{z}_0}{\sigma_s\sqrt{1-\rho^2}})\phi(\tilde{z}_0)d\tilde{z}_0 - \int_0^{+\infty}\tilde{z}_0\phi(\tilde{z}_0)d\tilde{z}_0 < 0$$

Hence, there exists a threshold $\hat{\sigma}_c$ such that $L \ge 0$ if $\sigma_c \in (0,\hat{\sigma}_c]$ and $L < 0$ otherwise. In summary, ω_r^0 and ω_r^1 increases in σ_c if $\rho \ge 0$ or $\mu_c \le c_1$; otherwise, ω_r^0 and ω_r^1 decreases in σ_c if $\sigma_c \in (0,\hat{\sigma}_c]$ and increases otherwise.

In terms of the effect of the correlation, I also have

$$\begin{aligned}\frac{\partial M(\sigma_s,\sigma_c,\rho;K_r)}{\partial \rho} = \sigma_c\Bigg(&\int_{-\infty}^{\frac{\tau_1(K_r)-\mu_s}{\sigma_s}}\int_{-\infty}^{+\infty}\Big[-\frac{\rho}{\sqrt{1-\rho^2}}\tilde{z}_2+\tilde{z}_1\Big]\phi(\tilde{z}_2)d\tilde{z}_2\phi(\tilde{z}_1)d\tilde{z}_1 \\ &+\int_{\frac{\tau_1(K_r)-\mu_s}{\sigma_s}}^{\frac{\tau_3(K_r)-\mu_s}{\sigma_s}}\int_{-\infty}^{\frac{c_2-\mu_c-\rho\sigma_c\tilde{z}_1}{\sigma_c\sqrt{1-\rho^2}}}\Big[-\frac{\rho}{\sqrt{1-\rho^2}}\tilde{z}_2+\tilde{z}_1\Big]\phi(\tilde{z}_2)d\tilde{z}_2\phi(\tilde{z}_1)d\tilde{z}_1 \\ &+\int_{\frac{\tau_3(K_r)-\mu_s}{\sigma_s}}^{+\infty}\int_{-\infty}^{\frac{c_1-\mu_c-\rho\sigma_c\tilde{z}_1}{\sigma_c\sqrt{1-\rho^2}}}\Big[-\frac{\rho}{\sqrt{1-\rho^2}}\tilde{z}_2+\tilde{z}_1\Big]\phi(\tilde{z}_2)d\tilde{z}_2\phi(\tilde{z}_1)d\tilde{z}_1\Bigg)\end{aligned}$$

Let $W = \frac{\partial M(\sigma_s,\sigma_c,\rho;K_r)}{\partial \rho}/\sigma_c$, then $W\Big|_{\sigma_c\to 0} \le 0$ where the equality is achieved when $c_1 > \mu_c$, and $W\Big|_{\sigma_c\to+\infty} = -\int_{\frac{\tau_1(K_r)-\mu_s}{\sigma_s}}^{+\infty}\int_{-\frac{\rho\tilde{z}_1}{\sqrt{1-\rho^2}}}^{+\infty}\Big[-\frac{\rho}{\sqrt{1-\rho^2}}\tilde{z}_2+\tilde{z}_1\Big]\phi(\tilde{z}_2)d\tilde{z}_2\phi(\tilde{z}_1)d\tilde{z}_1 < 0.$

Moreover,

$$\frac{dW}{d\sigma_c} = -\left(\int_{\frac{\tau_3(K_r)-\mu_s}{\sigma_s}}^{+\infty} \frac{c_1-\mu_c}{\beta_r \sigma_c^2 \sqrt{1-\rho^2}} \Big[\frac{\sigma_c \tilde{z}_1 - \rho(c_1-\mu_c)}{\sigma_c(1-\rho^2)} \Big] \phi\Big(\frac{c_1-\mu_c-\rho\sigma_c\tilde{z}_1}{\sigma_c\sqrt{1-\rho^2}} \Big) \phi(\tilde{z}_1) d\tilde{z}_1 \right.$$
$$\left. + \int_{\frac{\tau_1(K_r)-\mu_s}{\sigma_s}}^{\frac{\tau_3(K_r)-\mu_s}{\sigma_s}} \frac{c_2-\mu_c}{\beta_r \sigma_c^2 \sqrt{1-\rho^2}} \Big[\frac{\sigma_c \tilde{z}_1 - \rho(c_2-\mu_c)}{\sigma_c(1-\rho^2)} \Big] \phi\Big(\frac{c_2-\mu_c-\rho\sigma_c\tilde{z}_1}{\sigma_c\sqrt{1-\rho^2}} \Big) \phi(\tilde{z}_1) d\tilde{z}_1 \right)$$

If $c_2 < \mu_c$ and $\rho > 0$, I have $\frac{dW}{d\sigma_c} < 0$; hence, $\frac{\partial M(\sigma_s,\sigma_c,\rho;K_r)}{\partial \rho} < 0$; if $c_2 < \mu_c$ and $\rho < 0$, considering two cases: (1) σ_c is relatively small, then $\frac{dW}{d\sigma_c} < 0$; (2) σ_c becomes relatively large, then it is possible that $\frac{dW}{d\sigma_c}$ is positive. Under case (2), if $\frac{dW}{d\sigma_c} < 0$, similarly, I have $\frac{\partial M(\sigma_s,\sigma_c,\rho;K_r)}{\partial \rho} < 0$; otherwise, I know that W first decreases and then increases in σ_c; moreover, I have $W\Big|_{\sigma_c \to 0} \leq 0$ and $W\Big|_{\sigma_c \to +\infty} < 0$; hence, I also have $\frac{\partial M(\sigma_s,\sigma_c,\rho;K_r)}{\partial \rho} < 0$. For the case that $c_2 > \mu_c$, similarly, I can derive that $\frac{\partial M(\sigma_s,\sigma_c,\rho;K_r)}{\partial \rho} < 0$. Therefore, ω_r^0 and ω_r^1 increases in ρ. □

Proof of Proposition 2.3: I show the results for any given K_r. There are two cases: (1) $K_f \leq \frac{D_h+D_{nh}}{\beta_f}$ and (2) $K_f > \frac{D_h+D_{nh}}{\beta_f}$.

Case (1): $K_f \leq \frac{D_h+D_{nh}}{\beta_f}$

(i) If $K_r \in [0, \frac{D_h+D_{nh}-\beta_f K_f}{\beta_r}]$, the expected cost can be written as

$$V(\sigma_s,\sigma_c,\rho;K_r) = (\mu_c - \beta_r c_d)K_r + \bar{c}_b(\beta_h D_h + \beta_{nh} D_{nh}) + c_d(D_h + D_{nh}) \tag{B.6}$$
$$+ \int_{-\infty}^{\frac{K_f-\mu_s}{\sigma_s}} \int_{-\infty}^{+\infty} \Big[(c_f - \beta_f c_d)(\sigma_s \tilde{z}_1 + \mu_c) \Big] \phi(\tilde{z}_2) d\tilde{z}_2 \phi(\tilde{z}_1) d\tilde{z}_1$$
$$+ \int_{\frac{K_f-\mu_s}{\sigma_s}}^{+\infty} \int_{-\infty}^{\infty} \Big[(c_f - \beta_f c_d) K_f \Big] \phi(\tilde{z}_2) d\tilde{z}_2 \phi(\tilde{z}_1) d\tilde{z}_1 \tag{B.7}$$
$$+ \int_{\frac{2K_f-\mu_s}{\sigma_s}}^{+\infty} \int_{-\infty}^{\infty} \Big[o_f(\sigma_s \tilde{z}_1 + \mu_c - 2K_f) \Big] \phi(\tilde{z}_2) d\tilde{z}_2 \phi(\tilde{z}_1) d\tilde{z}_1 + \omega_r K_r$$

From the expected cost expression (B.6), I can easily find that $V(\sigma_s,\sigma_c,\rho;K_r)$ is independent of σ_c and ρ. For the impact from rainfall variability, I have

$$\frac{\partial V(\sigma_s,\sigma_c,\rho;K_r)}{\partial \sigma_s} = \int_{-\infty}^{\frac{K_f-\mu_s}{\sigma_s}} \Big[(c_f - \beta_f c_d)\tilde{z}_1 \Big] \phi(\tilde{z}_1) d\tilde{z}_1 + \int_{\frac{2K_f-\mu_s}{\sigma_s}}^{+\infty} o_f \tilde{z}_1 \phi(\tilde{z}_1) d\tilde{z}_1$$
$$\frac{\partial^2 V(\sigma_s,\sigma_c,\rho;K_r)}{\partial \sigma_s^2} = -\frac{(K_f-\mu_s)^2}{\sigma_s^2}(c_f - \beta_f c_d) + o_f \frac{(2K_f-\mu_s)^2}{\sigma_s^3}$$

As $c_f - \beta_f c_d < 0$, I have $\frac{\partial^2 V(\sigma_s,\sigma_c,\rho;K_r)}{\partial \sigma_s^2} > 0$. Moreover, $\frac{\partial V(\sigma_s,\sigma_c,\rho;K_r)}{\partial \sigma_s}\Big|_{\sigma_s \to 0} = 0$; hence, $\frac{\partial V(\sigma_s,\sigma_c,\rho;K_r)}{\partial \sigma_s} > 0$, which means the expected cost increases in σ_s.

(ii) If $K_r \in [\frac{D_h + D_{nh} - \beta_f K_f}{\beta_r}, \min(\beta^U q_u, \frac{D_{nh}}{\beta_r})]$, the expected cost function is

$$
\begin{aligned}
V(\sigma_s,\sigma_c,\rho;K_r) = & \int_{-\infty}^{\frac{\tau_1(K_r)-\mu_s}{\sigma_s}} \int_{-\infty}^{+\infty} \Big[(\sigma_c\sqrt{1-\rho^2}\tilde{z}_2 + \mu_c + \rho\sigma_c\tilde{z}_1 - \beta_r c_d)K_r + \\
& c_d(D_h + D_{nh}) + (c_f - \beta_f c_d)(\sigma_s\tilde{z}_1 + \mu_s)\Big]\phi(\tilde{z}_2)d\tilde{z}_2\phi(\tilde{z}_1)d\tilde{z}_1 \\
& + \int_{\frac{\tau_1(K_r)-\mu_s}{\sigma_s}}^{\frac{K_f-\mu_s}{\sigma_s}} \int_{\frac{c_2-\mu_c-\rho\sigma_c\tilde{z}_1}{\sigma_c\sqrt{1-\rho^2}}}^{+\infty} \Big[(\frac{\sigma_c\sqrt{1-\rho^2}\tilde{z}_2 + \mu_c + \rho\sigma_c\tilde{z}_1}{\beta_r})(D_h + D_{nh}) - \\
& (\frac{\sigma_c\sqrt{1-\rho^2}\tilde{z}_2 + \mu_c + \rho\sigma_c\tilde{z}_1}{\beta_r} - \frac{c_f}{\beta_f})\beta_f(\sigma_s\tilde{z}_1 + \mu_s)\Big]\phi(\tilde{z}_2)d\tilde{z}_2\phi(\tilde{z}_1)d\tilde{z}_1 \\
& + \int_{\frac{K_f-\mu_s}{\sigma_s}}^{\frac{2K_f-\mu_s}{\sigma_s}} \int_{\frac{c_2-\mu_c-\rho\sigma_c\tilde{z}_1}{\sigma_c\sqrt{1-\rho^2}}}^{+\infty} \Big[(\frac{\sigma_c\sqrt{1-\rho^2}\tilde{z}_2 + \mu_c + \rho\sigma_c\tilde{z}_1}{\beta_r})(D_h + D_{nh}) - \\
& (\frac{\sigma_c\sqrt{1-\rho^2}\tilde{z}_2 + \mu_c + \rho\sigma_c\tilde{z}_1}{\beta_r} - \frac{c_f}{\beta_f})\beta_f K_f\Big]\phi(\tilde{z}_2)d\tilde{z}_2\phi(\tilde{z}_1)d\tilde{z}_1 \\
& + \int_{\frac{2K_f-\mu_s}{\sigma_s}}^{+\infty} \int_{\frac{c_1-\mu_c-\rho\sigma_c\tilde{z}_1}{\sigma_c\sqrt{1-\rho^2}}}^{+\infty} \Big[(\frac{\sigma_c\sqrt{1-\rho^2}\tilde{z}_2 + \mu_c + \rho\sigma_c\tilde{z}_1}{\beta_r})(D_h + D_{nh}) - \\
& (\frac{\sigma_c\sqrt{1-\rho^2}\tilde{z}_2 + \mu_c + \rho\sigma_c\tilde{z}_1}{\beta_r} - \frac{c_f}{\beta_f})\beta_f K_f + o_f(\sigma_s\tilde{z}_1 + \mu_s - 2K_f)\Big]\phi(\tilde{z}_2)d\tilde{z}_2\phi(\tilde{z}_1)d\tilde{z}_1 \\
& + \int_{\frac{\tau_1(K_r)-\mu_s}{\sigma_s}}^{\frac{\tau_3(K_r)-\mu_s}{\sigma_s}} \int_{-\infty}^{\frac{c_2-\mu_c-\rho\sigma_c\tilde{z}_1}{\sigma_c\sqrt{1-\rho^2}}} \Big[(\frac{\sigma_c\sqrt{1-\rho^2}\tilde{z}_2 + \mu_c + \rho\sigma_c\tilde{z}_1}{\beta_r} - \frac{c_f}{\beta_f})\beta_r K_r + \\
& \frac{c_f}{\beta_f}(D_h + D_{nh})\Big]\phi(\tilde{z}_2)d\tilde{z}_2\phi(\tilde{z}_1)d\tilde{z}_1 \\
& + \int_{\frac{\tau_3(K_r)-\mu_s}{\sigma_s}}^{+\infty} \int_{-\infty}^{\frac{c_1-\mu_c-\rho\sigma_c\tilde{z}_1}{\sigma_c\sqrt{1-\rho^2}}} \Big[(\frac{\sigma_c\sqrt{1-\rho^2}\tilde{z}_2 + \mu_c + \rho\sigma_c\tilde{z}_1}{\beta_r} - \frac{c_f - o_f}{\beta_f})\beta_r K_r + \\
& \frac{c_f - o_f}{\beta_f}(D_h + D_{nh}) + o_f(\sigma_s\tilde{z}_1 + \mu_s - 2K_f)\Big]\phi(\tilde{z}_2)d\tilde{z}_2\phi(\tilde{z}_1)d\tilde{z}_1 \\
& + \int_{\frac{\tau_3(K_r)-\mu_s}{\sigma_s}}^{\frac{2K_f-\mu_s}{\sigma_s}} \int_{\frac{c_1-\mu_c-\rho\sigma_c\tilde{z}_1}{\sigma_c\sqrt{1-\rho^2}}}^{\frac{c_2-\mu_c-\rho\sigma_c\tilde{z}_1}{\sigma_c\sqrt{1-\rho^2}}} \Big[(\frac{\sigma_c\sqrt{1-\rho^2}\tilde{z}_2 + \mu_c + \rho\sigma_c\tilde{z}_1}{\beta_r})(D_h + D_{nh}) - \\
& (\frac{\sigma_c\sqrt{1-\rho^2}\tilde{z}_2 + \mu_c + \rho\sigma_c\tilde{z}_1}{\beta_r} - \frac{c_f}{\beta_f})\beta_f(\sigma_s\tilde{z}_1 + \mu_s - K_f)\Big]\phi(\tilde{z}_2)d\tilde{z}_2\phi(\tilde{z}_1)d\tilde{z}_1 \\
& + c_b(D_h + D_{nh}) + \omega_r K_r
\end{aligned}
$$

The first order partial derivative with respect to σ_c is

$$\frac{\partial V(\sigma_s,\sigma_c,\rho;K_r)}{\partial \sigma_c} = \int_{-\infty}^{\frac{\tau_1(K_r)-\mu_s}{\sigma_s}} \int_{-\infty}^{+\infty} \Big[\frac{\sqrt{1-\rho^2}\tilde{z}_2+\rho\tilde{z}_1}{\beta_r}\beta_r K_r\Big]\phi(\tilde{z}_2)d\tilde{z}_2\phi(\tilde{z}_1)d\tilde{z}_1$$
$$+ \int_{\frac{\tau_1(K_r)-\mu_s}{\sigma_s}}^{\frac{K_f-\mu_s}{\sigma_s}} \int_{\frac{c_2-\mu_c-\rho\sigma_c\tilde{z}_1}{\sigma_c\sqrt{1-\rho^2}}}^{+\infty} \Big[\frac{\sqrt{1-\rho^2}\tilde{z}_2+\rho\tilde{z}_1}{\beta_r}(D_h+D_{nh}-\beta_f(\sigma_s\tilde{z}_1+\mu_s))\Big]\phi(\tilde{z}_2)d\tilde{z}_2\phi(\tilde{z}_1)d\tilde{z}_1$$
$$+ \int_{\frac{K_f-\mu_s}{\sigma_s}}^{\frac{2K_f-\mu_s}{\sigma_s}} \int_{\frac{c_2-\mu_c-\rho\sigma_c\tilde{z}_1}{\sigma_c\sqrt{1-\rho^2}}}^{+\infty} \Big[\frac{\sqrt{1-\rho^2}\tilde{z}_2+\rho\tilde{z}_1}{\beta_r}(D_h+D_{nh}-\beta_f K_f)\Big]\phi(\tilde{z}_2)d\tilde{z}_2\phi(\tilde{z}_1)d\tilde{z}_1$$
$$+ \int_{\frac{2K_f-\mu_s}{\sigma_s}}^{+\infty} \int_{\frac{c_1-\mu_c-\rho\sigma_c\tilde{z}_1}{\sigma_c\sqrt{1-\rho^2}}}^{+\infty} \Big[\frac{\sqrt{1-\rho^2}\tilde{z}_2+\rho\tilde{z}_1}{\beta_r}(D_h+D_{nh}-\beta_f K_f)\Big]\phi(\tilde{z}_2)d\tilde{z}_2\phi(\tilde{z}_1)d\tilde{z}_1$$
$$+ \int_{\frac{\tau_1(K_r)-\mu_s}{\sigma_s}}^{\frac{\tau_3(K_r)-\mu_s}{\sigma_s}} \int_{-\infty}^{\frac{c_2-\mu_c-\rho\sigma_c\tilde{z}_1}{\sigma_c\sqrt{1-\rho^2}}} \Big[\frac{\sqrt{1-\rho^2}\tilde{z}_2+\rho\tilde{z}_1}{\beta_r}\beta_r K_r\Big]\phi(\tilde{z}_2)d\tilde{z}_2\phi(\tilde{z}_1)d\tilde{z}_1$$
$$+ \int_{\frac{\tau_3(K_r)-\mu_s}{\sigma_s}}^{+\infty} \int_{-\infty}^{\frac{c_1-\mu_c-\rho\sigma_c\tilde{z}_1}{\sigma_c\sqrt{1-\rho^2}}} \Big[\frac{\sqrt{1-\rho^2}\tilde{z}_2+\rho\tilde{z}_1}{\beta_r}\beta_r K_r\Big]\phi(\tilde{z}_2)d\tilde{z}_2\phi(\tilde{z}_1)d\tilde{z}_1$$
$$+ \int_{\frac{\tau_3(K_r)-\mu_s}{\sigma_s}}^{\frac{2K_f-\mu_s}{\sigma_s}} \int_{\frac{c_1-\mu_c-\rho\sigma_c\tilde{z}_1}{\sigma_c\sqrt{1-\rho^2}}}^{\frac{c_2-\mu_c-\rho\sigma_c\tilde{z}_1}{\sigma_c\sqrt{1-\rho^2}}} \Big[\frac{\sqrt{1-\rho^2}\tilde{z}_2+\rho\tilde{z}_1}{\beta_r}(D_h+D_{nh}-\beta_f(\sigma_s\tilde{z}_1+\mu_s-K_f))\Big]\phi(\tilde{z}_2)d\tilde{z}_2\phi(\tilde{z}_1)d\tilde{z}_1$$

Then

$$\frac{\partial^2 V(\sigma_s,\sigma_c,\rho;K_r)}{\partial \sigma_c^2} =$$
$$\frac{(c_2-\mu_c)^2}{\beta_r\sigma_c^3\sqrt{1-\rho^2}} \int_{\frac{\tau_1(K_r)-\mu_s}{\sigma_s}}^{\frac{K_f-\mu_s}{\sigma_s}} (D_h+D_{nh}-\beta_f(\sigma_s\tilde{z}_1+\mu_s))\phi(\frac{c_2-\mu_c-\rho\sigma_c\tilde{z}_1}{\sigma_c\sqrt{1-\rho^2}})\phi(\tilde{z}_1)d\tilde{z}_1$$
$$+ \frac{(c_2-\mu_c)^2}{\beta_r\sigma_c^3\sqrt{1-\rho^2}} \int_{\frac{K_f-\mu_s}{\sigma_s}}^{\frac{2K_f-\mu_s}{\sigma_s}} (D_h+D_{nh}-\beta_f K_f)\phi(\frac{c_2-\mu_c-\rho\sigma_c\tilde{z}_1}{\sigma_c\sqrt{1-\rho^2}})\phi(\tilde{z}_1)d\tilde{z}_1$$
$$+ \frac{(c_1-\mu_c)^2}{\beta_r\sigma_c^3\sqrt{1-\rho^2}} \int_{\frac{2K_f-\mu_s}{\sigma_s}}^{+\infty} (D_h+D_{nh}-\beta_f K_f)\phi(\frac{c_1-\mu_c-\rho\sigma_c\tilde{z}_1}{\sigma_c\sqrt{1-\rho^2}})\phi(\tilde{z}_1)d\tilde{z}_1$$
$$- \frac{(c_2-\mu_c)^2}{\sigma_c^3\sqrt{1-\rho^2}} \int_{\frac{\tau_1(K_r)-\mu_s}{\sigma_s}}^{\frac{\tau_3(K_r)-\mu_s}{\sigma_s}} K_r\phi(\frac{c_2-\mu_c-\rho\sigma_c\tilde{z}_1}{\sigma_c\sqrt{1-\rho^2}})\phi(\tilde{z}_1)d\tilde{z}_1$$
$$- \frac{(c_1-\mu_c)^2}{\sigma_c^3\sqrt{1-\rho^2}} \int_{\frac{\tau_3(K_r)-\mu_s}{\sigma_s}}^{+\infty} K_r\phi(\frac{c_1-\mu_c-\rho\sigma_c\tilde{z}_1}{\sigma_c\sqrt{1-\rho^2}})\phi(\tilde{z}_1)d\tilde{z}_1$$
$$- \frac{(c_2-\mu_c)^2}{\beta_r\sigma_c^3\sqrt{1-\rho^2}} \int_{\frac{\tau_3(K_r)-\mu_s}{\sigma_s}}^{\frac{2K_f-\mu_s}{\sigma_s}} (D_h+D_{nh}-\beta_f(\sigma_s\tilde{z}_1+\mu_s-K_f))\phi(\frac{c_2-\mu_c-\rho\sigma_c\tilde{z}_1}{\sigma_c\sqrt{1-\rho^2}})\phi(\tilde{z}_1)d\tilde{z}_1$$
$$+ \frac{(c_1-\mu_c)^2}{\beta_r\sigma_c^3\sqrt{1-\rho^2}} \int_{\frac{\tau_3(K_r)-\mu_s}{\sigma_s}}^{\frac{2K_f-\mu_s}{\sigma_s}} (D_h+D_{nh}-\beta_f(\sigma_s\tilde{z}_1+\mu_s-K_f))\phi(\frac{c_1-\mu_c-\rho\sigma_c\tilde{z}_1}{\sigma_c\sqrt{1-\rho^2}})\phi(\tilde{z}_1)d\tilde{z}_1 < 0$$

I also have $\frac{\partial V(\sigma_s,\sigma_c,\rho;K_r)}{\partial \sigma_c}\Big|_{\sigma_c\to 0}=0$ if $\mu_c \le c_1$. If $\mu_c > c_2$, then

$$\frac{\partial V(\sigma_s,\sigma_c,\rho;K_r)}{\partial \sigma_c}\Big|_{\sigma_c\to 0}=\int_{-\infty}^{\frac{\tau_1(K_r)-\mu_s}{\sigma_s}} \rho\tilde{z}_1 K_r\phi(\tilde{z}_1)d\tilde{z}_1+$$

$$\int_{\frac{\tau_1(K_r)-\mu_s}{\sigma_s}}^{\frac{K_f-\mu_s}{\sigma_s}} \frac{\rho\tilde{z}_1}{\beta_r}(D_h+D_{nh}-\beta_f(\sigma_s\tilde{z}_1+\mu_s))\phi(\tilde{z}_1)d\tilde{z}_1+\int_{\frac{K_f-\mu_s}{\sigma_s}}^{+\infty}\frac{\rho\tilde{z}_1}{\beta_r}(D_h+D_{nh}-\beta_f K_f)\phi(\tilde{z}_1)d\tilde{z}_1$$

Taking the derivative with respect to σ_s, I have

$$d\left(\frac{\partial V(\sigma_s,\sigma_c,\rho;K_r)}{\partial \sigma_c}\Big|_{\sigma_c\to 0}\right)/d\sigma_s=\int_{\frac{\tau_1(K_r)-\mu_s}{\sigma_s}}^{\frac{K_f-\mu_s}{\sigma_s}} -\frac{\rho\beta_f(\tilde{z}_1)^2}{\beta_r}\phi(\tilde{z}_1)d\tilde{z}_1$$

then, $\frac{\partial V(\sigma_s,\sigma_c,\rho;K_r)}{\partial \sigma_c}\Big|_{\sigma_c\to 0}$ is increasing, decreasing and independent of σ_s if $\rho<0$, $\rho>0$ and $\rho=0$, respectively. Hence, if $\rho<0$, $\frac{\partial V(\sigma_s,\sigma_c,\rho;K_r)}{\partial \sigma_c}\Big|_{\sigma_c\to 0}>0$; otherwise, $\frac{\partial V(\sigma_s,\sigma_c,\rho;K_r)}{\partial \sigma_c}\Big|_{\sigma_c\to 0}\le 0$. As $\frac{\partial^2 V(\sigma_s,\sigma_c,\rho;K_r)}{\partial \sigma_c^2}<0$; hence, if $\rho\ge 0$, I know that $\frac{\partial V(\sigma_s,\sigma_c,\rho;K_r)}{\partial \sigma_c}<0$, which implies that $V(\sigma_s,\sigma_c,\rho;K_r)$ decreases in σ_c; otherwise, I need to investigate $\frac{\partial V(\sigma_s,\sigma_c,\rho;K_r)}{\partial \sigma_c}\Big|_{\sigma_c\to+\infty}$. I find that $\frac{\partial V(\sigma_s,\sigma_c,\rho;K_r)}{\partial \sigma_c}\Big|_{\sigma_c\to+\infty}$ decreases in σ_s and $\frac{\partial V(\sigma_s,\sigma_c,\rho;K_r)}{\partial \sigma_c}\Big|_{\sigma_c\to+\infty,\sigma_s\to 0}=0$, thus $\frac{\partial V(\sigma_s,\sigma_c,\rho;K_r)}{\partial \sigma_c}\Big|_{\sigma_c\to+\infty}<0$. Then there exists a threshold $\bar{\sigma}_c$ such that the expected cost increases in σ_c if $\sigma_c\in(0,\bar{\sigma}_c]$ and decreases in σ_c otherwise. These results also hold under the case $c_1<\mu_c\le c_2$. Therefore, in summary, I have

- If $\mu_c \le c_1$ or $\rho\ge 0$, the expected cost $V(\sigma_s,\sigma_c,\rho;K_r)$ decreases in σ_c;
- If $\mu_c > c_1$ and $\rho<0$, the expected cost increases in σ_c if $\sigma_c\in(0,\bar{\sigma}_c]$ and decreases otherwise.

Similarly, I can get the first-order partial derivative with respective to σ_s The first-order partial derivative with respect to σ_s is

$$\frac{\partial V(\sigma_s,\sigma_c,\rho;K_r)}{\partial \sigma_s} = \int_{-\infty}^{+\infty}\int_{-\infty}^{\frac{\tau_1(K_r)-\mu_s-\rho\sigma_s\tilde{z}_0}{\sigma_s\sqrt{1-\rho^2}}}\Big[(c_f-\beta_f c_d)(\sqrt{1-\rho^2}\tilde{z}_3+\rho\tilde{z}_0)\Big]\phi(\tilde{z}_3)d\tilde{z}_3\phi(\tilde{z}_0)d\tilde{z}_0$$
$$+\int_{\frac{c_2-\mu_c}{\sigma_c}}^{+\infty}\int_{\frac{\tau_1(K_r)-\mu_s-\rho\sigma_s\tilde{z}_0}{\sigma_s\sqrt{1-\rho^2}}}^{\frac{K_f-\mu_s-\rho\sigma_s\tilde{z}_0}{\sigma_s\sqrt{1-\rho^2}}}\Big[-(\frac{\sigma_c\tilde{z}_0+\mu_c}{\beta_r}-\frac{c_f}{\beta_f})\beta_f(\sqrt{1-\rho^2}\tilde{z}_3+\rho\tilde{z}_0)\Big]\phi(\tilde{z}_3)d\tilde{z}_3\phi(\tilde{z}_0)d\tilde{z}_0$$
$$+\int_{\frac{c_1-\mu_c}{\sigma_c}}^{+\infty}\int_{\frac{2K_f-\mu_s-\rho\sigma_s\tilde{z}_0}{\sigma_s\sqrt{1-\rho^2}}}^{+\infty}\Big[o_f(\sqrt{1-\rho^2}\tilde{z}_3+\rho\tilde{z}_0)\Big]\phi(\tilde{z}_3)d\tilde{z}_3\phi(\tilde{z}_0)d\tilde{z}_0$$
$$+\int_{-\infty}^{\frac{c_1-\mu_c}{\sigma_c}}\int_{\frac{\tau_3(K_r)-\mu_s-\rho\sigma_s\tilde{z}_0}{\sigma_s\sqrt{1-\rho^2}}}^{+\infty}\Big[o_f(\sqrt{1-\rho^2}\tilde{z}_3+\rho\tilde{z}_0)\Big]\phi(\tilde{z}_3)d\tilde{z}_3\phi(\tilde{z}_0)d\tilde{z}_0$$
$$+\int_{\frac{c_1-\mu_c}{\sigma_c}}^{\frac{c_2-\mu_c}{\sigma_c}}\int_{\frac{\tau_3(K_r)-\mu_s-\rho\sigma_s\tilde{z}_0}{\sigma_s\sqrt{1-\rho^2}}}^{\frac{2K_f-\mu_s-\rho\sigma_s\tilde{z}_0}{\sigma_s\sqrt{1-\rho^2}}}\Big[-(\frac{\sigma_c\tilde{z}_0+\mu_c}{\beta_r}-\frac{c_f}{\beta_f})\beta_f(\sqrt{1-\rho^2}\tilde{z}_3+\rho\tilde{z}_0)\Big]\phi(\tilde{z}_3)d\tilde{z}_3\phi(\tilde{z}_0)d\tilde{z}_0$$

then I have

$$\frac{\partial^2 V(\sigma_s,\sigma_c,\rho;K_r)}{\partial \sigma_s^2} = \frac{(\tau_1(K_r)-\mu_s)^2}{\sigma_s^3\sqrt{1-\rho^2}}\int_{-\infty}^{+\infty}(\beta_f c_d-c_f)\phi(\frac{\tau_1(K_r)-\mu_s-\rho\sigma_s\tilde{z}_0}{\sigma_s\sqrt{1-\rho^2}})\phi(\tilde{z}_0)d\tilde{z}_0$$
$$-\frac{(\tau_1(K_r)-\mu_s)^2}{\sigma_s^3\sqrt{1-\rho^2}}\int_{\frac{c_2-\mu_c}{\sigma_c}}^{+\infty}(\frac{\sigma_c\tilde{z}_0+\mu_c}{\beta_r}-\frac{c_f}{\beta_f})\beta_f\phi(\frac{\tau_1(K_r)-\mu_s-\rho\sigma_s\tilde{z}_0}{\sigma_s\sqrt{1-\rho^2}})\phi(\tilde{z}_0)d\tilde{z}_0$$
$$+\frac{(K_f-\mu_s)^2}{\sigma_s^3\sqrt{1-\rho^2}}\int_{\frac{c_2-\mu_c}{\sigma_c}}^{+\infty}(\frac{\sigma_c\tilde{z}_0+\mu_c}{\beta_r}-\frac{c_f}{\beta_f})\beta_f\phi(\frac{K_f-\mu_s-\rho\sigma_s\tilde{z}_0}{\sigma_s\sqrt{1-\rho^2}})\phi(\tilde{z}_0)d\tilde{z}_0$$
$$+\frac{(2K_f-\mu_s)^2}{\sigma_s^3\sqrt{1-\rho^2}}\int_{\frac{c_1-\mu_c}{\sigma_c}}^{+\infty}o_f\phi(\frac{2K_f-\mu_s-\rho\sigma_s\tilde{z}_0}{\sigma_s\sqrt{1-\rho^2}})\phi(\tilde{z}_0)d\tilde{z}_0$$
$$+\frac{(\tau_3(K_r)-\mu_s)^2}{\sigma_s^3\sqrt{1-\rho^2}}\int_{-\infty}^{\frac{c_1-\mu_c}{\sigma_c}}o_f\phi(\frac{\tau_3(K_r)-\mu_s-\rho\sigma_s\tilde{z}_0}{\sigma_s\sqrt{1-\rho^2}})\phi(\tilde{z}_0)d\tilde{z}_0$$
$$+\frac{(2K_f-\mu_s)^2}{\sigma_s^3\sqrt{1-\rho^2}}\int_{\frac{c_1-\mu_c}{\sigma_c}}^{\frac{c_2-\mu_c}{\sigma_c}}(\frac{\sigma_c\tilde{z}_0+\mu_c}{\beta_r}-\frac{c_f}{\beta_f})\beta_f\phi(\frac{2K_f-\mu_s-\rho\sigma_s\tilde{z}_0}{\sigma_s\sqrt{1-\rho^2}})\phi(\tilde{z}_0)d\tilde{z}_0$$
$$-\frac{(\tau_3(K_r)-\mu_s)^2}{\sigma_s^3\sqrt{1-\rho^2}}\int_{\frac{c_1-\mu_c}{\sigma_c}}^{\frac{c_2-\mu_c}{\sigma_c}}(\frac{\sigma_c\tilde{z}_0+\mu_c}{\beta_r}-\frac{c_f}{\beta_f})\beta_f\phi(\frac{\tau_3(K_r)-\mu_s-\rho\sigma_s\tilde{z}_0}{\sigma_s\sqrt{1-\rho^2}})\phi(\tilde{z}_0)d\tilde{z}_0 \geq 0$$

Moreover, $\frac{\partial V(\sigma_s,\sigma_c,\rho;K_r)}{\partial \sigma_s}\Big|_{\sigma_s\to 0} = 0$; hence, $\frac{\partial V(\sigma_s,\sigma_c,\rho;K_r)}{\partial \sigma_s} > 0$, which implies that $V(\sigma_s,\sigma_c,\rho;K_r)$ increases in σ_s. Following the same way, I can show that $\frac{\partial V(\sigma_s,\sigma_c,\rho;K_r)}{\partial \rho} < 0$ (details are omitted), which implies that the expected cost decreases in ρ.

Although I prove these results for any given K_r, it is easy to show that they also hold under the optimal K_r^*. Therefore

(i) if $\omega_r \geq \omega_r^1$, the optimal expected cost V^* is independent of ρ and σ_c and increases in σ_s;

(ii)if $\omega_r < \omega_r^1$, V^* decreases in ρ and increases in σ_s; moreover, if $\mu_c \leq c_1$ or $\rho \geq 0$, V^* decreases in σ_c; otherwise, the optimal expected cost increases in σ_c on $\sigma_c \in (0, \bar{\sigma}_c(K_f)]$ and decreases on $(\bar{\sigma}_c(K_f), +\infty)$.

Using correlation for illustration, I show the global effect on the optimal expected cost. As the correlation coefficient ρ increases, the thresholds ω_r^0 and ω_r^1 increase. Now I consider the case that ω_r is initially larger than ω_r^1. From the results above, I know that the optimal expected cost V^* initially is independent of ρ. However, as ω_r^0 and ω_r^1 also increase in ρ such that a sufficiently large ρ may make ω_r^1 or both thresholds larger than ω_r, in this regard, V^* is first independent of and then decreases in ρ. If ω_r is initially smaller than ω_r^1, then I observe that V^* decreases in ρ globally. In summary, I can conclude that V^* decreases in ρ globally for all cases. I can derive the global effects of the variabilities on the optimal expected cost similarly. Hence I complete the proofs of Proposition 2.3. □

Proof of Proposition 2.4 If $\omega_r \geq \omega_r^1$ or $\omega_r < \omega_r^0$, K_r^* is independent of σ_s, σ_c and ρ; otherwise, by the implicit function theorem, I have $\frac{dK_r^*}{d\sigma_c} = -\frac{\partial^2 V(\sigma_s,\sigma_c,\rho;K_r)}{\partial K_r \partial \sigma_c} / \frac{\partial^2 V(\sigma_s,\sigma_c,\rho;K_r)}{\partial K_r^2}$. I know that $\frac{\partial^2 V(\sigma_s,\sigma_c,\rho;K_r)}{\partial K_r^2} > 0$, then the sign of $\frac{dK_r^*}{d\sigma_c}$ depends on $\frac{\partial M(\sigma_s,\sigma_c,\rho;K_r)}{\partial \sigma_c}$. Similarly, the signs of $\frac{dK_r^*}{d\sigma_s}$ and $\frac{dK_r^*}{d\rho}$ depend on $\frac{\partial M(\sigma_s,\sigma_c,\rho;K_r)}{\partial \sigma_s}$ and $\frac{\partial M(\sigma_s,\sigma_c,\rho;K_r)}{\partial \rho}$, respectively. I show these results in the proof of Lemma 1; hence, I can easily conclude that, if $\omega_r \in (\omega_r^0, \omega_r^1)$, K_r^* increases in ρ and decreases in σ_s. As σ_c increases, K_r^* increases if $\rho \geq 0$ or $\mu_c \leq c_1$; otherwise, K_r^* decreases if $\sigma_c \in (0, \hat{\sigma}_c]$ and increases otherwise.

For the global effect, I may note that the thresholds, except ω_r^2, also change with the variabilities and correlation. Considering the case that ω_r is initially larger than ω_r^1, as ρ increases, from Lemma 1, I know that ω_r^0 and ω_r^1 increases. If the increasing of ω_r^0 and ω_r^1 does not make $\omega_r^1 > \omega_r$, then, as I proved, K_r^* is independent of ρ; however, the global effects is K_r^* remains constant and then increases in ρ if I have $\omega_r^0 < \omega_r < \omega_r^1$ when ρ is sufficiently large. Nevertheless, I can conclude that K_r^* increases in ρ globally. This result also holds under another possible scenario that

the final increased ω_r^0 is larger than ω_r. Following similar arguments, I can also show that the global effects of σ_c and σ_s on the optimal recycling capacity K_r^*, which are presented in Proposition 2.4. □

Proof of Lemma 2.2: Following the closed form of ω_r^2, it is easy for us to conclude that ω_r^2 is independent of β_f and increasing in β_r. For the effects of β_r and β_f on ω_r^1, I take the first order partial derivative of $M(\beta_r, \beta_f; K_f)\big|_{K_r=\frac{D_h+D_{nh}-\beta_f K_f}{\beta_r}}$ with respect to β_r as

$$\begin{aligned}\frac{\partial M(\beta_r,\beta_f;K_f)}{\partial \beta_r} = &\int_{\underline{c}_r}^{\bar{c}_r}\int_{s_0}^{K_f} -c_d\psi(\tilde{s},\tilde{c}_r)d\tilde{s}d\tilde{c}_r + \int_{\underline{c}_r}^{c_2}\int_{K_f}^{2K_f} -\frac{c_f}{\beta_f}\psi(\tilde{s},\tilde{c}_r)d\tilde{s}d\tilde{c}_r \\ &+ \int_{\underline{c}_r}^{c_1}\int_{2K_f}^{+\infty} -\frac{c_f-o_f}{\beta_f}\psi(\tilde{s},\tilde{c}_r)d\tilde{s}d\tilde{c}_r\end{aligned}$$

As $c_1 \geq \underline{c}_r$, then I have $\frac{\partial V(\beta_r,\beta_f;K_f)}{\partial \beta_r} < 0$(this is also true if $c_1 < \underline{c}_r$). Hence, ω_r^1 increases in β_r. Similarly, I can show ω_r^1 decreases in β_f. □

Proof of Proposition 2.5: If $\omega_r \geq \omega_r^2$, I have

$$\begin{aligned}V^* = &\int_{\underline{c}_r}^{\bar{c}_r}\int_{s_0}^{K_f} \left(c_f\tilde{s} + c_d(D_h+D_{nh}-\beta_f\tilde{s})\right)\psi(\tilde{s},\tilde{c}_r)d\tilde{s}d\tilde{c}_r \\ &+ \int_{\underline{c}_r}^{\bar{c}_r}\int_{K_f}^{+\infty} \left(c_f K_f + c_d(D_h+D_{nh}-\beta_f K_f)\right)\psi_f(\tilde{s},\tilde{c}_r)d\tilde{s}d\tilde{c}_r \\ &+ \int_{\underline{c}_r}^{\bar{c}_r}\int_{2K_f}^{+\infty} o_f(\tilde{s}-2K_f)\psi_f(\tilde{s},\tilde{c}_r)d\tilde{s}d\tilde{c}_r + \bar{c}_b(\beta_h D_h + \beta_{nh}D_{nh})\end{aligned}$$

which, obviously, is independent of β_r. Moreover, I take the first-order derivative with respect to β_f

$$\frac{dV^*}{d\beta_f} = \int_{\underline{c}_r}^{\bar{c}_r}\int_{s_0}^{K_f} -\tilde{s}\psi(\tilde{s},\tilde{c}_r)d\tilde{s}d\tilde{c}_r + \int_{\underline{c}_r}^{\bar{c}_r}\int_{K_f}^{+\infty} -K_f\psi(\tilde{s},\tilde{c}_r)d\tilde{s}d\tilde{c}_r$$

which is negative. Hence, V^* decreases in β_f. Following from these results immediately, I find that reducing freshwater leakage ratio is more beneficial than reducing recycled water leakage.

If $\omega_r^1 \leq \omega_r < \omega_r^2$, I have

$$\frac{\partial V^*}{\partial \beta_r} = -\frac{D_h+D_{nh}-\beta_f K_f}{\beta_r^2}(\mu_c+\omega_r) < 0$$

Similarly, I have

$$\frac{\partial V^*}{\partial \beta_f} = -(\mu_c - \beta_r c_d + \omega_r)\frac{K_f}{\beta_r} - \int_{\underline{c}_r}^{\bar{c}_r}\int_{s0}^{K_f} c_d \tilde{s}\psi(\tilde{s},\tilde{c}_r)d\tilde{s}d\tilde{c}_r$$
$$- \int_{\underline{c}_r}^{\bar{c}_r}\int_{K_f}^{+\infty} c_d K_f \psi(\tilde{s},\tilde{c}_r)d\tilde{s}d\tilde{c}_r$$

I then have

$$\frac{\partial V^*}{\partial \beta_f} = \begin{cases} < 0, & \text{if } \omega_r > \underline{\omega}_r^2 \\ \geq 0, & \text{otherwise} \end{cases}$$

where $\underline{\omega}_r^2 = \omega_r^2 - \frac{\underset{\tilde{c}_r,\tilde{s}}{E}[\min(K_f,\tilde{s})]}{K_f}\beta_r c_d$. However, I can show that $\underline{\omega}_r^2 < \omega_r^1$; hence, in this case, $\omega_r > \underline{\omega}_r^2$ is always true. Therefore, V^* decreases in β_f. Comparing the marginal benefits of reducing β_f and β_r, I find that

$$\frac{\partial V^*}{\partial \beta_r} - \frac{\partial V^*}{\partial \beta_f} = -\frac{D_h + D_{nh} - \beta_f K_f}{\beta_r^2}(\mu_c + \omega_r) + (\mu_c - \beta_r c_d + \omega_r)\frac{K_f}{\beta_r}$$
$$+ \underset{\tilde{c}_r,\tilde{s}}{E}[\min(K_f,\tilde{s})]c_d$$
$$= \beta_f \frac{K_f(\mu_c + \omega_r)}{\beta_r^2} - \frac{D_h + D_{nh}}{\beta_r^2}(\mu_c + \omega_r) + (\mu_c - \beta_r c_d + \omega_r)\frac{K_f}{\beta_r}$$
$$+ \underset{\tilde{c}_r,\tilde{s}}{E}[\min(K_f,\tilde{s})]c_d$$

Let

$$C(\beta_r) = \frac{D_h + D_{nh}}{K_f} - \frac{(\omega_r - \omega_r^2)\beta_r}{\mu_c + \omega_r} - \frac{\underset{\tilde{c}_r,\tilde{s}}{E}[\min(K_f,\tilde{s})]c_d\beta_r^2}{K_f(\mu_c + \omega_r)}$$

then

$$\frac{\partial V^*}{\partial \beta_r} - \frac{\partial V^*}{\partial \beta_f} = \begin{cases} \geq 0, & \text{if } \beta_f \geq C(\beta_r); \\ < 0, & \text{otherwise} \end{cases}$$

Hence, in this case, it is optimal to reduce the freshwater leakage ratio in priority if $\beta_f \geq C(\beta_r)$ and reduce recycled water leakage ratio otherwise.

If $\omega_r < \omega_r^1$, for any given K_r, I have

$$\begin{aligned}\frac{\partial V(\beta_r,\beta_f;K_f)}{\partial \beta_r} = &\int_{\underline{c}_r}^{\bar{c}_r}\int_{s_0}^{\tau_1} -c_d K_r \psi(\tilde{s},\tilde{c}_r)d\tilde{s}d\tilde{c}_r + \int_{c_2}^{\bar{c}_r}\int_{\tau_1}^{K_f} -\frac{\tilde{c}_r}{\beta_r}\frac{D_h+D_{nh}-\beta_f\tilde{s}}{\beta_r}\psi(\tilde{s},\tilde{c}_r)d\tilde{s}d\tilde{c}_r \\ &+ \int_{c_2}^{\bar{c}_r}\int_{\tau_1}^{K_f} -\frac{\tilde{c}_r}{\beta_r}\frac{D_h+D_{nh}-\beta_f K_f}{\beta_r}\psi(\tilde{s},\tilde{c}_r)d\tilde{s}d\tilde{c}_r \\ &+ \int_{c_1}^{\bar{c}_r}\int_{2K_f}^{+\infty} -\frac{\tilde{c}_r}{\beta_r}\frac{D_h+D_{nh}-\beta_f K_f}{\beta_r}\psi(\tilde{s},\tilde{c}_r)d\tilde{s}d\tilde{c}_r \\ &+ \int_{\underline{c}_r}^{c_2}\int_{K_f}^{2K_f} -\frac{c_f}{\beta_f}K_r\psi(\tilde{s},\tilde{c}_r)d\tilde{s}d\tilde{c}_r + \int_{\underline{c}_r}^{c_1}\int_{2K_f}^{+\infty} -\frac{c_f-o_f}{\beta_f}K_r\psi(\tilde{s},\tilde{c}_r)d\tilde{s}d\tilde{c}_r \\ &+ \int_{c_1}^{c_2}\int_{\tau_3}^{2K_f} -\frac{\tilde{c}_r}{\beta_r}\frac{D_h+D_{nh}-\beta_f(\tilde{s}-K_f)}{\beta_r}\psi(\tilde{s},\tilde{c}_r)d\tilde{s}d\tilde{c}_r\end{aligned}$$

Hence, $\frac{\partial V(\beta_r,\beta_f;K_f)}{\partial \beta_r} < 0$, which implies that the optimal expected cost decreases in β_r. Similarly, I show V^* decreases in β_f.

In summary, I have

- If $\omega_r \geq \omega_r^2$, V^* is independent of β_r and decreasing in β_f
- If $\omega_r^1 \leq \omega_r < \omega_r^2$, V^* decreases in β_r and β_f
- If $\omega_r < \omega_r^1$, V^* decreases in β_r and β_f

From Lemma 2.2, I know how ω_r^2 and ω_r^1 change with β_r and β_f; hence, it is easy to show that V^* is globally decreasing in β_r and β_f. □

Proof of Lemma 2.3: omitted. □

Proof of Proposition 2.6: If $\omega_r \geq \omega_r^2$, I know that

$$\text{DW} = D_h + D_{nh} - \beta_f \underset{\tilde{c}_r,\tilde{s}}{E}[\min(K_f,\tilde{s})]$$

Obviously, it decreases in K_f.

If $\omega_r^1 \leq \omega_r < \omega_r^2$, then

$$\text{DW} = \beta_f \underset{\tilde{c}_r,\tilde{s}}{E}[(K_f-\tilde{s})^+]$$

which increases in K_f.

If $\omega_r^0 < \omega_r < \omega_r^1$, then

$$\mathrm{DW} = \underset{\tilde{c}_r, \tilde{s}}{E}[D_h + D_{nh} - \beta_f \tilde{s} - \beta_r K_r^*]$$

From Corollary 2.2, I know that K_r^* increases in K_f in this region; hence, DW decreases in K_f.

If $\omega_r \leq \omega_r^0$, I can see that DW is independent of K_f.

For the global effect, if $\omega_r \geq \omega_r^2$, as ω_r^2 is independent of K_r; hence, the global effect is the same as the characterized local effect.

If $\omega_r^1 \leq \omega_r < \omega_r^2$, I know that ω_r^1 increases in K_f. Define $\bar{\omega}_r = \omega_r^1 \Big|_{K_f=(D_h+D_{nh})/\beta_f}$, then (i) if $\bar{\omega}_r < \omega_r < \omega_r^2$, the increasing of K_f does not make ω_r^1 larger than $\bar{\omega}_r$, then the global effect is still DW increases in K_f; (ii) otherwise, there exists a threshold $\bar{K}_f$ such that $\omega_r^1 < \omega_r$ when K_f increases from s_0 to $\bar{K}_f$ and $\omega_r^1 \geq \omega_r$ when K_f further increases; hence, DW increases on $[s_0, \bar{K}_f)$ and decreases on $[\bar{K}_f, (D_h + D_{nh})/\beta_f]$.

If $\omega_r < \omega_r^1$, I can similarly show that DW globally decreases in K_f. □

Proof of Proposition 2.7: Omitted. □

Proof of Proposition 2.8: Omitted. □

Proof of Proposition 2.9: Omitted. □